Copper Complex Catalyzed Hydrolysis of Amides

by

Karen Mrejen

A thesis submitted to the Faculty of Graduate Studies and Research of McGill University in partial fulfillment of the requirements for the degree of Masters of Science

June 1991
Department of Chemistry
McGill University
Montreal, Quebec, Canada

To my parents Jacob and Anita

and to a special Friend

Abstract

Diaqua Cu(II) complexes are effective catalysts in promoting the hydrolysis of activated and unactivated amides.

The complex [Cu(2,2'-dipyridylamine)$(OH_2)_2$]$^{+2}$ efficiently catalyzes the hydrolysis of the acyl-activated amides trifluoro-N-methyl-*p*-nitroacetanilide (**MNTA**), *p*-nitrotrifluoroacetanilide (**NTA**), and *p*-methoxytrifluoroacetanilide (**MTA**).

A cooperative effect between N-methylmorpholine buffer and [Cu(2,2'-dipyridylamine)$(OH_2)_2$]$^{+2}$ is observed in the hydrolysis of *p*-methoxytrifluoroacet-anilide.

[Cu(2,2'-dipyridylamine)$(OH_2)_2$]$^{+2}$ hydrolyzes the unactivated amides with poor leaving groups formamide (**FA**) and N-methylformamide (**MFA**). In contrast, the monoaqua complex [Cu(2,2':6',2"-terpyridine)(OH_2)]$^{+2}$ is not active. A detailed mechanism of the copper complex catalyzed hydrolysis reactions is proposed to explain the structural requirements of an amide-cleaving catalyst.

A copper complex is shown to be an effective metalloprotein model. A potential hapten capable of generating catalytic metalloantibodies with peptidase activity has been proposed. The role of the metal ion in carboxypeptidase A is compared to that of the metal ion in [Cu(2,2'-dipyridylamine)$(OH_2)_2$]$^{+2}$.

Résumé

Les complexes diaqua du Cuivre(II) sont des catalyseurs efficaces lors de l'hydrolyse d'amides acylés activés trifluoro-N-méthyl-*p*-nitroacétanilide (**MNTA**), *p*-nitrotrifluoroacétanilide (**NTA**) et *p*-méthoxytrifluoroacétanilide (**MTA**).

Un effect coopératif entre le tampon N-méthylmorpholine et le complexe [Cu(2,2'-dipyridylamine)$(OH_2)_2]^{+2}$ augmente la vitesse de la réaction lors de l'hydrolyse du *p*-méthoxytrifluoroacétanilide.

Le complexe [Cu(2,2'-dipyridylamine)$(OH_2)_2]^{+2}$ hydrolyse les amides non-activés ayant de mauvais groupes partants, comme le formamide (**FA**) et le N-méthylformamide (**MFA**). Au contraire, le complexe monoaqua [Cu(2,2':6',2"-terpyridine)$(OH_2)]^{+2}$ n'est pas actif. Un mécanisme détaillé de la réaction d'hydrolyse catalysée par un complexe de cuivre est proposé pour expliquer les conformations structurales requises pour un tel catalyseur.

Il est démontré qu'un complexe de cuivre peut servir de modèle efficace pour les métalloprotéines. Un haptène potentiel, capable de générer des métalloanticorps catalytiques ayant une activité de peptidase, a été proposé. Le rôle de l'ion métallique de la carbopeptidase A est comparé a celui de l'ion métallique du complexe [Cu(2,2'-dipyridylamine)$(OH_2)_2]^{+2}$.

Acknowledgements

I am deeply grateful to my research supervisor, Prof. Jik Chin, for his enlightening discussions and his intellectual insight. His enthusiasm and support throughout this study is greatly appreciated.

I would like to thank Dr. Vrej Jubian, Dr. Stephen Kawai, Barry Linkletter, Dr. Mariusz Banaszczyk, Warren Chew, Jung-Hee Kim, Dr. Andrew Moore, James Connolly, Daphne Wahnon, and Bryan Takasaki for their friendship and their uselful discussions. I would also like to thank Dr. Françoise Sauriol for her assistance in NMR experiments and Yves St. Denis for translating the abstract of this thesis into french.

GLOSSARY OF SYMBOLS AND ABBREVIATIONS

δ	chemical shift
ε	extinction coefficient
λ	wavelength
Arg	arginine
Asn	aspargine
b.p.	boiling point
CHES	[2-(cyclohexylamino)ethanesulfonic acid]
CPA	carboxypeptidase A
dien	diethylenetriamine
dpa	2,2'-dipyridylamine
DSS	3-(trimethylsilyl)-1-propanesulfonic acid (2,2-dimethyl-2-silapentane-5-sulfonate)
en	ethylenediamine
Eq.	equation
FA	formamide
g	gram(s)
GAC	general acid catalysis
GBC	general base catalysis
Glu	glutamic acid
His	histidine
hrs	hour(s)
L	Litre(s)
Li	bidentate diamine ligand
Lit.	literature
MES	4-morpholineethanesulfonic acid
MFA	N-methylformamide
min	minute(s)
MNTA	trifluoro-N-methyl-*p*-nitroacetanilide
M-OH	metal-hydroxide
mol	mole(s)
m.p.	melting point
MTA	*p*-methoxytrifluoroacetanilide
NEM	N-ethylmorpholine

neo	neocuproine (2,9-dimethyl-1,10-phenanthroline)
NMR	nuclear magnetic resonance
NTA	*p*-nitrotrifluoroacetanilide
Phe	phenylalanine
ppm	parts per million
terp	2,2':6',2''-terpyridine
TMED	N,N,N',N'-tetramethylethylenediamine
TMS	tetramethylsilane
tren	tris(2-aminoethyl)amine
trien	triethylenetetramine
trpn	tris(3-aminopropyl)amine
Tyr	tyrosine
UV-vis	ultraviolet-visible
sec	second(s)

GLOSSARY OF STRUCTURES

Complexes:

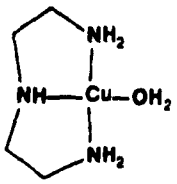

11 $[(dien)Cu(OH_2)]^{+2}$

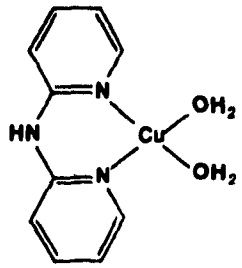

2 $[(dpa)Cu(OH_2)_2]^{+2}$

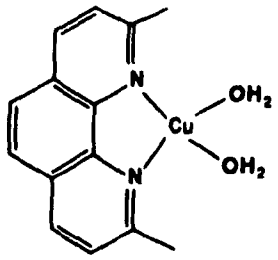

10 $[(neo)Cu(OH_2)_2]^{+2}$

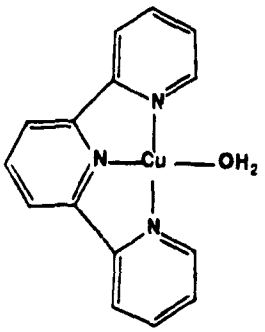

3

$[(terp)Cu(OH_2)]^{+2}$

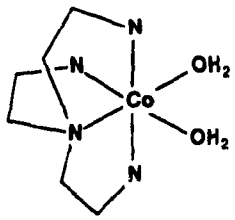

6

$[(tren)Co(OH_2)_2]^{+3}$

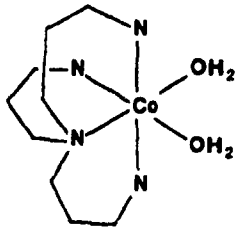

4

$[(trpn)Co(OH_2)_2]^{+3}$

Materials:

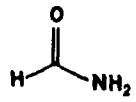

FA Formamide

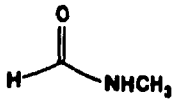

MFA N-methylformamide

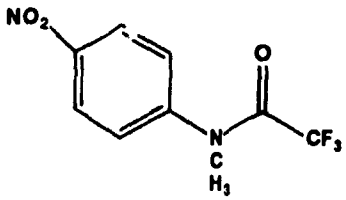

MNTA trifluoro-N-methyl-*p*-nitroacetanilide

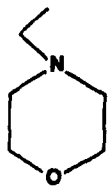

NEM N-ethylmorpholine

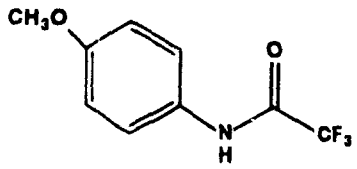

MTA — *p*-methoxytrifluoroacetanilide

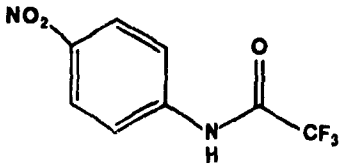

NTA — *p*-nitrotrifluoroacetanilide

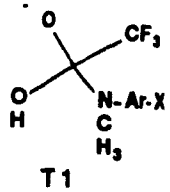

T1 — anionic tetrahedral intermediate

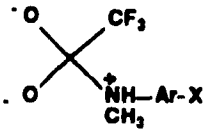

T2 zwitterionic tetrahedral intermediate

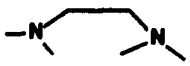

TMED N,N,N,N'-tetramethylethylenediamine

Table of Contents

3. Results

4. Discussion

1. Introduction

1.1 Proteins

Proteins are an essential part of the cell machinery. They are made of polypeptide chains which interact through disulfide bridges, hydrophobic interactions, hydrogen bonds, and electrostatic interactions. The twenty two amino acids found in nature are the building blocks of the polypeptide chain. The specific sequence by which these amino acids are joined determines the folding pattern of the polypeptides, and ultimately, the function of the resulting protein. The protein can function as a hormone, antibody, transport molecule, receptor, or enzyme.[1,2,3]

As the cell functions to maintain life, these protein molecules are continuously synthesized. They perform crucial cellular tasks and are then degraded. The amide bond linkage that forms the backbone of protein molecules are highly resistant to hydrolysis. In nature many enzymes function to catalyze the hydrolysis of amides. Some of these peptidases, for example carboxypeptidases, thermolysin, and angiotensin converting enzyme, are activated by metal ions.[4,5,6] However, other peptidases such as chymotrypsin, pepsin, and papain do not have any metals associated with them.[7,8]

Over the years, enormous interest has evolved in understanding the mechanism of action of peptidases. Numerous elegant models of peptidases, both metallic and non-metallic, have been designed and studied.[9-11] Although simple model studies do not prove enzyme mechanisms, detailed mechanistic studies of these simple model systems can give valuable insight into how enzymes work, and consequently, yield important information on the principles of catalysis.

In general, carboxylate esters are more reactive and therefore easier to hydrolyze than carboxylate amides. Furthermore, since the hydrolysis of esters and amides are mechanistically related, peptidases are not only highly efficient at hydrolyzing amides, but esters as well. In order to understand the structural requirements of a simple catalyst, or an enzyme, for hydrolyzing esters or amides, it is essential to understand the mechanism of hydrolysis of esters and amides in the absence of any catalysts. The simple hydrolysis of carboxylate esters, which has led the way to the development of peptidase models, will be discussed first.

1.2 Hydrolysis of Carboxylate Esters

The mechanism of hydrolysis of carboxylic esters has been extensively investigated and the process is well understood.[12, 13] Cleavage of either the acyl-oxygen bond or the alkyl-oxygen bond is possible. Both are observed and lead to the same products. Oxygen labelling studies have revealed that it is the acyl-oxygen cleavage which is more common

in both acid and base catalyzed hydrolysis reactions. The mechanisms are shown in Scheme 1.1.

Scheme 1.1

a) Base catalyzed hydrolysis of carboxylic esters

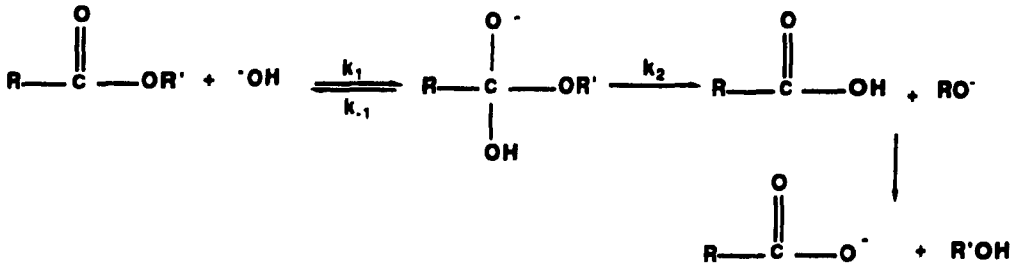

b) Acid catalyzed hydrolysis of carboxylic esters

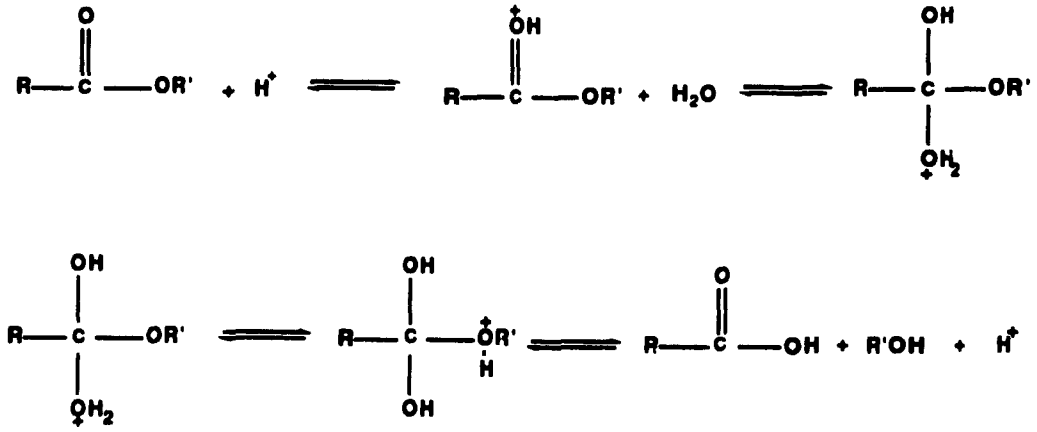

In acidic solution the ester hydrolysis reaction is reversible whereas in aqueous alkaline solution the reaction is irreversible. Substituents have a strong effect in the hydrolysis of esters. Electron withdrawing groups in either the acyl or the alkoxy group of an ester facilitates hydrolysis. The addition of hydroxide forms the tetrahedral intermediate which can either lose the hydroxide or the alkoxide (Scheme 1.1a). If the alkoxide is a better leaving group than the hydroxide ($k_2 > k_{-1}$), k_1 is the rate limiting step. However, if the alkoxide is a poorer leaving group than the hydroxide ($k_2 < k_{-1}$), k_2 is the rate limiting step.

The structural requirements of a simple catalyst for hydrolyzing esters with poor leaving groups are not necessarily the same as those for hydrolyzing esters with good leaving groups.[14-16] A catalyst that gives a large rate-acceleration for the rate of an activated ester hydrolysis may have little or no effect on the rate of an unactivated ester hydrolysis. For example, imidazole is an efficient nucleophilic catalyst for hydrolyzing *p*-nitrophenyl acetate whereas it is not a nucleophilic catalyst for hydrolyzing ethyl acetate.[14] Since *p*-nitrophenoxide is a good leaving group, the tetrahedral intermediate formed from imidazole and *p*-nitrophenyl acetate can eliminate *p*-nitrophenoxide efficiently ($k_2 > k_{-1}$, Scheme 1.2A). On the other hand, ethoxide is a much poorer leaving group than imidazole resulting in the breakdown of the tetrahedral intermediate to starting material ($k_{-1} >> k_2$, Scheme 1.2B). Thus, imidazole reverts to a general base mechanism for hydrolyzing ethyl acetate (Scheme 1.2C).

Scheme 1.2

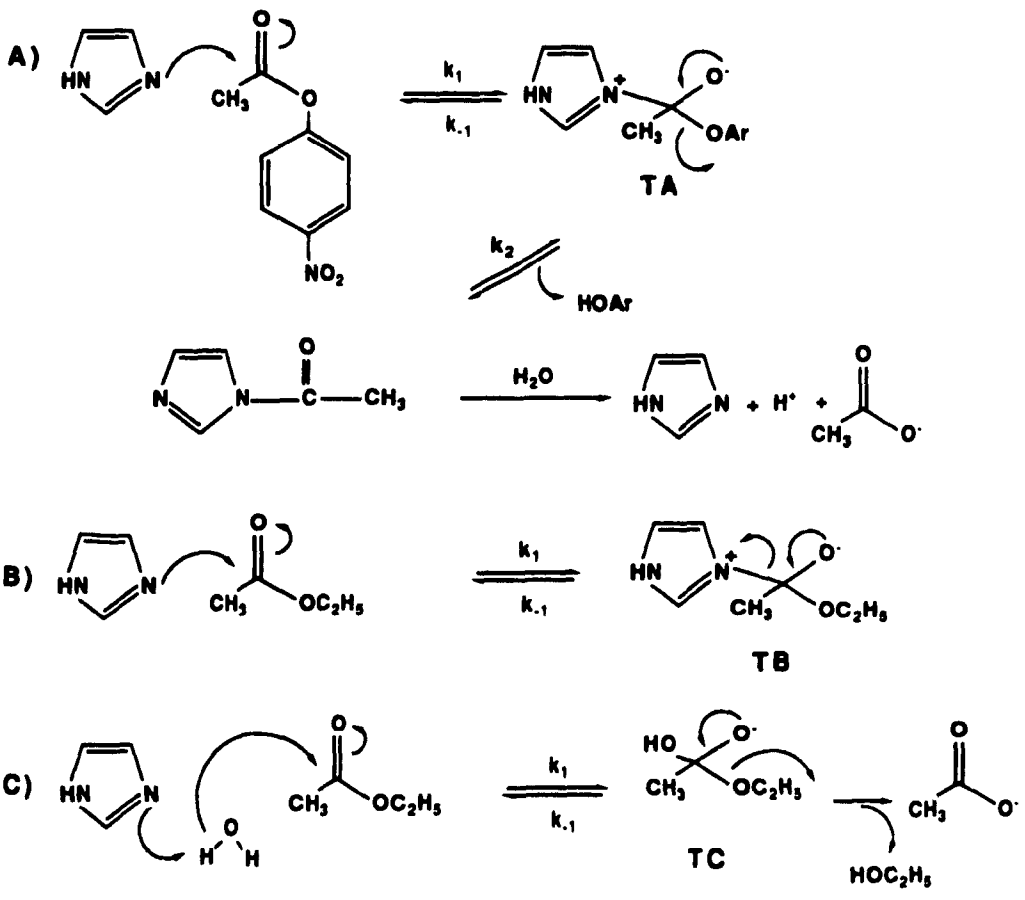

One way to distinguish between nucleophilic and general base catalysis is by solvent isotope effect studies.[14] The solvent isotope effect is small or absent in the nucleophilic mechanism for ester hydrolysis since a solvent molecule is not directly involved (Scheme 1.2A). Thus the solvent isotope effect is small for imidazole catalyzed hydrolysis of *p*-nitrophenyl acetate. In contrast, a large solvent isotope effect is observed for imidazole catalyzed hydrolysis of ethyl acetate since a solvent molecule is directly involved (Scheme 1.2C).

Due to the stability of amides and the difficulty associated with monitoring the hydrolysis reaction, most artificial enzymes have been tested for hydrolyzing activated substrates, for instance *p*-nitrophenyl esters. *p*-Nitrophenyl esters are convenient because they offer favorable reaction times and their hydrolysis can be followed spectrophotometrically. Thus various chymotrypsin models that hydrolyze *p*-nitrophenyl esters have been studied.[11-16] However, since the mechanism for the hydrolysis of activated esters is not always the same as that for the hydrolysis of unactivated esters, artificial enzymes should be tested for both activated and unactivated substrates.

1.3 Metal-Catalyzed Ester Hydrolysis

Metal ions were found to participate in enzyme mediated hydrolysis of esters and amides. Kroll[18] first demonstrated the possible role of divalent metal ions in the catalyzed hydrolysis of amino acid esters. The mechanism proposed was that of a cupric ion Lewis acid activation of the carbonyl group to attack by an external hydroxide (Scheme 1.3, where M= Cu(II)).

Scheme 1.3

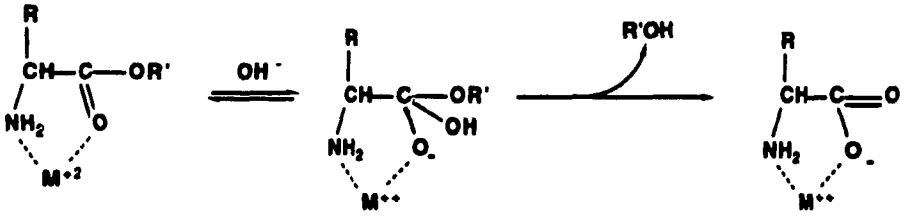

Buckingham and Sargeson[19] studied the hydrolysis of the ester bond in $[(en)_2CoX(NH_2CH_2COOR)]^{+2}$ (where R= CH_3, $CH(CH_3)_2$, C_2H_5; X=Cl^-, Br^-; en =

ethylenediamine). They showed that the hydrolysis reaction proceeds by two separate paths: the metal-hydroxide mechanism (Scheme 1.4, path **A**) and the Lewis acid mechanism (Scheme 1.4, path **B**).

Scheme 1.4

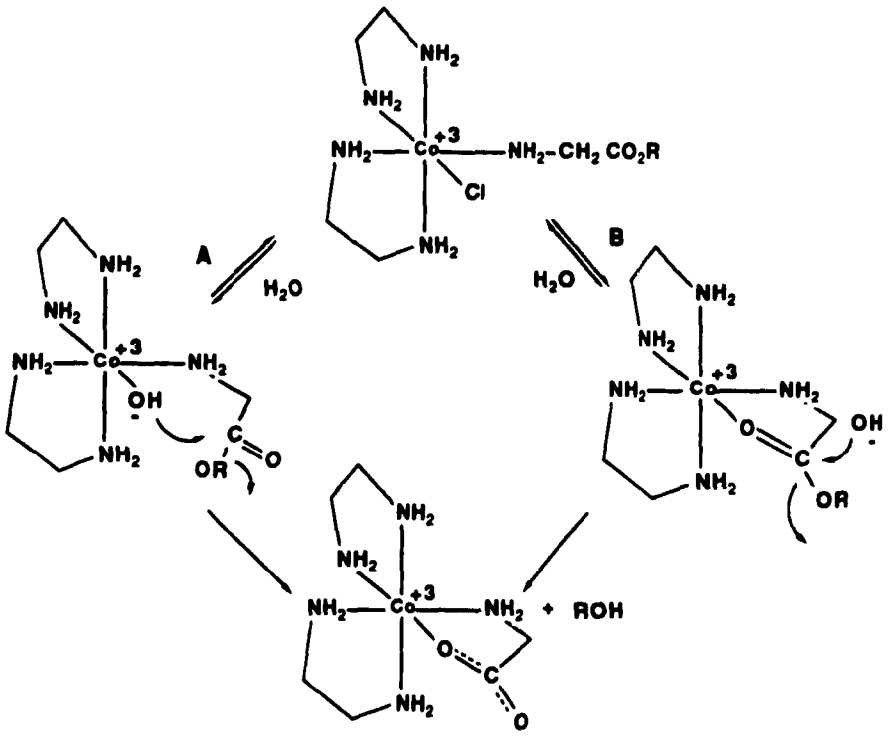

The polarization of the carbonyl, by the metal in path **B**, is responsible for up to 10^6 fold acceleration of the base hydrolysis of the glycine ester. The alternative mechanism, path **A**, shows a cis attack by a coordinated hydroxyl. ^{18}O labelling experiments have revealed that path **A** and **B** contribute about equally to the formation of the bidentate glycine product when R= $CH(CH_3)_2$. The ring size formed as a result of intramolecular hydroxide attack, pH, and the bulkiness of the amino acid ester, are important factors in determining which mechanism predominates.[19]

Recently, considerable interest has evolved in developing simple metal complexes that catalyze the hydrolysis of esters with poor leaving groups. Unlike imidazole (section 1.2), a simple zinc-hydroxide complex (**1**, Scheme 1.5) is an efficient nucleophilic catalyst for hydrolyzing methyl trifluoroacetate.[20] However, the zinc complex is not an efficient nucleophilic catalyst for hydrolyzing methyl acetate. This goes against the Lewis acid

mechanism and the reactivity-selectivity principle[21] since a greater rate-acceleration is obtained for a more reactive ester (methyl trifluoroacetate) than for a less reactive ester (methyl acetate). The metal-hydroxide mechanism shown in Scheme 1.5 was used to explain this catalytic effect.

Scheme 1.5

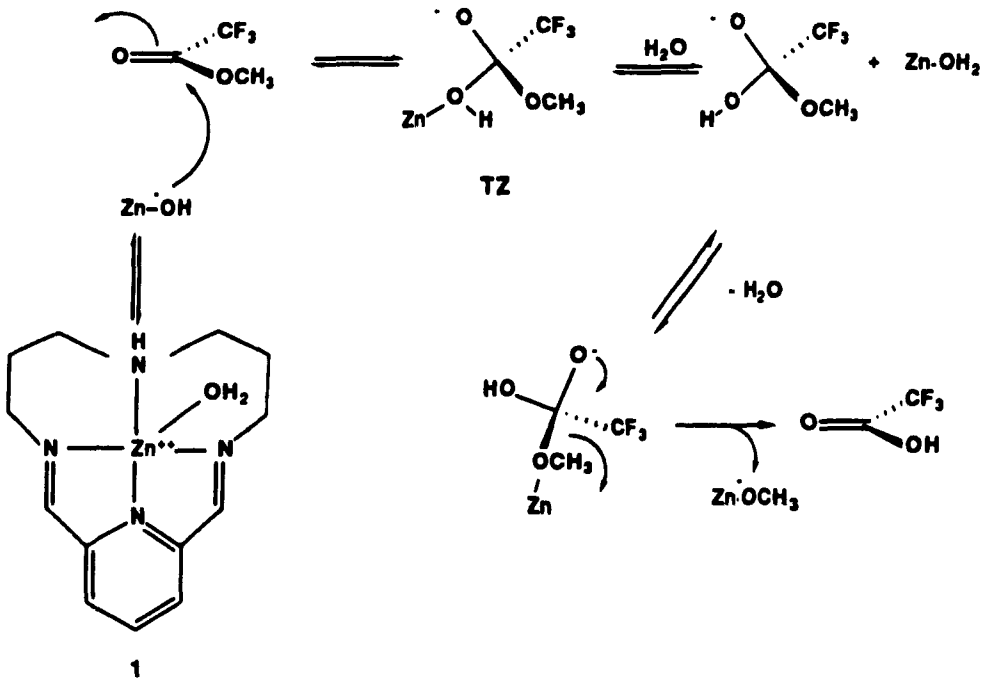

The mechanism involves nucleophilic attack of the zinc-hydroxide on methyl trifluoroacetate followed by zinc migration and elimination of the zinc methoxide. The zinc migration can take place rapidly since zinc ion is substitutionally labile.[22] However, for methyl acetate hydrolysis, the lifetime of the tetrahedral intermediate (**TZ**, Scheme 1.5) is too short for even this rapid zinc migration to take place. Thus **1** is an efficient nucleophilic catalyst for hydrolyzing methyl trifluoroacetate but not for hydrolyzing methyl acetate.

Two water molecules bound to a metal center is required for hydrolyzing unactivated esters like methyl acetate.[23] For example, **2** shown below, efficiently catalyzes the hydrolysis of methyl acetate. The pH-rate profile for **2** catalyzed hydrolysis of methyl acetate showed that the active form of the catalyst is the aqua-hydroxy metal complex. The hydrolysis mechanism involves coordination of the ester carbonyl group followed by intramolecular metal-hydroxide attack on the coordinated ester. Thus the proposed bifunctional mechanism includes both the Lewis acid and the metal-hydroxide mechanism

(Scheme 1.6). Lack of any solvent isotope effect indicates that the metal-hydroxide is a nucleophilic catalyst rather than a general base catalyst. Although **2** is slightly less reactive than **1**, **3**, or imidazole, for hydrolyzing *p*-nitrophenyl acetate, it is the only efficient catalyst for hydrolyzing methyl acetate. Thus, *p*-nitrophenyl acetate is not always appropriate for testing catalysts that hydrolyze unactivted esters.

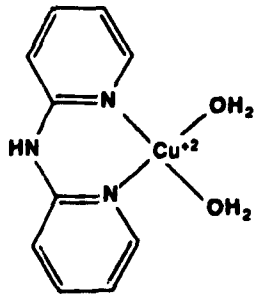

2

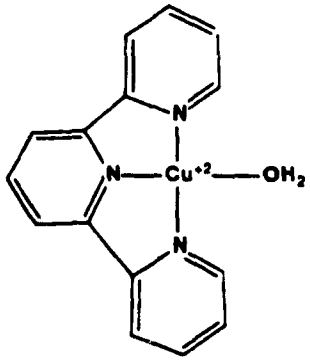

3

Scheme 1.6

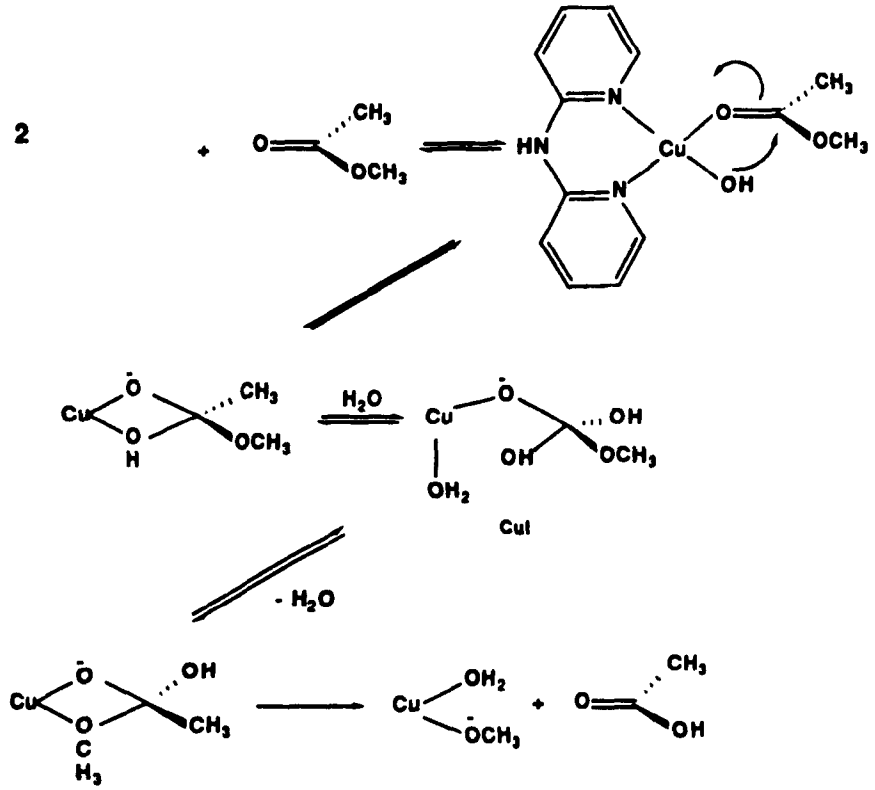

A cis diaqua cobalt complex (**4**, Scheme 1.7) was also found to catalyze the hydrolysis of methyl acetate. The catalytic cycle is shown in Scheme 1.7.

Scheme 1.7

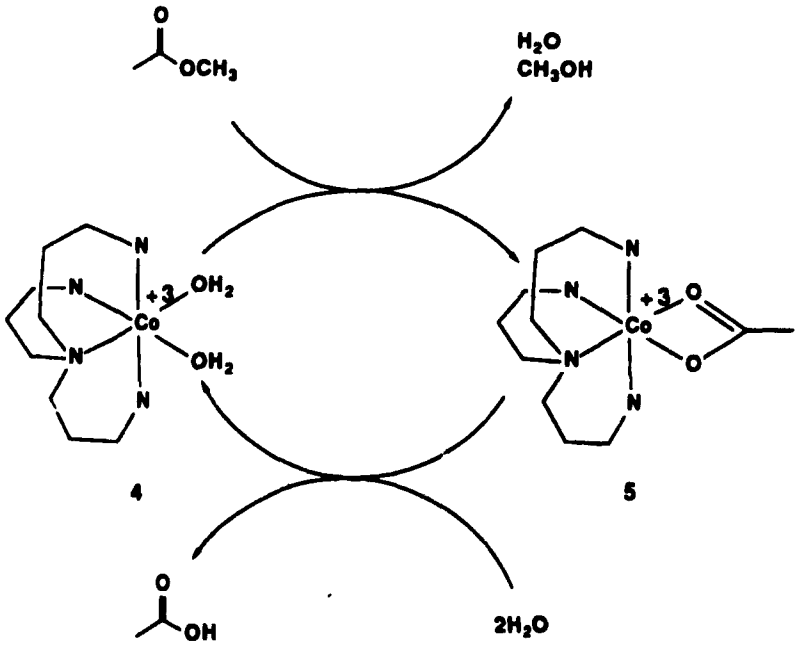

As with the copper complex (Scheme 1.6), the mechanism involves coordination of the ester to the metal complex followed by intramolecular metal-hydroxide attack. This requires the formation of a four-membered ring complex (**5**, Scheme 1.7). Although, in general, four-membered rings are strained and difficult to form, in this case the four-membered ring intermediate in the catalytic cycle **5** could easily be isolated and its X-ray structure determined.[25] Interestingly, the stability of the four-membered ring complex **5** is h ghly sensitive to the tetraamine ligand structure. For example, **6** shown below, a close structural analog of **4** does not form the four-membered ring acetato complex. Instead it forms a monodentate acetate complex. **6** unlike **4**, is not active at hydrolyzing methyl acetate.[26]

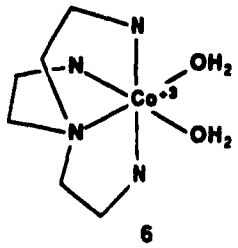

6

1.4 Hydrolysis of Amides

Amide-cleaving enzymes are an important part of the protein machinery present in biological systems.[1-8] The enzymes papain and ficin require intact thiol groups for activity. The serine hydroxyl group is the reactive nucleophile in the enzymes trypsin, chymotrypsin, substilisn, thrombin, and cholinesterases.[2] A number of dipeptidases, and exopeptidases such as carboxypeptidase A, require metals for activity. Metals such as Zn(II), Co(II), Mn(II), Mg(II), Fe(II), Cd(II), Ni(II), and Ca(II), have been found in several enzymes' active sites. Structure-reactivity relationships of these peptidases have been elucidated through the use of site-directed mutagenesis, X-ray crystallography, kinetic and mechanistic studies, and enzyme models. Although interest in understanding amide hydrolysis exists, the design of a functioning artificial peptidase has never been reported. Only oxidative cleavage of peptide bonds has been observed.[27] This may be partly due to the lack of a sensitive assay capable of detecting modest increments in the rate of amide hydrolysis.[28]

Still and Kahn[28] have recently developed a sensitive radioassay for detecting trace amounts of hydrolysis of unactivated amides. The pseudo-first order rate constant for the hydrolysis of a tripeptide attached to a solid support, shown below, at neutral pH and room temperature, was found to be 3×10^{-9} sec^{-1}. This corresponds to a half-life of about seven years.

Radioassay, due to its high sensitivity and convenient detection by liquid scintillation counting, was found to be adequate for the detection of the hydrolysis products. A peptide radiolabelled with ^{14}C, shown as * below, at the alpha carbon of the carboxy-terminal residues was added to a polymer support in the form of small beads (P_2).

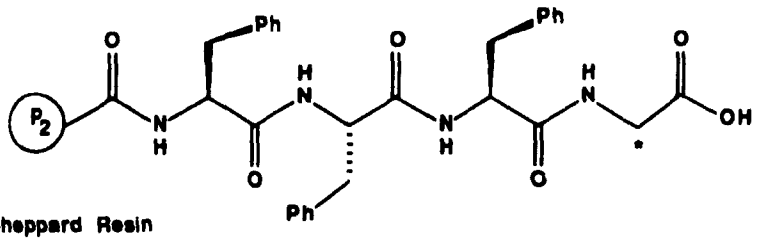

P_2= Sheppard Resin

All the bonds linking the radiolabel to the polymer backbone were either amide or carbon-carbon bonds. Scintillation counting of the filtrate obtained from the simple filtration of the water insoluble polymer-bound label (hydrolysis product) measured the extent to which the radiolabel had been released into solution. This was converted to the

rate of peptide cleavage. This method allowed easy separation of the products from the starting materials.

The amide bond is a planar hybrid existing in the two resonance forms shown in Scheme 1.8. Since the electron releasing nature of the nitrogen participates in a significant ground state stabilization to the carbonyl group, the hydrolysis of amides requires much more vigorous conditions than that of esters.[12, 13, 29]

Scheme 1.8

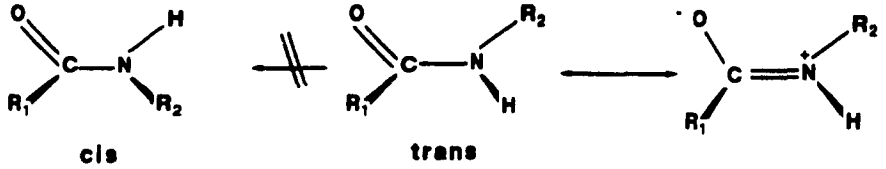

Proteins are polymers of amino acids joined through amide bonds. The resulting peptide linkage has trans geometry. This sterically favored geometry does not readily isomerize to the cis isomer through rotation about the C-N bond since such a rotation would destroy the resonance overlap.[29]

During amide hydrolysis, as the tetrahedral intermediate is formed, the stabilization of the amide bond is lost. Amide hydrolysis can occur with either acid or base catalysis. In basic medium, a mechanism similar to that of ester hydrolysis occurs. This is shown in Scheme 1.9.[12, 13]

Scheme 1.9

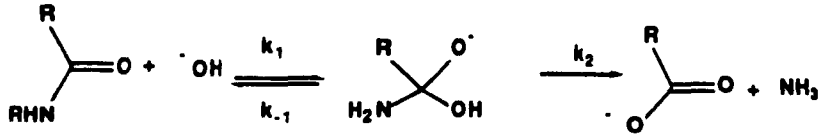

Amine ions NH_2^- are poorer leaving groups than hydroxides, and alkoxides. Thus, $k_{-1} >> k_2$, and k_2 (the breakdown of the tetrahedral intermediate) is the rate limiting step. In some cases, the breakdown of the tetrahedral intermediate in the forward direction is accompanied by a proton switch from the oxygen to the nitrogen and a dioxyanion intermediate forms.[30-32] This aspect of amide hydrolysis will be discussed in greater detail in the discussion.

For acid catalyzed hydrolysis of amides, there are two protonation sites: the amide oxygen and the amide nitrogen. The amide oxygen is more basic and hence the site of protonation (Scheme 1.10).[12, 13]

Scheme 1.10

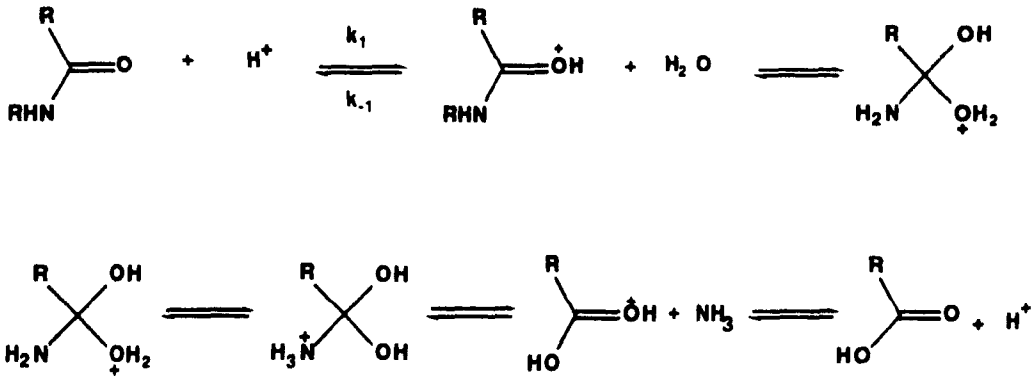

Increased rates of amide hydrolysis were observed in models which use an intramolecular nucleophilic mechanism.[23-25, 33-40] For example[38], when comparing the hydrolysis of gamma-hydroxybutyramide to that of acetamide and to that of butyramide, it was found that the respective ratios for the rate constants for the acid catalyzed reactions were 9:1 and 15:1. For the base catalyzed reaction, the ratios for the rate constants were 8:1 and 22:1 respectively. The introduction of a hydroxyl group in the gamma position of butyramide increased the ratio of acid to alkaline hydrolysis by a factor of 15 to 22. The intramolecular hydroxide hydrolysis reactions proposed for gamma-hydroxybutyramide are shown in Scheme 1.11.

Scheme 1.11

A) Acidic medium B) Basic medium C) Neutral medium

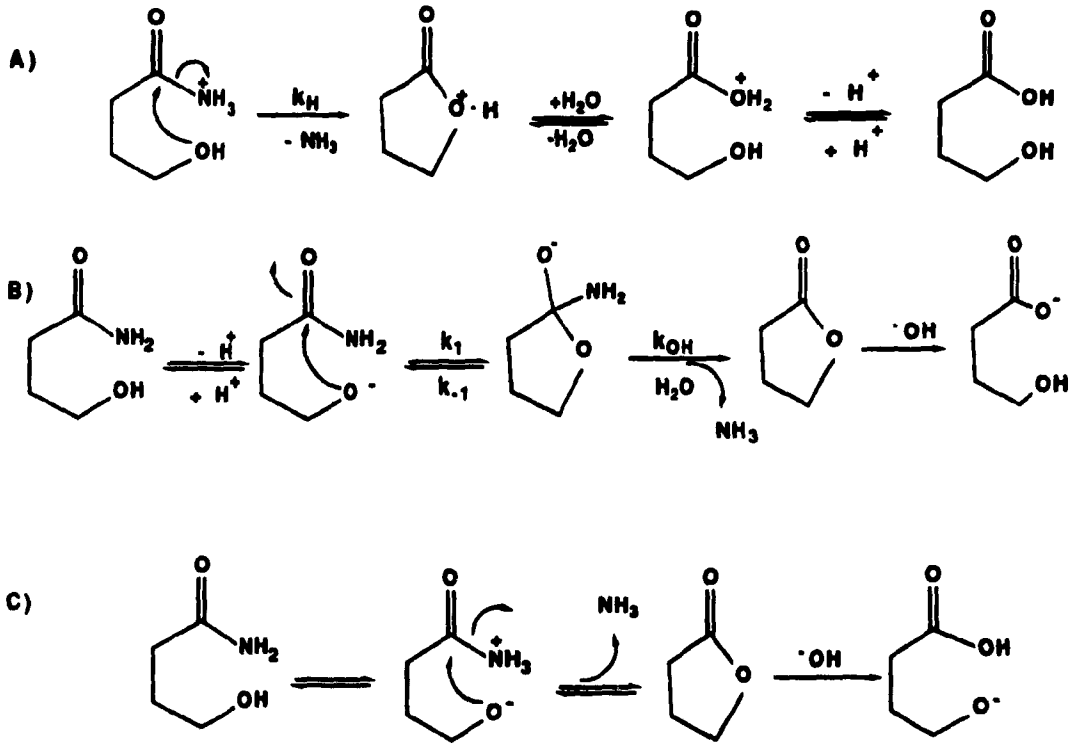

The pH rate profile revealed that at neutral conditions (pH 6.16, 100°C, C in Scheme 1.11) an 800 fold rate enhancement over the hydrolysis rate of butyramide was observed. This implied a significant participation of the gamma-hydroxyl group in the intramolecular amide hydrolysis reaction. Increases in the rates of amide hydrolysis reactions have also been observed with intramolecular carboxylate functional groups and metal ions.[17, 34, 39-41]

Greater rates of intramolecular reactions compared to the corresponding intermolecular reactions is due to lowering of the activation entropy.[33,40] Similarly, enzymes lower activation entropy by binding reacting substrates. Jencks showed that an effective molarity of up to 10^8 M may be obtained by completely eliminating the activation entropy.[33]

1.5 Metal-Catalyzed Amide Hydrolysis

The first studies of metal ion catalyzed hydrolysis of peptide bonds were done by Westheimer and Meriwether.[42] Three possible mechanisms were postulated for the hydrolysis of the sample peptide phenylalanylgylcine. These are shown in Scheme 1.12. The first reaction depicts the spontaneous intramolecular hydrolysis of the peptide. Release of an ammonium ion occurs as a stable six membered ring is formed (Scheme 1.12 **A**). The second reaction (k_2) shows exocyclic peptide bond cleavage whereas the third reaction (k_3) reveals endocyclic bond cleavage (Scheme 1.12 **B** and **C**).[42]

Scheme 1.12

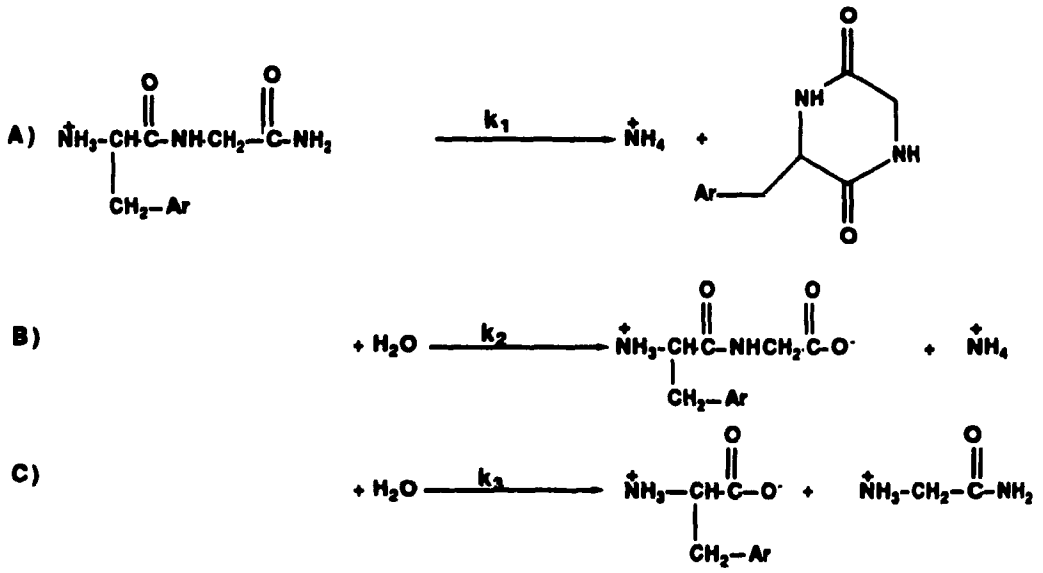

Without metal only 10% hydrolysis of the sample peptide was measured. This value increased to 95% with Cu(II), 70% with Co(II), 60% with Ni(II), and no rate enhancement was observed with Zn(II). It was proposed that these divalent transition metal ions functioned in a Lewis acid fashion, thus facilitating the attack of an external hydroxide, or a water molecule, onto the amide bond. The addition of copper metal was believed to catalyze k_2 and k_3, but suppress k_1. However, these metals were observed to accelerate peptide hydrolysis in an indiscriminate manner.[42]

As with metal catalyzed hydrolysis of esters, metal-catalyzed hydrolysis of amides can take place by a Lewis acid mechanism or the metal-hydroxide mechanism.[19] The two mechanisms are kinetically indistinguishable with substitutionally labile metal ions.[19,43] Sargeson and Buckingham[19] used substitutionally inert cobalt complexes to show that both

the Lewis acid and the metal-hydroxide mechanisms can give substantial rate-enhancements for hydrolyzing amides.

Elegant ^{18}O labelling experiments showed that the amide bond in cis-$[(en)_2Co(OH/OH_2)(glyNH_2)]^{+2/+3}$ (Scheme 1.13) is hydrolyzed primarily by the metal-hydroxide mechanism at neutral pH. In contrast, the amide bond in the complex $[(trien)Co(OH/OH_2)(glyNH_2)]^{+2/+3}$, hydrolyzes primarily by the Lewis acid mechanism (Scheme 1.14). At pH 7 the intramolecular metal-hydroxide mechanism is about 100 times faster than the intermolecular Lewis acid mechanism (Scheme 1.4).[19]

Scheme 1.13

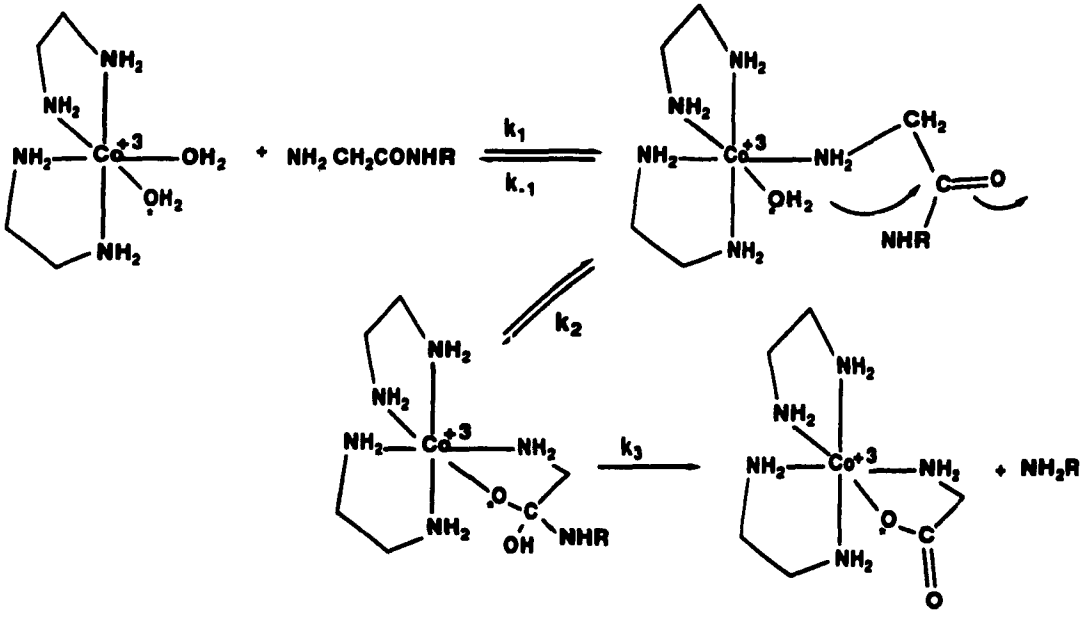

Scheme 1.14

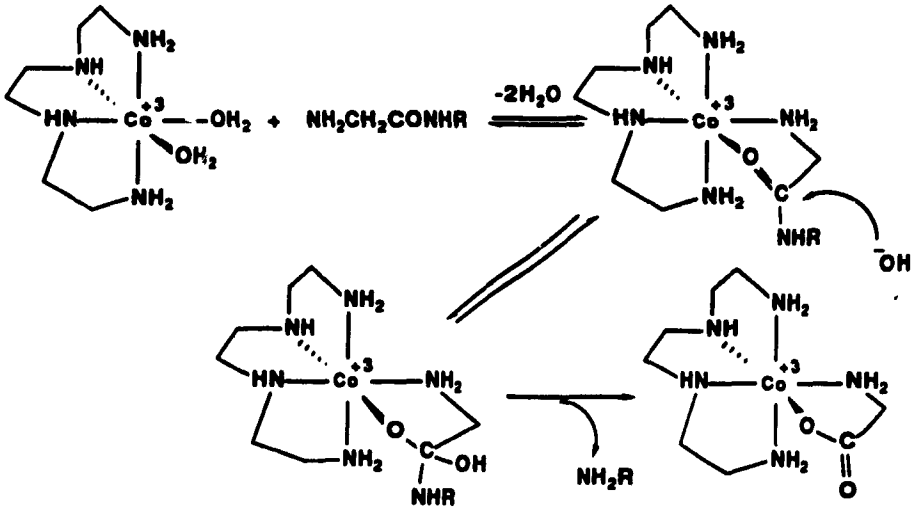

More recently, simple carboxypeptidase models have been designed based on the Lewis acid mechanism as well as on the metal-hydroxide mechanism.[43-45] In one Lewis acid mechanism based model,[44] (Scheme 1.15) the cobalt bound amide was covalently linked to a phenol group to model the tyrosine hydroxyl group in the active site of carboxypeptidase A. The phenol group was shown to increase the rate of amide hydrolysis by about 50 fold.

Scheme 1.15

1. R = H, R' = CO_2 H
2. R = R' = H
3. R = CH_3 , R' = H

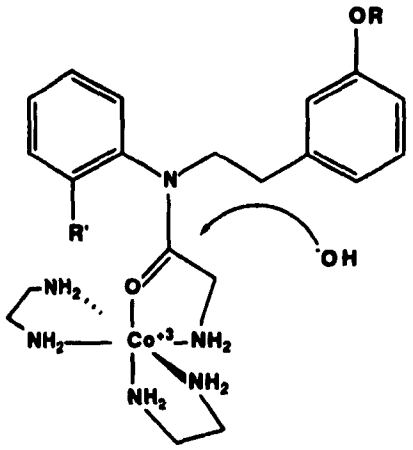

In the metal-hydroxide mechanism based model,[45] (Scheme 1.16) an intramolecular carboxyl group was added to mimic the glutamate group in the active site of carboxypeptidase A. The carboxyl group gave a 30 fold increase in the rate of the amide hydrolysis.

Scheme 1.16

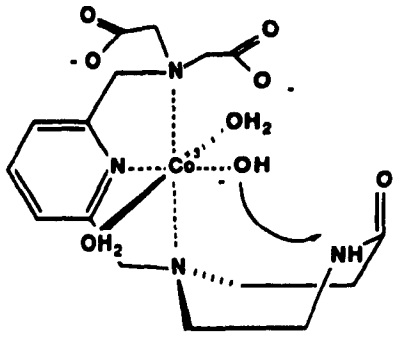

In most peptidase models the amides are either highly activated or they are covalently linked to the catalytic groups. Recently, catalytic hydrolysis of an unactivated amide by free Cu(II) metal was demonstrated.[46] At pH 7.5 and 23°C one equivalent of $Cu(ClO_4)_2$ catalyzed the hydrolysis of **7** (Scheme 1.17), which is the addition product of N-benzyl-N',N'-dimethylethylenediamine, the metal chelating portion, to acrylamide. K_{obs} for the reaction, with 8 mmol dm^{-3} of **7**, was 3.4×10^{-6} s^{-1}. The reaction proceeded to about 97% completion whereas the control **8**, at 50°C, revealed less than 2% hydrolysis. The catalytic cycle for the Cu(II) catalyzed hydrolysis of **7** is shown in Scheme 1.17.

Scheme 1.17

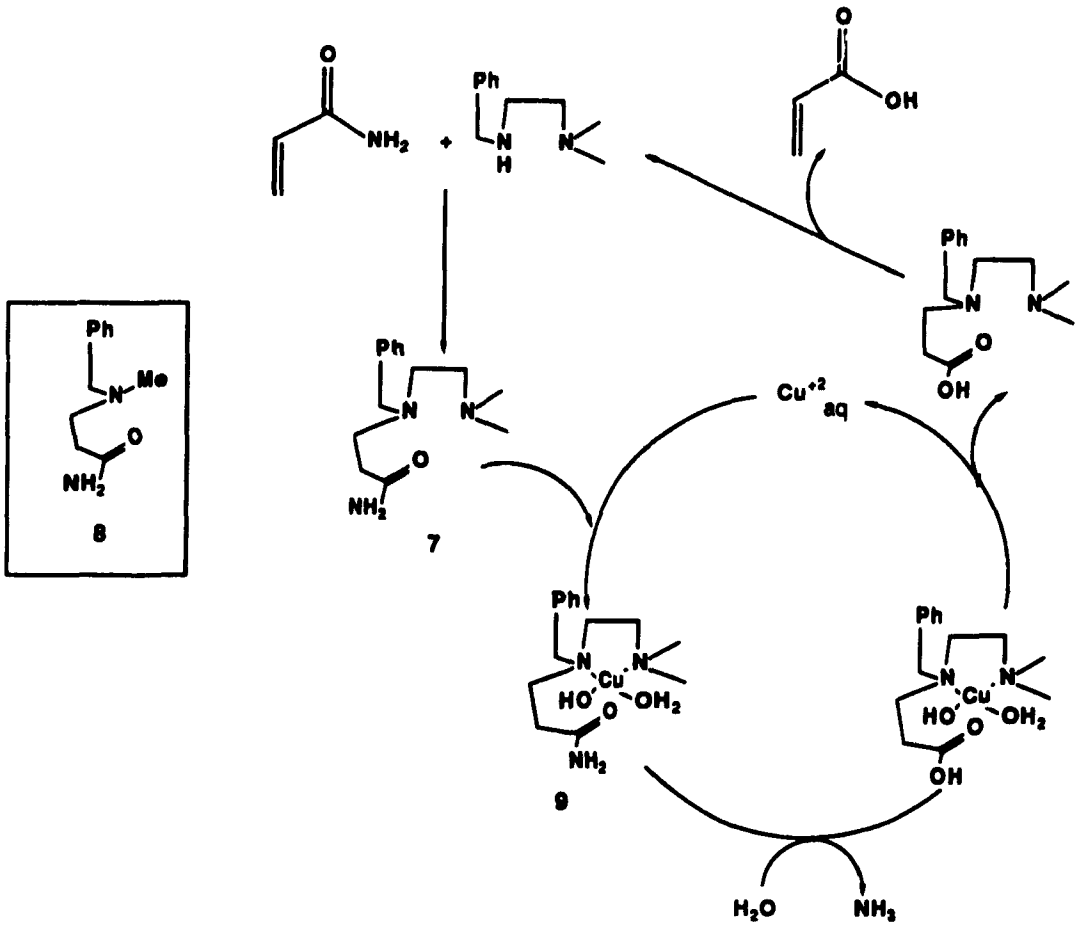

One half of an equivalent of Cu(II) with 8 mmol dm^{-3} of **7**, at pH 7.5 and 50°C, proceeded to 97% completion. Although complexation of the metal is weak, proper chelate ring size is believed to be the key factor in the observed rate increase. Lewis acid activation

in **9** requires a six membered ring which is known to be not as stable as a five membered ring. Because of this, the amide is believed to be hydrolyzed by an intracomplex metal-hydroxide, with no Lewis acid activation by the metal. For copper complexes the copper hydroxide mechanism is more efficient than that of the Lewis acid activation mechanism.[34] Although this system (Scheme 1.17) displays catalytic turnover, the amide substrate requires a Michael addition site. This imposes a structural requirement in the amide substrate to be hydrolyzed.

The purpose of this thesis is to investigate the structural requirements of a simple catalyst for hydrolyzing both activated and unactivated amides without any constraints.

Plan of Study

Considerable interest exists in determining the role of the metal ion in amide hydrolysis. The first possibility is that the metal ion directly activates the amide by coordinating to the amide carbonyl making it more susceptible to nucleophilic attack (**A**). The second possibility is that the metal ion coordinates to a water molecule subsequently generating a metal-hydroxide which attacks the amide (**B**).

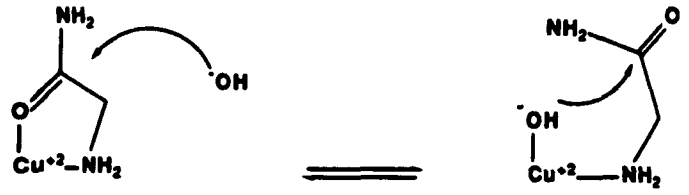

A **B**

The two mechanisms are kinetically indistinguishable. Furthermore **A** and **B** do not represent true catalytic systems since the products are tightly bound to the metal complexes preventing any catalytic turnover.

Two fundamentally important questions may be raised at this point. First, what is the structural requirements of a simple metal complex that would hydrolyze amides with catalytic turnover? Second, what is the role of the metal ion in that simple catalytic system? The effects of monoaqua and diaqua copper complexes on the rate of hydrolysis of activated and unactivated amides will be investigated. Detailed kinetic and mechanistic studies will be carried out in order to address these questions.

Metal-buffer cooperativity plays an important role in metalloprotease catalyzed hydrolysis of amides. However, only metalloenzymes have been observed to hydrolyze free amide substrates through such a mechanism. The structural requirements of a metal complex, capable of metal-buffer cooperative free amide hydrolysis, will be investigated.

2. Experimental

2.1 Instruments

^{1}H NMR and ^{31}P NMR spectra were recorded on Varian XL200 and Varian XL300 spectrometers respectively. For ^{1}H NMR tetramethylsilane (TMS, $CDCl_3$) and 3-trimethylsilyl-1-propanesulfonic acid (DSS, D_2O) were used as internal standards. For ^{31}P NMR, trimethylphosphate was used as an external reference.

Melting points were determined using an Electrothermal MP apparatus. UV-vis absorption spectra were recorded on a Hewlett-Packard 8451A diode array spectrophotometer equipped with a Lauda RM6 thermostat.

Titrations and pH-stat experiments were performed using a Radiometer PHM63 pH meter equipped with a Radiometer RTS822 automatic titrator.

2.2 Materials

MES (4-morpholineethanesulfonic acid), CHES [2-(cyclohexylamino)ethanesulfonic acid], and NEM (N-ethylmorpholine), were purchased from Aldrich (and were used without purification). N,N,N',N'-tetramethylethylenediamine (TMED), and sodium acetate were purchased from Aldrich (and were used without purification).

The synthesis of the activated amides, trifluoro-N-methyl-*p*-nitroacetanilide (**MNTA**), *p*-nitrotrifluoroacetanilide (**NTA**) and *p*-methoxytrifluoroacetanilide (**MTA**) were carried out by the procedure of *Tatlow* et al.[47] **MNTA**: yield: 80%; mp: 122-125°C (Lit. mp: 126.5-128°C). **NTA**: yield: 89%; mp: 150-152°C (Lit. mp: 151.5-153°C). **MTA**: yield: 90%; mp: 112-115°C (Lit. mp: 100-113°C). These compounds gave satisfactory ^{1}H NMR spectra.

Formamide (**FA**) and N-methylformamide (**MFA**) were purchased from Aldrich and purified by vacuum distillation.

Phenylphosphonic acid was purchased from Aldrich. Its disodium salt was made by adding two equivalents of aqueous NaOH (0.1M) to an aqueous phenylphosphonic acid solution (2 g, 10 mmol). The solution (pH 9-10) was then lyophilized.

The ligands 2,2'-dipyridylamine (dpa), 2,2':6',2''-Terpyridine (terp), and Tris(2-aminoethyl)amine (tren) were purchased from Aldrich and were used without purification.

Synthesis of Ligands

Tris(3-aminopropyl)amine (trpn) was synthesized by the method described by Mariusz Banaszczyk.[25]

Synthesis of Complexes

[(dpa)$CuCl_2$]; [(terp)CuCl]Cl; [(neo)$CuCl_2$]; [(dien)CuCl]Cl:

To a solution of ligand (1 g, 5.4 mmol) in ethanol (30 mL) was added $CuCl_2$ (0.73 g, 5.4 mmol) also in ethanol (30 mL). The corresponding green complex precipitated out of solution. The precipitate was filtered and dried under vacuum.

[(trpn)Co(CO_3)](ClO_4)H_2O; [(tren)Co(CO_3)](ClO_4)H_2O:

The ligand (trpn or tren; 1.5 g) was added dropwise to a stirring solution of lead oxide (4.5 g, 20 mmol, 30 mL H_2O) and aqueous sodium bicarbonate (3.0 g, 36 mmol, 30 mL H_2O). One equivalent of aqueous Co(II) perchlorate hexahydrate was added dropwise and the resulting solution was stirred at room temperature. After two days the red solution was filtered over celite and the filtrate's pH was lowered to six with aqueous perchloricacid (5 M). The volume of the solution was reduced under vacuum. Upon crystallization of a purple precipitate, ethanol was added.[25]

[(trpn)Co(OH_2)$_2$]$^{+3}$ (4); [(tren)Co(OH_2)$_2$]$^{+3}$ (6):

To a solution of the Co(III) carbonato complex (0.2 g, 0.47 mmol) was added aqueous perchloric acid (2.5-5.0 equivalents) and the resulting mixture was stirred under a water aspirator for 2-6 hours.[25]

2.3 Kinetics

Hydrolysis of Activated Amides with Good Leaving Groups

The non-complexing buffers NEM, CHES, and MES (0.1 N) were used to make stock solutions of the Cu(II) catalysts at the desired pH. The pH of the solution was adjusted with aqueous NaOH (0.1N). The reactions were followed at optimum pH for each complex at 25°C. Ionic strength of the reaction solution was not controlled since the rate of amide hydrolysis did not change significantly with added NaCl (0.1 N). The hydrolyses of the activated amides, **MNTA** and **NTA** were followed spectrophotometrically by monitoring the change of absorbance at 400 nm. The conditions

were pseudo first order, where the concentration of the Cu(II) catalyst was 1 mM and that of the amide was 0.1 mM (10 fold excess of complex).

In a typical experiment, a freshly prepared solution (2 mL) of the Cu(II) complex (1 mM) was made with the appropriate buffer (0.1N) at the desired pH (or pD when in D_2O). The Cu(II) solution was thermostatted for five minutes at 25°C. Injection of 10 µl of a stock solution of the amide (20 mM, dioxane) initiated the hydrolysis reaction. The pH of the solution did not change by more than 0.05 units at the end of the reaction. Experiments were run in triplicate and were reproducible to within 5 % error.

To demonstrate catalytic turnover, excess substrate (1 mM, 25°C) was used over the Cu(II) complex (0.1 mM, pH 8.0). Under these conditions the reaction was followed spectrophotometrically at 490 nm (ε = 360) since the change in absorbance at 400 nm (ε = 18 200) was too large to monitor a reaction.

First order rate constants were calculated from the slopes of the linear plots of optical density against time by converting to concentration units (ε = 18 200 for 400 nm and ε = 360 for 490 nm) and by dividing by the initial amide concentration. Rates of hydrolysis of the amide substrate in the absence of the catalyst were measured and, when not negligible, were subtracted from the rate of catalytic hydrolysis.

Hydrolysis of an Activated Amide with a Poor Leaving Group

The non-complexing buffer NEM (10-50 mM) was used to make stock solutions of the Cu(II) catalyst at pH 8. The pH of the solution was adjusted with aqueous NaOH (0.1 N). The hydrolysis of the activated amide MTA was followed spectrophotometrically by monitoring the change in absorbance at 290 nm due to the decrease in the concentration of substrate. Since the concentration of the catalyst does not change during the reaction, the conditions were pseudo first order where the concentration of the Cu(II) catalyst was 0.3 mM and that of MTA was 0.05 mM (6 fold excess of complex).

A freshly prepared solution (2 mL) of the Cu(II) complex (0.3 mM) was made with NEM buffer (10-50 mM) at pH 8. The Cu(II) solution was thermostatted for five minutes at 50°C. Injection of 2.5 µL of a stock solution of the amide (40 mM, dioxane) initiated the hydrolysis reaction. The pH of the solution did not change by more than 0 05 units at the end of the reaction. Experiments were run in triplicate and were reproducible to within 5 % error.

First order rate constants were calculated from the slopes of the linear plots of optical density against time by converting to concentration units; where $\varepsilon = \varepsilon_{substrate} - \varepsilon_{product} = 7964 - 550 = 7414$. The extinction coefficients, ε, were determined

experimentally at 290 nm by taking the slopes of the linear plots of optical density against concentration of substrate (or product). The hydrolysis rates of the amide substrate in the absence of the catalyst were measured. These were compared to the rates of Cu(II) complex catalyzed amide hydrolysis in the presence of NEM buffer.

Hydrolysis of Unactivated Amides

One equivalent of **MFA** in D_2O (40 μl of a 0.5 M solution) was added to a freshly prepared solution of the Cu(II) complex (10 mM, 2 mL). The pD of the resulting solution was adjusted with aqueous NaOH (0.1N, D_2O). The sample was then placed in an NMR tube. The tube was then sealed and heated in a water bath maintained at 100°C. The $[(dpa)Cu(OH_2)_2]^{+2}$ (10 mM) catalyzed hydrolysis of **FA** (10 mM) and **MFA** (10 mM), at 100°C, was monitored by ^1H NMR spectroscopy. The progress of the **FA** hydrolysis reaction was followed by a decrease in the aldehyde peak [δ = 8.08; with respect to DSS]. For the **MFA** hydrolysis reaction, a decrease in the ^1H NMR signal of the aldehyde and methyl peaks [δ = 8.08, δ = 2.75] are accompanied by an increase in the product's methyl peak [δ = 2.58] (free methylamine). The references used to monitor the **MFA** and **FA** hydrolysis reactions were tetramethylammonium fluoride [δ = 3.18] and dioxane [δ = 3.71] respectively. The kinetic experiments were reproducible to within 10 % error.

Since the catalyst concentration does not change during the reaction, the data was treated as pseudo-first order reactions. The first order hydrolysis reaction rates for the $[(dpa)Cu(OH_2)_2]^{+2}$ catalyzed hydrolysis of unactivated amides were calculated by fitting the linear graph of the logarithm of the percent of substrate present (at time t) vs time (hrs) according to the first order equation:[48]

$$A_t = A_0 e^{-kt} \quad \text{or} \quad \ln(A_t/A_0) = -kt$$

where A_t is the concentration of substrate left at time **t**, A_0 is the initial concentration of substrate which was present at t=0, and **k** is the first order rate constant in sec^{-1}.

2.4 Titrations

A 5 mL sample of a 1 mM solution of $[(dpa)Cu(OH_2)_2]^{+2}$ complex in water (or D_2O, 25°C) was titrated with a 0.01N NaOH solution.

2.5 ^{31}P NMR

A solution of the Co(III) diaqua complex in D_2O (50 mM, 2 mL) was mixed with 1.0 equivalent (40 µl) of the disodium salt of phenylphosphonic acid (2.5 M). The solution was adjusted to pD 6.5 with aqueous NaOH (0.1N, D_2O) and was then allowed to equilibrate for one hour before the spectrum was recorded.

3. Results

3.1 Hydrolysis of Activated Amides

The mechanisms of hydroxide catalyzed hydrolysis of acyl-activated amides is well known.[30-32] The acyl-activated amides trifluoro-N-methyl-*p*-nitroacetanilide (**MNTA**), *p*-nitrotrifluoroacetanilide (**NTA**), and *p*-methoxytrifluoroacetanilide (**MTA**), displayed below, are used to study the hydrolytic reactions catalyzed by the simple Cu(II) complexes $[(dpa)Cu(OH_2)_2]^{+2}$ (**2**), $[(terp)Cu(OH_2)]^{+2}$ (**3**), $[(neo)Cu(OH_2)_2]^{+2}$ (**10**), and $[(dien)Cu(OH_2)]^{+2}$ (**11**).

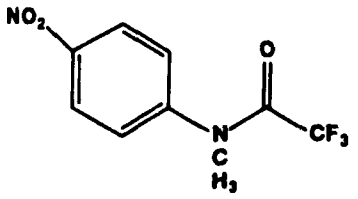

MNTA

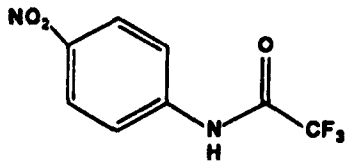

NTA

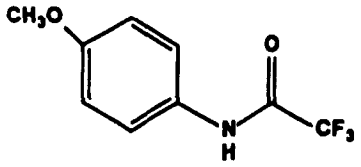

MTA

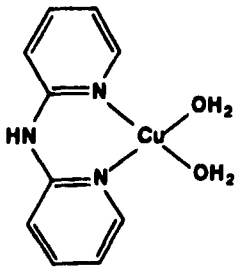

2

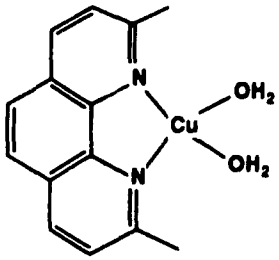

10

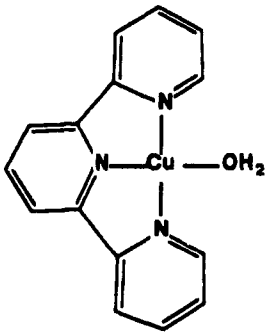

3

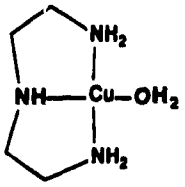

11

Pseudo-first order rate constants are obtained for Cu(II) complex catalyzed hydrolysis of **MNTA**, **NTA**, and **MTA**. These rate constants are compared to the amide's hydroxide (uncatalyzed) rate of hydrolysis.

Hydrolysis of Activated Amides with Good Leaving Groups

Cu(II) Complex Catalyzed Hydrolysis of MNTA

The pH and pD rate profiles for the $[(dpa)Cu(OH_2)_2]^{+2}$ (1 mM, 25°C) catalyzed hydrolysis of **MNTA** (0.1 mM) are shown in Figure 3.1 and 3.2 respectively. The data points are averages from three consecutive runs. The pH and pD rate profiles for **MNTA** were fit according to the equation displayed below using a non-linear least squares curve fitting program.[49]

$$\log k_{obs} = \log \left\{ \frac{k_2 K_a}{K_a + [H^+]} \right\}$$

where k_2 is the rate constant for the hydrolysis reaction catalyzed by the aqua-hydroxy Cu(II) complex. K_a is the first acid dissociation constant for the diaqua Cu(II) complex species. The calculated values are depicted with the appropriate pH (pD) rate profiles. The rate equation is derived in the discussion.

An increase in the hydrolysis rate of the activated amide **MNTA** is observed with the diaqua copper complexes $[(dpa)Cu(OH_2)_2]^{+2}$ and $[(neo)Cu(OH_2)_2]^{+2}$. No significant rate enhancement is observed with monoaqua Cu(II) complexes. Table 3.1 summarizes these results.

Table 3.1 k_{obs} for the hydroxide[50] (uncatalyzed), and Cu(II) (1 mM) complex catalyzed hydrolysis of the activated amide **MNTA** (0.1 mM). The relative rates compared to the hydroxide rate at pH 8.00, 25°C are also displayed.

Catalyst	Substrate MNTA trifluro-N-methyl-*p*-nitroacetanilide	
	Rate (sec^{-1})	Rel. Rate
Hydroxide (pH 8.04)[50]	1.8×10^{-4}	1.0
$[(dpa)Cu(OH)(OH_2)]^+$	7.3×10^{-4}	4.1
$[(Neo)Cu(OH)(OH_2)]^+$	3.4×10^{-4}	1.9
$[(terp)Cu(OH)]^+$	1.5×10^{-4}	0.83
$[(dien)Cu(OH)]^+$	1.5×10^{-4}	0.83

The second order rate constant for the hydrolysis reaction of MNTA is highest for the hydroxide ion (k_{obs} = 180 sec^{-1} M^{-1}).[50] This hydroxide catalyzed reaction is very sensitive to pH.[50] At neutral pH the Cu(II) diaqua catalysts are more efficient than hydroxide.

$[(dpa)Cu(OH_2)_2]^{+2}$ Catalyzed Hydrolysis of MNTA

Further experiments were performed with the most effective catalyst, $[(dpa)Cu(OH_2)_2]^{+2}$. Titration of the complex showed that pKa_1 of the complex is 7.2 in H_2O and 7.3 in D_2O. However, pKa_2 for the complex is too high to measure experimentally. Figure 3.1, which displays the pH rate profiles for the hydroxide[50] (uncatalyzed) and $[(dpa)Cu(OH_2)_2]^{+2}$ catalyzed hydrolysis reactions of MNTA, reveals that the catalyst is effective in its aqua-hydroxy form (between pH 6 and 8.5). At pH 8.5 the catalyzed reaction reaches its maximum rate.

Table 3.2 k_{obs}, at varying pH, for the $[(dpa)Cu(OH_2)_2]^{+2}$ (1 mM, 25°C) catalyzed hydrolysis of MNTA (0.1 mM). The rate enhancement over the background rate is also given.

pH	k_{obs} (sec^{-1})	$\log(k_{obs})$ sec^{-1}	Rate Enhancement
6.50	1.2×10^{-4}	-3.92	
7.00	2.6×10^{-4}	-3.58	14.0
7.45	5.7×10^{-4}	-3.24	
8.00	7.3×10^{-4}	-3.14	4.1
8.50	7.9×10^{-4}	-3.10	

Figure 3.1 pH-rate profiles for the hydroxide[50] (uncatalyzed) and $[(dpa)Cu(OH_2)_2]^{+2}$ catalyzed hydrolysis of **MNTA**. The calculated values are $k_2 = 8.8 \times 10^{-4}$ sec^{-1}, $K_a = 4.8 \times 10^{-8}$.

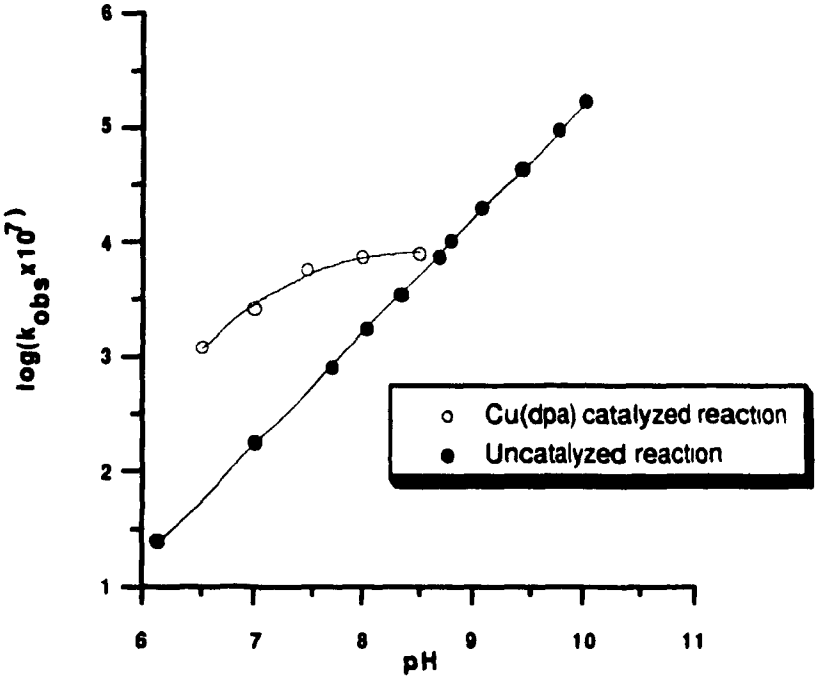

Kinetic Solvent Isotope Effect

Kinetic solvent isotope effects (KIE) on hydrolysis reaction rates give valuable information on the hydrolysis mechanism. If the rate limiting step involves proton transfer then a primary solvent isotope effect is expected (KIE > 2) since an O-D bond is more difficult to break then an O-H bond.[2b,51] Solvent isotope experiments were performed to determine whether proton transfer was the rate limiting step in the $[(dpa)Cu(OH_2)_2]^{+2}$ catalyzed hydrolysis reactions.

At pH's ranging from 7 to 8.5, the KIE for the $[(dpa)Cu(OH_2)_2]^{+2}$ catalyzed hydrolysis of **MNTA** is less than 2. Table 3.3B displays the ratio (k_{H2O}/k_{D2O}) for the first order rate constants for the catalyzed hydrolysis reactions at a specific pH (or pD where pD = pH + 0.4)[52]. The kinetic solvent isotope effect on k_2 is small (8.8/6.2 = 1.4 at pH 8.5) therefore proton transfer is not the rate limiting step for the $[(dpa)Cu(OH_2)_2]^{+2}$ catalyzed hydrolysis of **MNTA**.

Table 3.3 A) At varying pD, k_{obs} for the $[(dpa)Cu(OH_2)_2]^{+2}$ (1 mM) catalyzed hydrolysis of MNTA (0.1 mM) in D_2O at 25°C. B) KIE at varying pH (pD) for the hydrolysis reactions (k_{H2O}/k_{D2O}).

A)

pD	k_{obs} (sec^{-1})	$log(k_{obs})$ sec^{-1}
7.05	1.5×10^{-4}	-3.83
7.45	3.1×10^{-4}	-3.52
8.00	4.0×10^{-4}	-3.40
8.50	5.6×10^{-4}	-3.25
9.05	6.5×10^{-4}	-3.19

B)

pH pD	k_{H_2O} / k_{D_2O}
7.00	1.8
7.45	1.8
8.00	1.8
8.50	1.4

Figure 3.2 displays the pH and pD rate profiles for the $[(dpa)Cu(OH_2)_2]^{+2}$ catalyzed hydrolysis of MNTA. In either H_2O or D_2O the active species is the aqua-hydroxy copper complex.

Figure 3.2 The pH and pD rate profiles for the $[(dpa)Cu(OH_2)_2]^{+2}$ catalyzed hydrolysis of MNTA. For the pD rate profile the calculated values are $k_2 = 6.2 \times 10^{-4}$ sec^{-1}, $K_a = 2.8 \times 10^{-8}$.

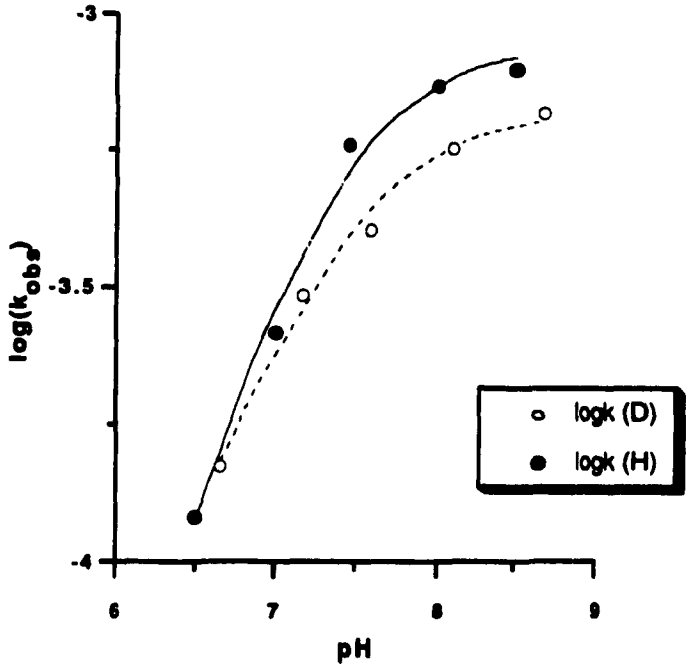

Buffer Catalysis

Examining the effects of buffers in both catalyzed and uncatalyzed amide hydrolysis reaction rates can help determine if the catalyst acts as a general base or a general acid in the Cu(II) complex catalyzed hydrolysis of amides. It can also indicate whether proton transfer is the rate limiting step.[51]

The non-complexing buffers (10-40 mM) MES, NEM, and CHES are not effective in catalyzing the hydrolysis of **MNTA**. At various concentrations of these buffers, the pseudo first order uncatalyzed rate constants are about equal to the hydroxide rate (k_{OH}) at pH 8.00. Furthermore, in the presence of these buffers the $[(dpa)Cu(OH_2)_2]^{+2}$ catalyzed rate (k_{Cu}) does not vary significantly (absence of cooperative effect between the metal and the buffer). These results indicate that these buffers maintain the appropriate pH without affecting the hydrolysis reaction rates.

Bifunctional buffers (general acid/general base), like phosphate and TMED, do not catalyze the hydrolysis reaction. Significant inhibition of the $[(dpa)Cu(OH_2)_2]^{+2}$ catalyzed hydrolysis of **MNTA** occurred with phosphate buffer (10 mM) and acetate buffer (10 mM). These results at pH 8.00 and 25°C are shown in Table 3.4. This inhibition is explained in the discussion.

Table 3.4 The effects of buffer in $[(dpa)Cu(OH)(OH_2)]^+$ (1 mM) catalyzed, hydrolysis of **MNTA** at pH 8 and 25°C.

Buffer	Conc mM	k_{obs}	Rel. Rate
NEM	10	7.3×10^{-4}	1.0
	40	9.0×10^{-4}	1.2
Na_2HPO_4	10	1.1×10^{-4}	0.15
$NaOCOCH_3$	10	8.2×10^{-5}	0.11
TMED	40	7.3×10^{-4}	1.0

Catalytic Turnover

The observation of pseudo-first order kinetics for several turnovers of $[(dpa)Cu(OH)(OH_2)]^+$ complex in buffered solution (NEM, 0.1N) containing an excess of **MNTA** (1 mM) confirms that the $[(dpa)Cu(OH)(OH_2)]^+$ complex (0.1 mM) functions catalytically at pH 8.00 and 25°C. Three turnovers for the reaction were observed at 490 nm. Figure 3.3 displays the relationship between the number of turnovers and time.

Table 3.5 Turnover number vs time for the $[(dpa)Cu(OH)(OH_2)]^+$ (0.1 mM) catalyzed hydrolysis of **MNTA** (1 mM).

Turnover	time (sec)
1	155
2	332
3	614

Figure 3.3 Plot of time vs Turnover number for the $[(dpa)Cu(OH)(OH_2)]^+$ catalyzed hydrolysis of **MNTA**.

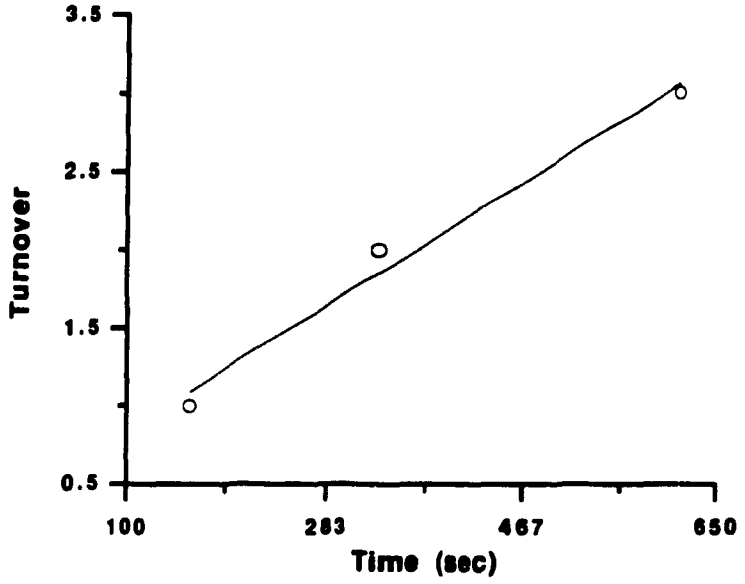

Figure 3.4 represents the typical change in the UV-vis spectrum during the $[(dpa)Cu(OH_2)_2]^{+2}$ (0.1 mM) catalyzed hydrolysis of **MNTA** (1 mM). The maximum change in absorbance was observed at 400 nm. This spectrum confirms the presence of the N-methyl-*p*-nitroanilide anion due to the hydrolysis reaction.

Figure 3.4 Absorbance spectra for the $[(dpa)Cu(OH_2)_2]^{+2}$ (0.1 mM, pH 8 and 25°C) catalyzed hydrolysis of **MNTA** (1 mM). The spectra were recorded at 30 second time intervals.

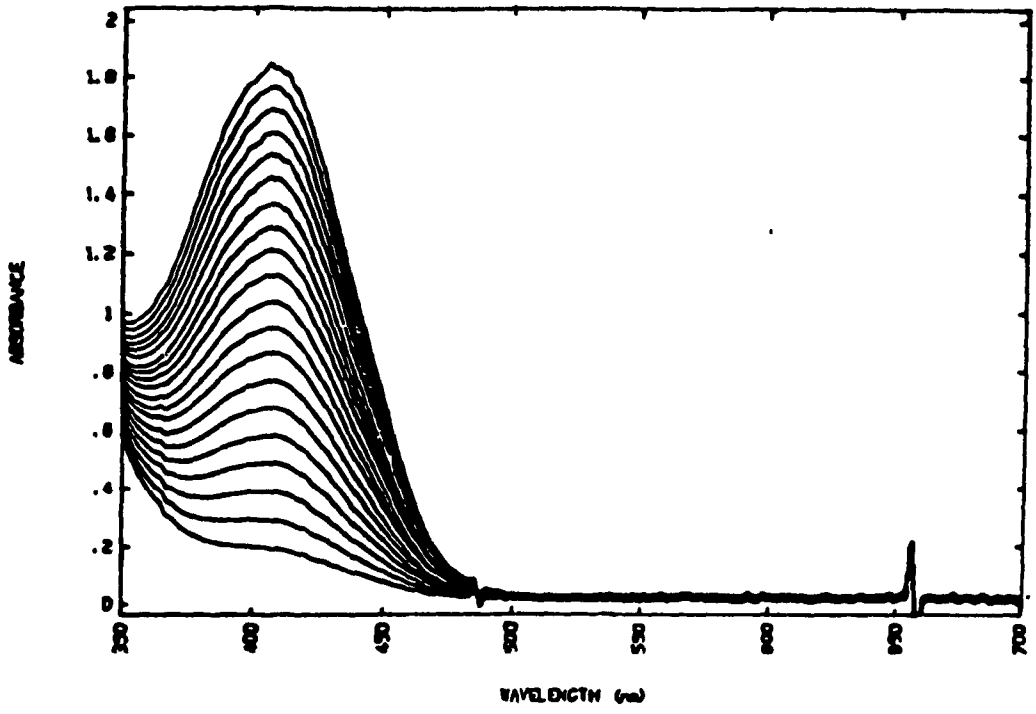

$[(neo)Cu(OH)(OH_2)]^+$ Catalyzed Hydrolysis of MNTA

A linear increase in the rate of the catalyzed hydrolysis of MNTA is observed with an increase in the concentration of $[(neo)Cu(OH)(OH_2)]^+$ at pH 8.00; Figure 3.5 displays this relationship. k_{obs} for this catalyst is 0.12 sec^{-1} M^{-1}.

Table 3.6 k_{obs} for the catalyzed hydrolysis of MNTA (0.1 mM) at different concentrations of $[(neo)Cu(OH)(OH_2)]^+$ at 25°C and pH 8.00.

Concentration mmol	k_{obs} (sec^{-1}) 10^{-4}	Relative Rate
0.0	1.6	1.0
0.5	2.0	1.3
1.0	3.4	2.1
2.0	4.8	3.0
3.0	6.1	3.8
4.5	6.8	4.3
5.0	7.8	4.9

Figure 3.5 Plot of k_{obs} vs concentration of $[(neo)Cu(OH)(OH_2)]^+$ for the catalyzed hydrolysis of MNTA.

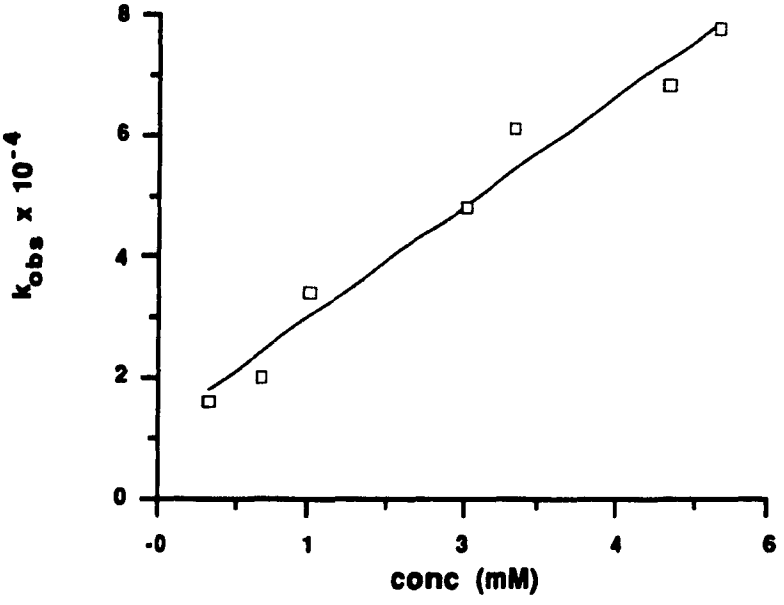

Cu(II) Complex Catalyzed Hydrolysis of NTA

The pH rate profiles for the catalyzed and uncatalyzed (hydroxide[50]) hydrolysis of NTA are displayed in Figure 3.6.

Table 3.7 k_{obs} for the $[(dpa)Cu(OH_2)_2]^{+2}$ (1 mM, 25°C) catalyzed hydrolysis of NTA (0.1 mM) at different pH's. The rate enhancement relative to the hydroxide rate, at the respective pH, is also shown.

pH	k_{obs} (sec^{-1})	$\log(k_{obs} \times 10^7)$	Rate Enhancement
6.50	2.9×10^{-5}	2.5	9.6
7.00	3.6×10^{-5}	2.6	
7.55	1.3×10^{-4}	3.1	6.0
8.00	1.6×10^{-4}	3.2	1.3
8.55	1.7×10^{-4}	3.2	0.66
9.05	1.9×10^{-4}	3.3	0.44
9.55	1.9×10^{-4}	3.3	

Figure 3.6 pH rate profiles for the hydroxide[50] (theoretical and experimental results)[50], and the $[(dpa)Cu(OH_2)_2]^{+2}$ catalyzed hydrolysis reactions of NTA.

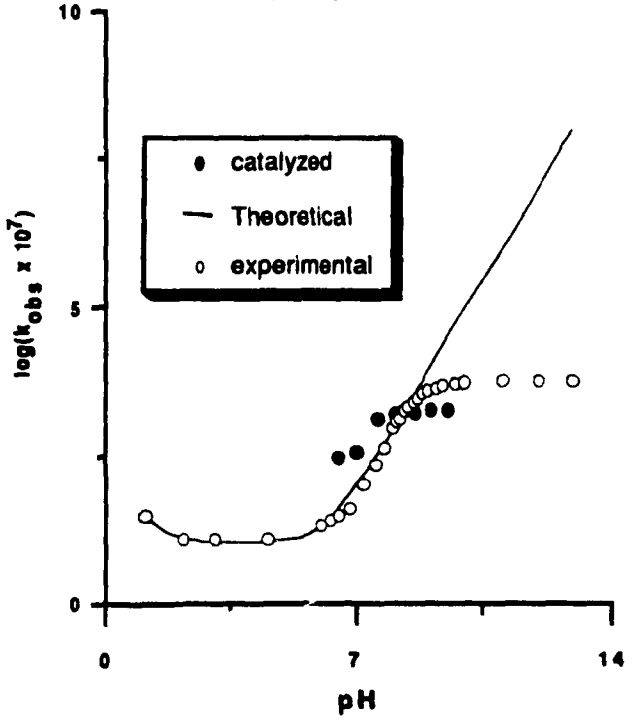

Due to the unusually low pKa of NTA, the $[(dpa)Cu(OH_2)_2]^{+2}$ catalyzed and uncatalyzed (experimental) hydrolysis rates reach a maximum around neutral pH where a plateau region forms (Figure 3.6). This ionization effect is more pronounced for the $[(dpa)Cu(OH_2)_2]^{+2}$ catalyzed reaction. This will be explained in greater detail in the discussion.

3.2 Metal-Buffer Cooperativity

Hydrolysis of an Activated Amide with a Poor Leaving Group

It is well known that amides with poor leaving groups may not have the same hydrolysis mechanism as that of amides with good leaving groups. This principle is examined in Cu(II) complex catalyzed hydrolysis reactions of the acyl-activated amide with a poor leaving group, *p*-methoxytrifluoroacetanilide (MTA), depicted below.

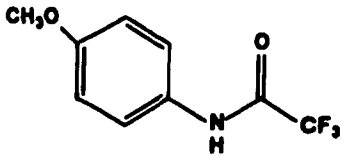

MTA

Figure 3.7 A UV scan displaying the **MTA** substrate disappearance at 270 nm, and the formation of the product, *p*-methoxyaniline, at 237 nm (in H_2O, pH 12).

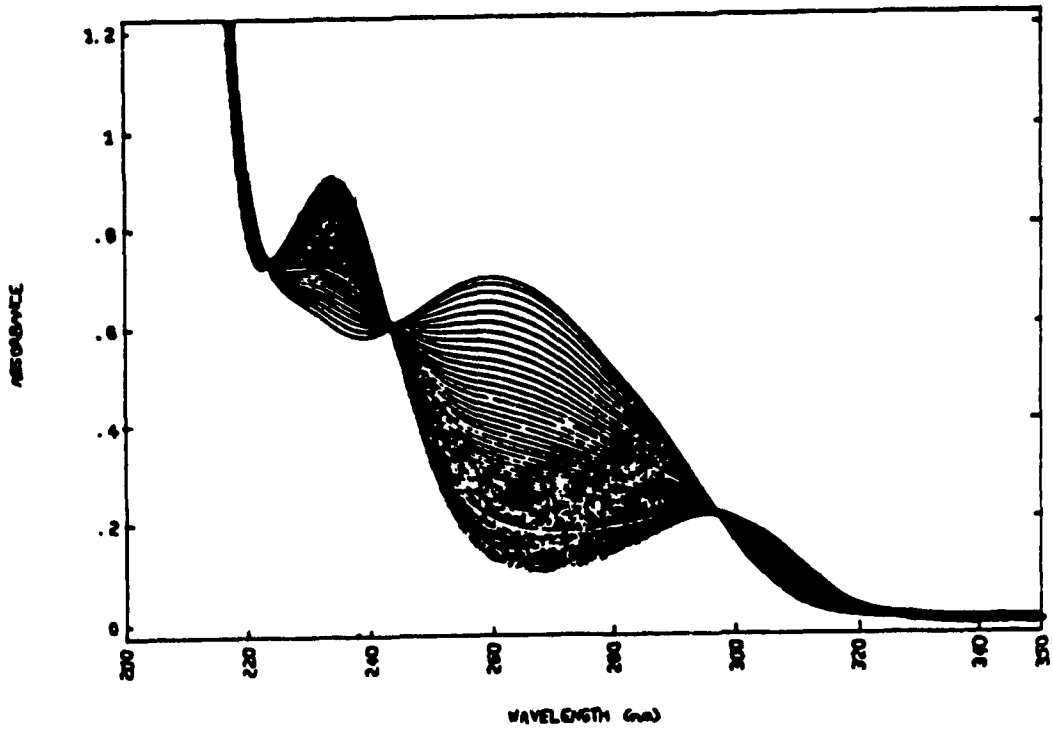

Difficulties in monitoring the reaction at the appropriate wavelength were encountered since Cu(II) complexes have significant absorbances between 200 and 350 nm.[58] In the presence of 0.3 mM Cu(II) complex, the ideal conditions to monitor a hydrolysis reaction are 50°C, pH 8, and 270 nm where the hydrolysis reaction is observed by measuring the absorbance change due to the decrease in the concentration of substrate (ε_{final} = 7414; where $\varepsilon_{final} = \varepsilon_{substrate} - \varepsilon_{product}$). The hydrolysis reactions are observed with $[(dpa)Cu(OH_2)_2]^{+2}$ and $[(dien)Cu(OH_2)]^{+2}$ since $[(terp)Cu(OH_2)]^{+2}$'s absorbance, at 270 nm, is too large to monitor a hydrolysis reaction.

The **MTA** hydrolysis reaction rates are much slower than those of the acyl-activated amides with good leaving groups (**NTA** and **MNTA**). The Cu(II) complex catalyzed hydrolysis reaction of **MTA** was monitored at 50°C and pH 8 where the $[(dpa)Cu(OH_2)_2]^{+2}$ complex is most effective. The pseudo-first order rate constants for $[(dpa)Cu(OH_2)_2]^{+2}$ catalyzed hydrolysis reactions were found with the non-complexing buffer NEM at concentrations between 10-50 mM, where high accuracy and reproducibility of the results were observed. The effects of the bifunctional buffers, acetate and phosphate, were not investigated since they were previously observed to inhibit amide hydrolysis reactions by binding to $[(dpa)Cu(OH_2)_2]^{+2}$ (Table 3.4).

To investigate metal-buffer cooperativity, the hydrolysis of **MTA** was followed at pH 8 and 50°C with a fixed concentration of $[(dpa)Cu(OH_2)_2]^{+2}$. Interestingly, Figure 3.8 shows that the rate of hydrolysis of **MTA** is more sensitive to the buffer in the presence of the metal complex than in its absence. The addition of equal amounts of the complex (0.3 mM) to a 10, 20, 30, 40, and 50 mM NEM solution results in a 1.3, 1.6, 1.5, 1.7, and a 1.9 fold rate increase respectively, over the buffer catalyzed rate. In contrast, the monoaqua complex $[(dien)Cu(OH_2)]^{+2}$ does not give any rate enhancement.

The $[(dpa)Cu(OH_2)_2]^{+2}$-buffer cooperativity effect is explained in mechanistic detail in the discussion.

Table 3.8 k_{obs} for the $[(dpa)Cu(OH_2)_2]^{+2}$ catalyzed hydrolysis of **MTA** at pH 8 and 50°C. The rate enhancement with respect to the uncatalyzed (buffer) reaction is also displayed.

NEM Conc mM	(sec^{-1}) k_{cat}	k_{uncat}	Rate enhancement
10	2.7×10^{-5}	3.5×10^{-5}	1.3
20	3.0×10^{-5}	4.9×10^{-5}	1.6
30	5.2×10^{-5}	7.7×10^{-5}	1.5
40	5.5×10^{-5}	9.3×10^{-5}	1.7
50	7.4×10^{-5}	1.4×10^{-4}	1.9

Figure 3.8 Plot of k_{obs} vs buffer concentration for the $[(dpa)Cu(OH_2)_2]^{+2}$ catalyzed, and buffer mediated (uncatalyzed), hydrolysis reaction of MTA at pH 8 and 50°C.

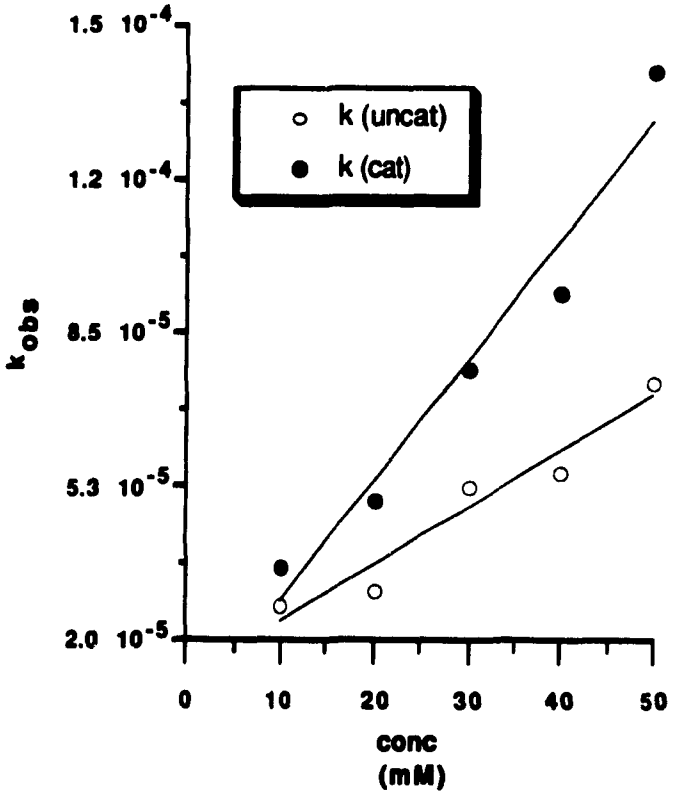

3.3 Hydrolysis of Unactivated Amides

The Cu(II) complex catalyzed hydrolysis of unactivated amides with poor leaving groups, N-methylformamide (**MFA**) and formamide (**FA**), were studied by ^1H NMR. Due to the difficulties associated with monitoring the reaction at 100°C (high temperature, and unusually large water peak in ^1H NMR), detailed mechanistic studies were difficult to perform. Figure 3.9 depicts the observed changes in signal intensity with respect to time for the $[(dpa)Cu(OH_2)_2]^{+2}$ catalyzed hydrolysis of **MFA** at 100°C. Figure 3.10 displays the plot of time vs change in signal intensity for this reaction.

The pD rate profiles for the $[(dpa)Cu(OH_2)_2]^{+2}$ catalyzed hydrolysis reactions of **MFA** and **FA** are shown in Figure 3.11 and Figure 3.12 respectively. The curves were fitted using the same equation and curve fitting program used for the activated amides. The values for k_2, (the rate constant for the hydrolysis reaction catalyzed by the aqua-hydroxy Cu(II) species), and K_a (the first dissociation constant for the Cu(II) complex) are displayed with the respective pD rate profiles.

The pD rate profiles and the pKa of the $[(dpa)Cu(OH_2)_2]^{+2}$ complex (7.3 in D_2O) imply that the active species in the catalyzed hydrolysis reaction is the aqua-hydroxy Cu(II) complex. $[(dpa)Cu(OH_2)_2]^{+2}$ gave a significant rate enhancement for the hydrolysis of **FA** whereas $[(terp)Cu(OH_2)_2]^{+2}$ gave no observable rate enhancement (Table 3.9).

Table 3.9 The observed reaction rates for the hydroxide and the $[(dpa)Cu(OH_2)_2]^{+2}$ (10 mM) catalyzed hydrolysis reactions of **FA** and **MFA** (at pD 8.00 and 100°C).

Substrate	k_{obs} (sec^{-1})		Rate Enhancement
	$[(dpa)Cu(OH_2)_2]^{+2}$	hydroxide	
Formamide	1.7×10^{-5}	1.0×10^{-7}	170
N-methylformamide	7.3×10^{-6}	7.4×10^{-7}	99

Figure 3.9 $[(dpa)Cu(OH)(OH_2)]^+$ (10 mM, pD 8.00 and 100°C) catalyzed hydrolysis of **MFA** (10 mM) at: a) T = 0 hrs; b) T = 40 hrs; c) T = 81 hrs; d) T = 130 hrs. An increase in the product's methyl peak [δ = 2.58] is followed by a decrease in the substrate's aldehyde and methyl peaks [δ = 8.08, δ = 2.75]. This is shown with respect to tetramethylammonium fluoride [δ = 3.18].

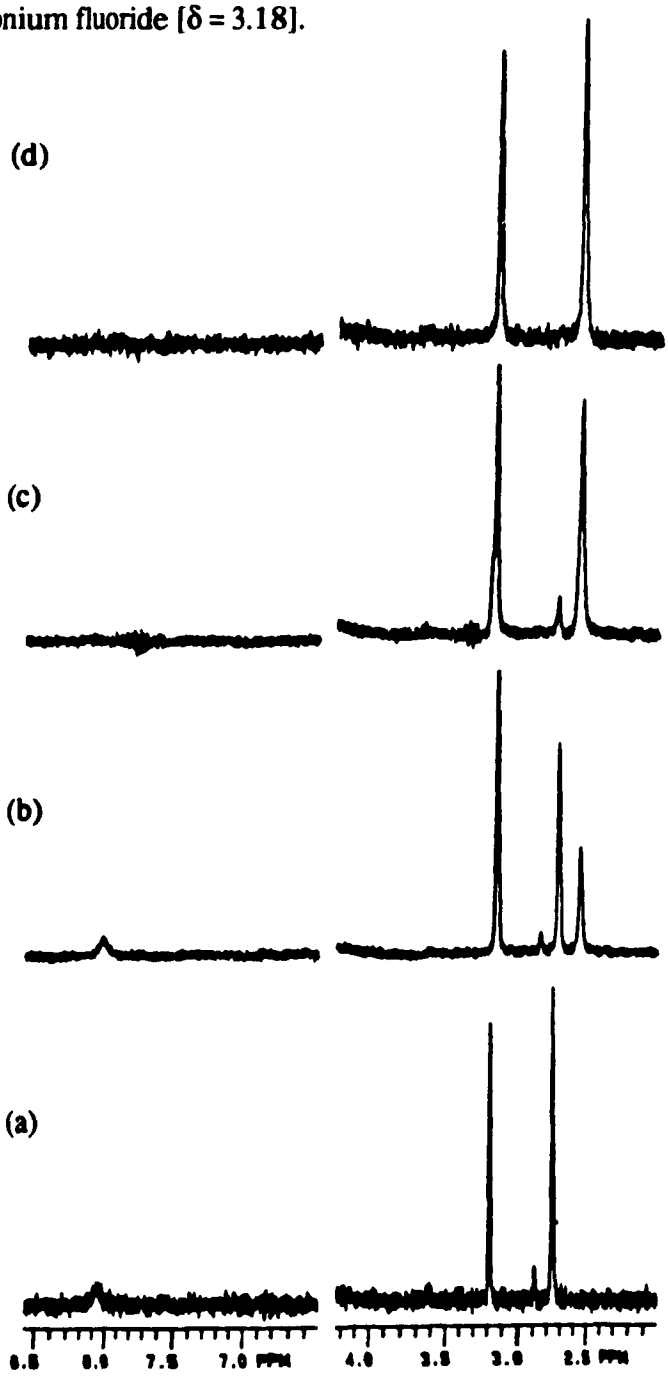

Table 3.10 $[(dpa)Cu(OH_2)_2]^{+2}$ (10 mM, 100°C) catalyzed hydrolysis of **MFA** (10 mM) at pD 8.00.

time (hrs)	ln(A/Ao)
24.0	-0 79
40.0	-1.40
59.0	-2.00
81.0	-2.60
105	-2.90

Figure 3.10 Time vs ln (A/Ao) of the methyl signal for the $[(dpa)Cu(OH_2)_2]^{+2}$ catalyzed hydrolysis of **MFA** at pD 8.00.

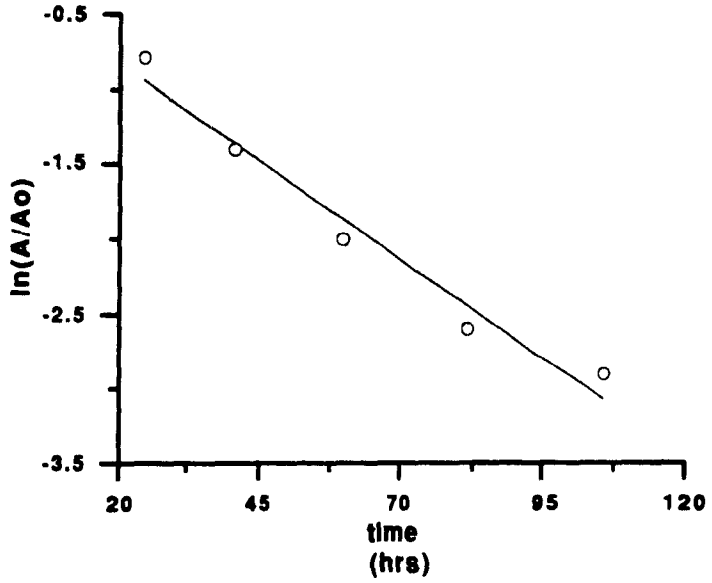

Table 3.11 $[(dpa)Cu(OH_2)_2]^{+2}$ (10 mM, 100°C) catalyzed hydrolysis of MFA (10 mM) at varying pD (pD = pH + 0.4)[52].

pD	$\log(k_{obs})$ (hrs^{-1})	k_{obs} (hrs^{-1})
5.90	-1.72	0.0189
6.50	-1.67	0.0214
6.95	-1.60	0.0249
7.50	-1.56	0.0277
8.00	-1.58	0.0264
8.50	-1.56	0.0276

Figure 3.11 pD rate profile for the $[(dpa)Cu(OH_2)_2]^{+2}$ catalyzed hydrolysis of MFA. For the pD rate profile the calculated values are k_2=2.8 x10^{-2} sec^{-1}, K_a=2.8 x10^{-7}.

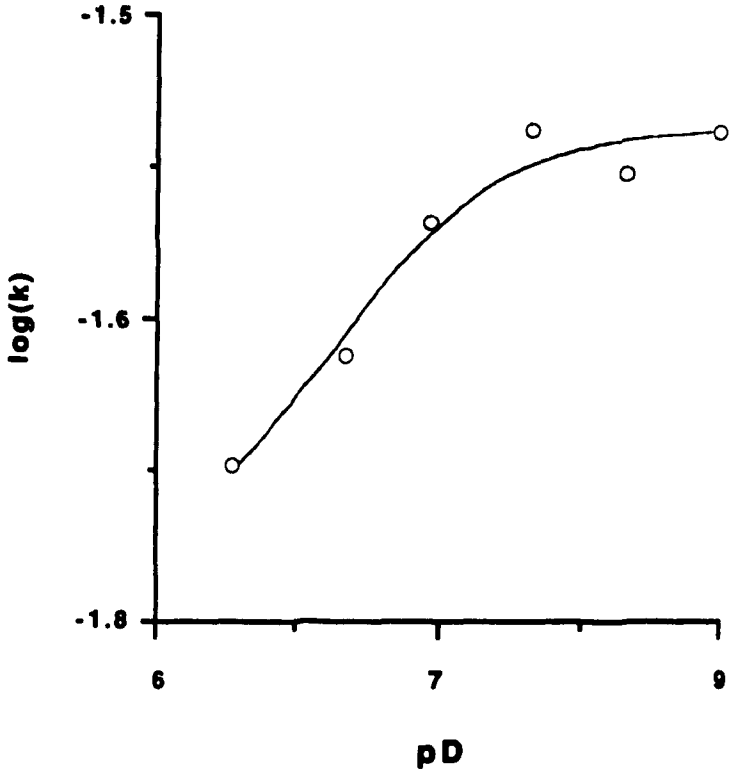

Table 3.12 $[(dpa)Cu(OH_2)_2]^{+2}$ (10 mM, 100°C) catalyzed hydrolysis of **FA** (10 mM) at varying pD.

pD	$\log(k_{obs})$ (hrs^{-1})	k_{obs} (hrs^{-1})
6.00	-1.71	0.0195
6.50	-1.40	0.0403
7.00	-1.37	0.0430
7.50	-1.26	0.0546
8.00	-1.22	0.0607

Figure 3.12 pD rate profile for the $[(dpa)Cu(OH_2)_2]^{+2}$ catalyzed hydrolysis of **FA**. For the pD rate profile the calculated values are $k_2=5.8 \times 10^{-2}$ sec^{-1}, $K_a=5.3 \times 10^{-7}$.

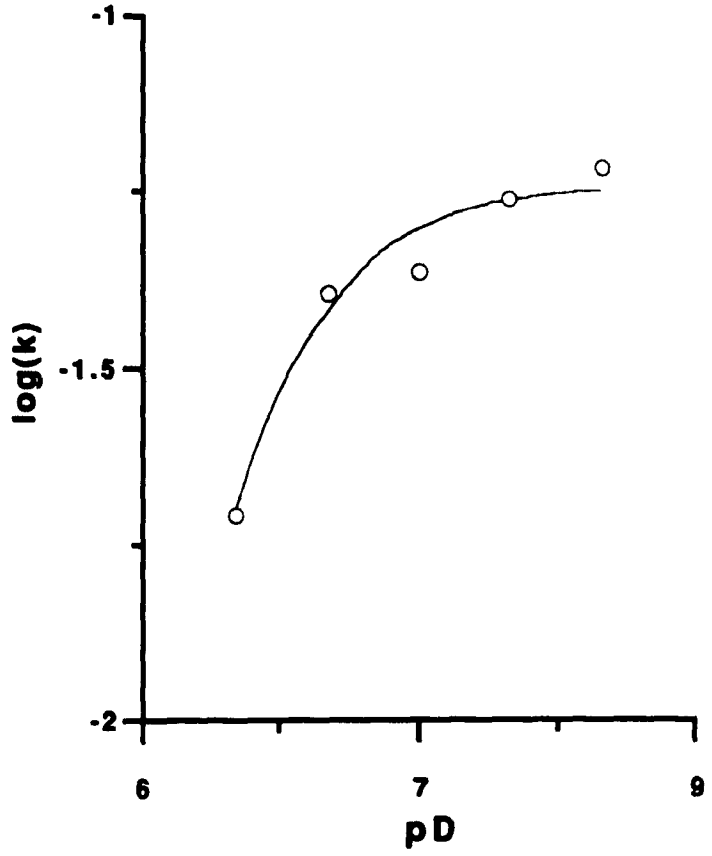

3.4 ^{31}P NMR Binding Studies

Investigating how substrates bind to metal complexes can give valuable insight into metal complex catalyzed hydrolysis reaction mechanisms.[54a-d] Since the phosphorus center of the disodium salt of phenylphosphonic acid closely resembles the tetrahedral intermediate formed during amide hydrolysis, it was chosen for binding studies.

^{31}P NMR is a valuable tool which helps assign the geometry of the phosphorus center in metal-phosphate chelates. Therefore, it is convenient to use ^{31}P NMR to study the interaction between diaqua metal complexes and the disodium salt of phenylphosphonic acid. Since Cu(II) is paramagnetic the Co(III) complexes of tren and trpn were used for these binding studies.

The disodium salt of phenylphosphonic acid binds to one equivalent of $[(trpn)Co(OH_2)_2]^{+3}$ in a bidentate fashion (Figure 3.13(a); 40.0 ppm), whereas with one equivalent of $[(tren)Co(OH_2)_2]^{+3}$ several species are observed (Figure 3.13(b); 10.5, 23.0, 24.0, 28.3, 29.2, 32.6 ppm). These peaks are free substrate (10.5 ppm), the monodentate Co(III) complex $[(tren)Co(OH_2)(ArPO_3)]^{+2}$ (23.0 and 24.0 ppm for the isomers), and other non-specific species.

Therefore, the disodium salt of phenylphosphonic acid binds completely to $[(trpn)Co(OH_2)_2]^{+3}$ whereas it only binds partially to $[(tren)Co(OH_2)_2]^{+3}$.

Figure 3.13 ^{31}P NMR of the disodium salt of phenylphosphonic acid with one equivalent of a) $[(trpn)Co(OH_2)_2]^{+3}$ b) $[(tren)Co(OH_2)_2]^{+3}$ (at 50 mM, 25°C, pD 6.5).

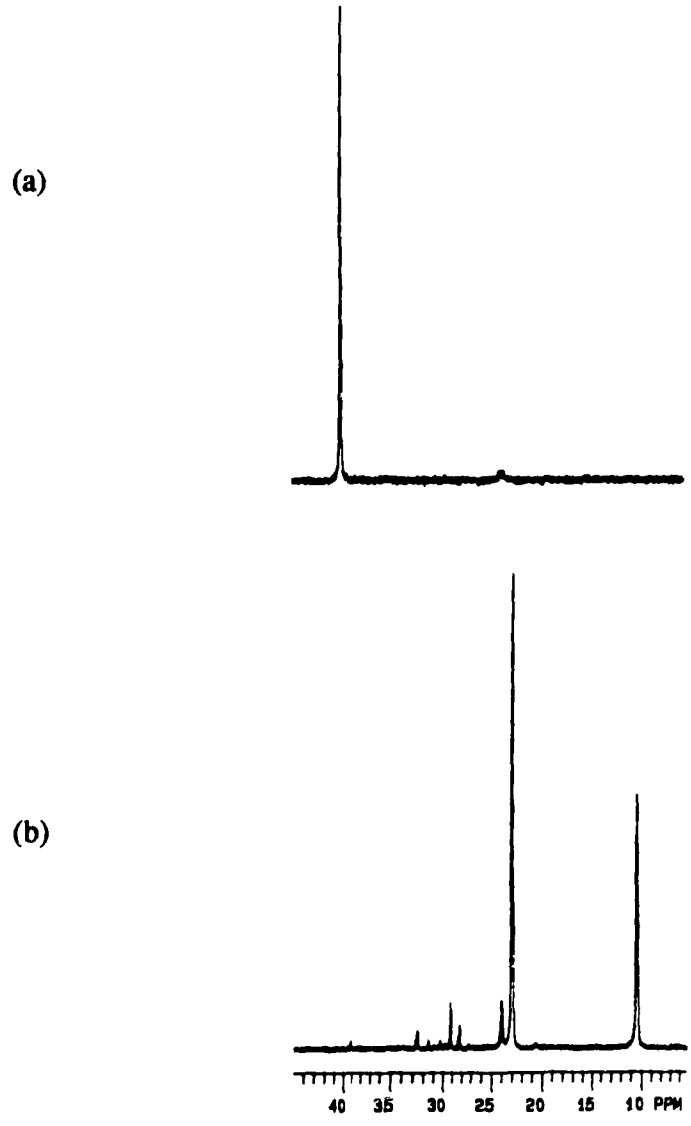

4. Discussion

4.1 Cu(II) Complexes

The paramagnetic, non-spherical Cu(II) metal ion has been intensively investigated for its unique chemical characteristics and its diverse biological roles.[55] Cu(II) metal complexes are known to have distinct stereochemistries such as square planar, square pyramidal, trigonal bipyramidal, or more commonly, distorted octahedral where the complex has four short bonds coplanar with the metal and two weakly bound water molecules in the axial positions. The reactivity of distorted octahedral Cu(II) complexes is similar to that of low spin d^8 square planar complexes. Evidence for this stems from Cu(II)'s labile nature where its characteristic rapid ligand exchange is in the order of 10^8 $M^{-1}sec^{-1}$. In addition, observed decreases in the rate of ligand exchange, with increased steric bulk of the ligand, indicates that Cu(II) complexes have a tendency to undergo bimolecular displacement reactions.[55]

To determine the structural requirements of a catalyst capable of hydrolyzing amides, the efficiencies of the diaqua complexes $[(dpa)Cu(OH_2)_2]^{+2}$ (**2**) and $[(neo)Cu(OH_2)_2]^{+2}$ (**10**), were compared to that of the monoaqua complexes $[(dien)Cu(OH_2)]^{+2}$ (**11**) and $[(terp)Cu(OH_2)]^{+2}$ (**3**).

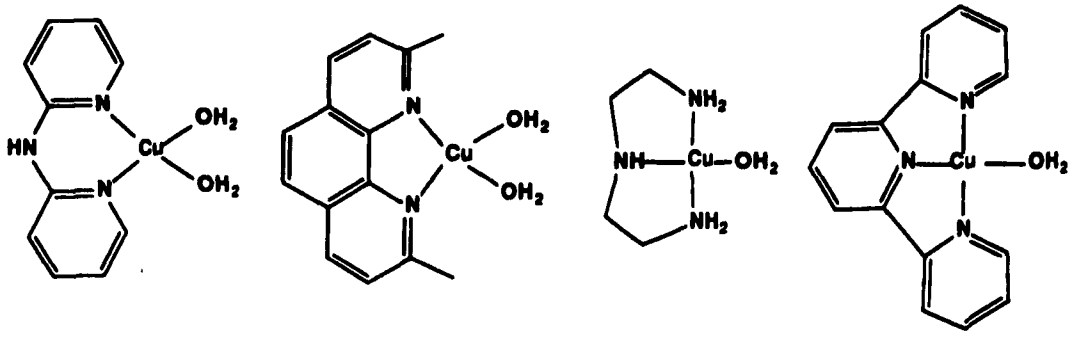

2 **10** **11** **3**

In solution, these four complexes have square planar geometries. The Cu(II) diaqua complexes (**2** and **10**) were observed to be effective catalysts for the hydrolysis of both activated and unactivated amides. The important equilibria in these complexes are the acid dissociation equilibria of the coordinated water molecules. This is displayed in Scheme 4.1.

Scheme 4.1

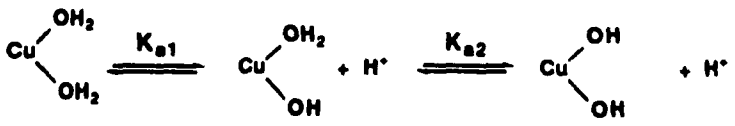

where

$$K_{a1} = \frac{[H^+]\ [Cu(OH)(OH_2)]^+}{[Cu(OH_2)_2]^{+2}} \qquad \text{Eq. (1)}$$

The metal increases the acidity of the coordinated water molecules. The value of pK_{a1} (7-8) is in between the pKa value of a free water molecule (15.7) and that of a hydronium ion (-1.7). pK_{a2} is too large to be measured experimentally. The pKa values can measure nucleophilicity. For instance, hydroxide ion is a stronger nucleophile than Cu-OH which in turn is a stronger nucleophile than water.[55,56]

These complexes can exist in their diaqua, aqua-hydroxy, and dihydroxy forms. In general cis diaqua Cu(II) complexes can form dimers.

(**2**) easily forms dimers at concentrations greater than 10 mM.[57,58] In contrast, (**10**) has two methyl groups *ortho* to the coordinating nitrogens which increases its steric bulk, and therefore prohibits the formation of dimers. The total catalyst concentration present in solution is the sum of the different species that the catalyst can form : [49,57,58]

$$[LiCu]_T = [LiCu(OH_2)_2]^{+2} + [LiCu(OH)(OH_2)]^+ + [LiCu(OH)_2] + [LiCu(OH)]_2^{+2} \qquad \text{Eq. (2)}$$

where $[LiCu]_T$ is the total catalyst concentration present in solution and Li is the ligand.

Scheme 4.2 shows the three paths by which an amide is hydrolyzed in solution. The amide (A) can be hydrolyzed by the diaqua copper complex, the aqua-hydroxy copper species, or by a water molecule.

Scheme 4.2

$$[LICu(OH_2)_2]^{+2} + A \xrightarrow{k_1} P$$

$$[LICu(OH)(OH_2)]^{+} + A \xrightarrow{k_2} P$$

$$H_2O + A \xrightarrow{k_3} P$$

The rate law for the hydrolysis of the amide is:

$$rate = (k_1 [LICu(OH_2)_2]^{+2} + k_2 [LICu(OH)(OH_2)]^{+} + k_3)[S] \qquad \text{Eq. 3}$$

where [S] is the concentration of the amide substrate. If we rearrange **Eq.1** we get:

$$[LICu(OH_2)_2]^{+2} = \frac{[H^+]\ [LICu(OH)(OH_2)]^{+}}{K_{a1}} \qquad \text{Eq. 4}$$

Rearranging **Eq.2** and taking into consideration that between pH 6 and 8.5 the concentrations of the dihydroxy species and, the concentration of the dimer (at low catalyst concentrations 0.1 mM-10 mM), are insignificant, we get **Eq. 5**:[57,58]

$$[LICu]_T - [LICu(OH_2)_2]^{+2} = [LICu(OH)(OH_2)]^{+} \qquad \text{Eq. 5}$$

The diaqua term in **Eq. 5** can be rewritten using **Eq. 4** to give **Eq. 6**:

$$[LICu]_T - \frac{[H^+]\ [LICu(OH)(OH_2)]^{+}}{K_{a1}} = [LICu(OH)(OH_2)]^{+} \qquad \text{Eq. 6}$$

Rearranging **Eq.6**, we get **Eq. 7**:

$$\frac{K_{a1}[LICu]_T}{K_{a1} + [H^+]} = [LICu(OH)(OH_2)]^+ \qquad \textbf{Eq. 7}$$

Between the pH range of interest, the reactions catalyzed by the diaqua Cu(II) complex (k_1) and the water catalyzed rate (k_3) are insignificant. Therefore, substituting **Eq. 4** and **Eq. 7** into **Eq. 3** (rate) we get **Eq. 8**:

$$\frac{rate}{[S]} = k_2 \cdot \frac{K_{a1}[LICu]_T}{K_{a1} + [H^+]} \qquad \textbf{Eq. 8}$$

The logarithm of the pseudo first order rate constant, k_{obs}, is shown in **Eq. 9** below. The pH rate profiles for the Cu(II) catalyzed hydrolysis of amides (Figures 3.1, 3.2, 3.9, and 3.10) were fit according to this equation.

$$\log k_{obs} = \log\left[\frac{k_2 K_{a1}}{K_{a1} + [H^+]}\right] \qquad \textbf{Eq.9}$$

4.2 Hydrolysis of Activated Amides

The Cu(II) catalyzed hydrolysis reactions of acyl-activated amides with good leaving groups and unactivated amides with poor leaving groups were investigated. To understand the structural requirements of a catalyst capable of hydrolyzing these amides effectively, it is critical to first understand the mechanism of the uncatalyzed reaction.

Base Catalyzed Amide Hydrolysis

Detailed mechanistic studies on the hydrolysis of acyl-activated amides were performed by Schowen.[30-32] Substituted trifluoro-N-methylacetanilides were the substrates studied. Scheme 4.3 displays a simplistic hydrolysis scheme for these amides. The electron-withdrawing group (CF_3) facilitates hydroxide attack and the tetrahedral intermediate (**T1**, Scheme 4.3) is quickly formed. Depending on the pH, decomposition of **T1** to products is catalyzed by either a water molecule (k_2), or a hydroxide ion (k_3), or both.

Scheme 4.3

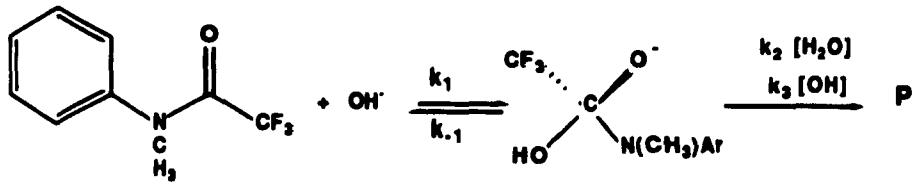

T1

Using the steady state assumption for **T1**, k_{obs} is :[30c]

$$k_{obs} = k_1 [OH] \left[\frac{k_2 + k_3 [OH]}{k_{-1} + k_2 + k_3 [OH]} \right] \qquad \textbf{Eq.10}$$

At low pH, $k_{-1} >>> k_2$ (**T1** prefers to revert back to starting material), and $k_2 > k_3$. Therefore, **Eq. 10** reduces to :

$$k_{obs} = \frac{k_1}{k_{-1}} \cdot k_2 [OH]$$

if $(k_1/k_{-1}) = K$ then: $k_{obs} = K\ k_2\ [OH]$ **Eq. 11**

At intermediate pH values $k_{-1} > k_3[OH]$, and $k_3[OH] > k_2$ thus k_{obs} becomes second order with respect to hydroxide concentration:

$$k_{obs} = \frac{k_1}{k_{-1}}\ k_3\ [OH]^2 = K k_3 [OH]^2 \qquad \textbf{Eq. 12}$$

At high pH, $k_3 >> k_{-1}$ and the term in brackets in **Eq. 10** approaches unity. k_{obs} reduces to:

$$k_{obs} = k_1\ [OH] \qquad \textbf{Eq. 13}$$

A change in the rate limiting step of the reaction, with a change in pH, implies that the reaction is multi-step as opposed to concerted.[30c,33] At low pH the hydrolysis reaction is first order with respect to hydroxide ion (**Eq. 11**). The rate determining step is the water catalyzed breakdown of **T1** to products (k_2, Scheme 4.3). At intermediate pH, the hydrolysis rate law is second order (**Eq. 12**). The rate determining step is the hydroxide catalyzed breakdown of **T1** (k_1, Scheme 4.3). At high pH the second step is so fast that the first step, formation of **T1** (k_3, Scheme 4.3), becomes the rate determining step. The observed rate has become first order with respect to hydroxide concentration (**Eq.13**).[30c,33]

To determine how **T1** is converted to products, through C-N bond cleavage and proton transfer steps, it is important to study the hydrolysis reaction at low hydroxide concentration where the rate limiting step is known to be the breakdown of **T1** to products. Under these conditions the mechanism for the breakdown of **T1** depends on the basicity of the leaving group. The pK_a of the doubly protonated leaving group determines the mechanism of the hydrolysis reaction.[30-32] A large pK_a indicates a leaving group capable of bearing a positive charge while a small pK_a indicates a leaving group capable of bearing a negative charge.[32] For trifluoro-N-methylacetanilides with poor leaving groups (electron donating groups attached to the anilide ring, $pK_a > 5$, Scheme 4.4A) the rate limiting step is proton transfer thereby forming a dianion (**T2**, Scheme 4.4A). C-N bond cleavage, which follows, is fast due to the driving force of the two alkoxides (**T2**).[30a-d,33]

Conversely, for trifluoro-N-methylacetanilides with good leaving groups (electron withdrawing groups on the anilide ring, $pK_a < 5$, Scheme 4.4B) the lifetime of the C-N bond in **T1** is so short that it cleaves prior to proton transfer.[30-33] Therefore, rate limiting C-N bond cleavage is followed by rapid intermolecular proton transfer.

Scheme 4.4

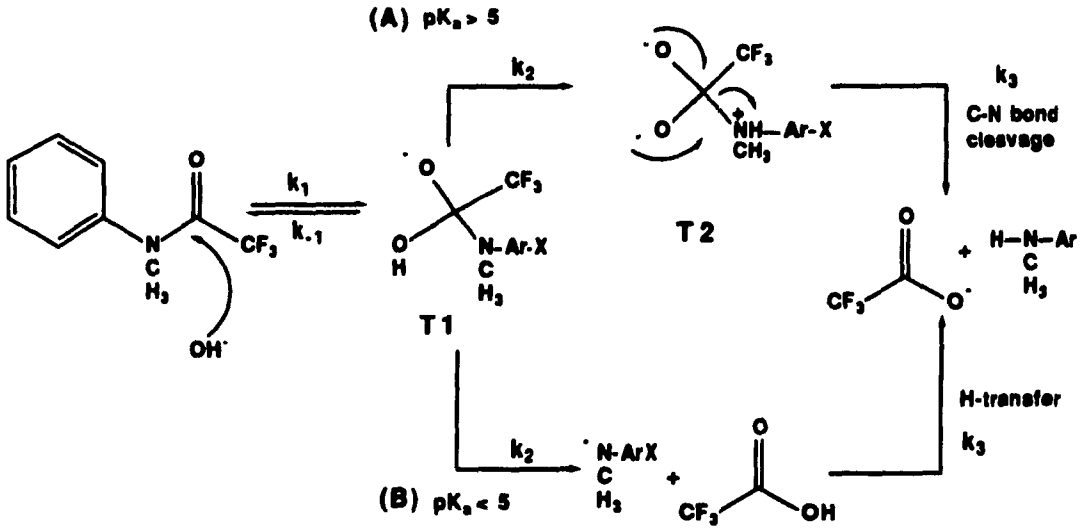

It is well known that proton transfer and C-N bond cleavage are two distinct steps in the breakdown mechanism of **T1** to products. Scheme 4.5 displays the possible transition state structures for the buffer catalyzed breakdown of **T1**. If proton transfer occurs prior to C-N bond cleavage then, theoretically, two transition states are possible in general acid catalyzed breakdown of **T1**. Firstly, if proton transfer is not the rate limiting step then 100% proton transfer occurs between **BH** and the leaving group in the transition state (Scheme 4.5C, **T3**). This implies that the amide is present as a zwitterionic intermediate in a transition state where proton transfer is fast and reversible (**T3**). Secondly, if proton transfer is the rate limiting step then only partial proton transfer between **BH** and the leaving group in the transition state (Scheme 4.5D, **T4**) occurs. **B** stabilizes this activated complex and the nitrogen carries only a partial positive charge (**T4**)[32]. **BH** is a GAC (general acid catalyst) and diffusion apart between **B** and the fully protonated amide becomes the rate limiting step. Electron donating substituents on the ring increase the reaction rate by increasing the electron density on the nitrogen, and by decreasing the C-N bond distance in **T1** thereby decreasing the basicity of the hydroxide in **T1**. This increases the extent of proton transfer in **T4** (**T4** is stabilized) and a faster reaction rate is observed.[30 a-d,32]

Scheme 4.5

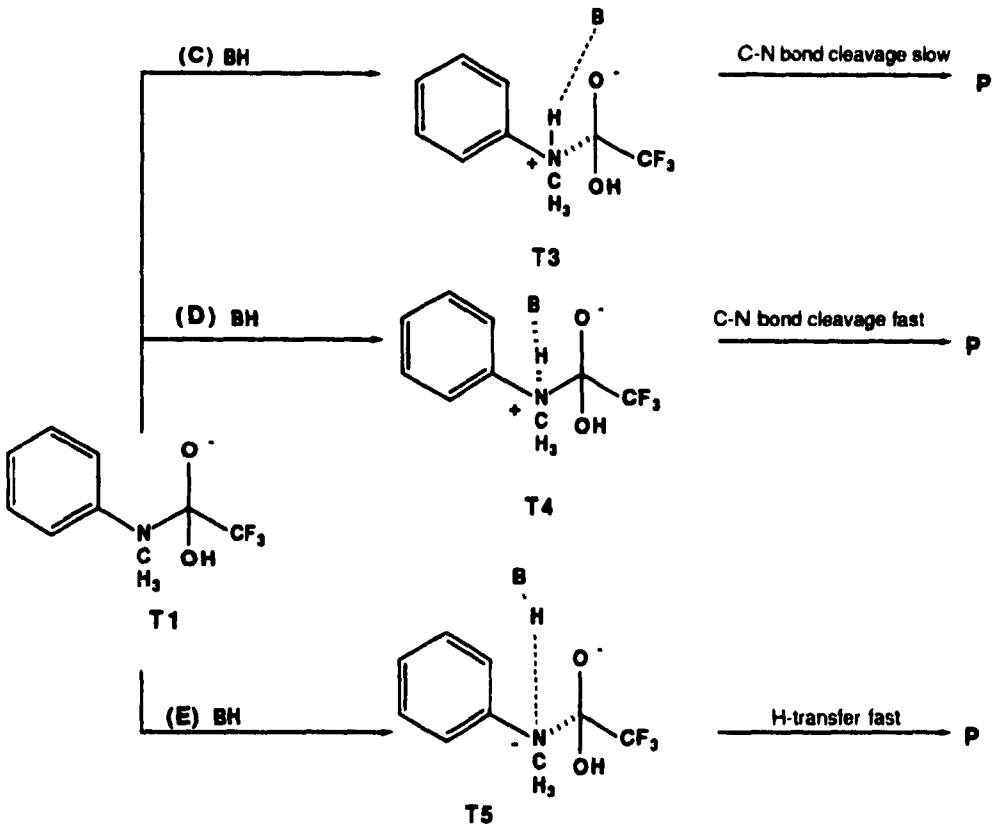

For the hydrolysis of amides with poor leaving groups ($pK_a > 5$, Scheme 4.4A) kinetic solvent isotope effects and the presence of buffer catalysis demonstrated that proton transfer is indeed the rate limiting step followed by rapid C-N bond cleavage. General acid (GAC), and general base (GBC) catalysis by buffers (**BH**) can facilitate the breakdown of **T1** to products. Thus, **T4** Scheme 4.5D displays the correct transition state for GAC breakdown of **T1** for amides with poor leaving groups.[30a-d,33]

For the hydrolysis of amides with good leaving groups ($pK_a < 5$, Scheme 4.4B), where the first step in the breakdown of **T1** to products is rate limiting C-N bond cleavage, the nitrogen in the transition state carries a partial negative charge (Scheme 4.5E, **T5**). Electron withdrawing substituents on the anilide ring will decrease the electron density on the nitrogen. This results in a lower energy transition state and an increased hydrolysis rate. The effect of a catalyst (**BH**) is minimal because it can only weakly hydrogen bond to the nitrogen in the transition state.

Cu(II) Complex Catalyzed Hydrolysis of Activated Amides with Good Leaving Groups

The structures of the two acyl-activated amides with good leaving groups which are studied, **MNTA** (trifluoro-N-methyl-*p*-nitroacetanilide) and **NTA** (*p*-nitrotrifluoroacetanilide), are displayed below.

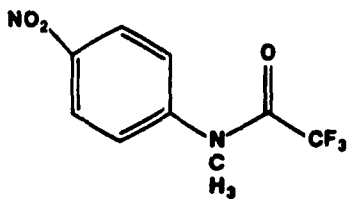

MNTA

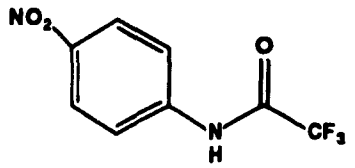

NTA

For **MNTA** and **NTA** the pKa for the doubly protonated leaving group is 0.5 and 1.0 respectively.[30c] These trifluoroacetanilides with good leaving groups have electron withdrawing groups in the anilide ring which increases the lability of the C-N bond. Since C-N bond breaking is the rate limiting step in the hydrolysis of activated amides with good leaving groups (pKa < 5, Scheme 4.4**B**), these amides possess higher hydroxide hydrolysis rates than those of their non-substituted counterparts.

Cu(II) Complex Catalyzed Hydrolysis of MNTA

For the hydrolysis of **MNTA**, between pH 1 and 4, the water catalyzed hydrolysis rate is observed ($k_{H2O} = 2 \times 10^{-7}$ sec^{-1}).[50] Above pH 4 the hydroxide catalyzed hydrolysis rate increases linearly with an increase in pH (Figure 3.1, uncatalyzed reaction).

Diaqua Cu(II) complexes (**2** and **10**) are efficient at catalyzing the hydrolysis of **MNTA** between pH 6.5 and 8.5. The pseudo first order rate constants for the hydrolysis of **MNTA** catalyzed by $[(dpa)Cu(OH_2)_2]^{+2}$ (**2**) and $[(neo)Cu(OH_2)_2]^{+2}$ (**10**), at pH 8.0 and 25°C, are 7.3×10^{-4} sec^{-1} and 3.4×10^{-4} sec^{-1} respectively (Table 3.1). A 4 and 2 fold rate enhancement over the uncatalyzed (hydroxide) rate (1.8×10^{-4} sec^{-1}) is achieved. The catalytic turnover time for (**2**) is about 229 sec (Table 3.5). The hydrolysis of **MNTA** is very sensitive to pH[50] and a larger rate enhancement is observed at pH 7 (Table 3.2).

For (2) catalyzed hydrolysis of **MNTA**, a 14 fold rate enhancement is observed at pH 7 whereas only a 4 fold rate enhancement is observed at pH 8.

Since (**10**) does not dimerize a linear increase in the amide's hydrolysis rate is observed with an increase in the concentration of (**10**) (1-5 mM; Table 3.6). The second order rate constant for (**10**) catalyzed hydrolysis of **MNTA** is 0.12 sec^{-1} M^{-1}.

Detailed mechanistic studies for the hydrolysis of **MNTA** were performed with $[(dpa)Cu(OH_2)_2]^{+2}$ (**2**) . In the presence and in the absence of (**2**), at pH 8 and 25°C, the addition of non-complexing buffers (NEM, CHES, MES) gave no observable rate enhancements. Furthermore, phosphate, TMED, and acetate buffers which are known to behave like general acid/general base catalysts, do not increase the (k_{OH} = 1.8 x 10^{-4})[50] hydrolysis rate at pH 8 and 25°C (Table 3.4).

For $[(dpa)Cu(OH_2)_2]^{+2}$ (**2**) catalyzed hydrolysis of **MNTA**, between pH 6.5 and 8.5, kinetic solvent isotope effects (KIE) were less than two (Table 3.3B). pKa_1 of (**2**) in H_2O and D_2O is 7.2 and 7.3 respectively. This difference in pKa_1 gives a small equilibrium isotope effect since Cu-OD is a stronger nucleophile than Cu-OH. This effect is minimized above pH 8 since the complex exists mostly in its aqua-hydroxy form (in both H_2O and D_2O).

For the hydrolysis of **MNTA**, the monoaqua complexes $[(terp)Cu(OH_2)]^{+2}$ (**3**) and $[(dien)Cu(OH_2)]^{+2}$ (**11**) gave no rate enhancements (Table 3.1). The simplest mechanisms accounting for the difference in reactivity between the diaqua and monoaqua complexes are shown in Scheme 4.6 below.

Based on the pKa of the copper coordinated water molecule (pKa= 7.2 for **2**; pKa= 8.0 for **10**) and the pH rate profile for the hydrolysis of **MNTA** catalyzed by (**2**) (Figure 3.1, catalyzed reaction) we propose that the aqua-hydroxy species is the active form of the catalyst. Two mechanisms for (**2**) catalyzed hydrolysis of **MNTA** are possible. The first mechanism involves intramolecular general base catalyzed attack of a water molecule to the coordinated amide followed by rate determining intramolecular general acid catalyzed C-N bond cleavage (Scheme 4.6**A**). The second mechanism involves intramolecular metal-hydroxide attack on the coordinated amide followed by rate determining C-N bond cleavage (Scheme 4.6**B**).

It is unlikely that the mechanism in Scheme 4.6**A** is correct since C-N bond cleavage of **MNTA** does not require a proton transfer step.[30-32] Furthermore, the kinetic isotope effect for (**2**) catalyzed hydrolysis of **MNTA** is insignificant (KIE = 1.4 at pH 8.5, Table 3.3B).

Scheme 4.6

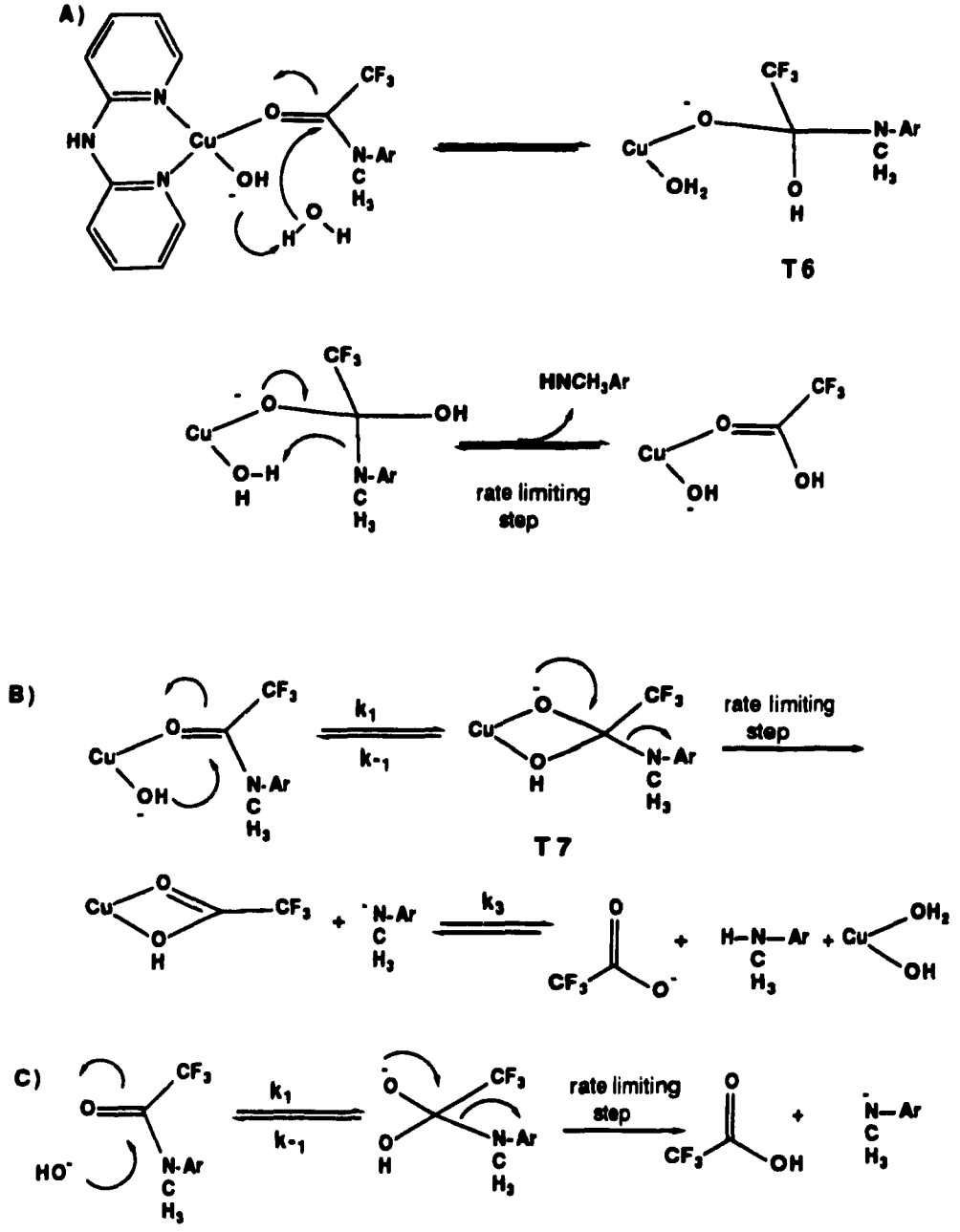

Except for the involvement of the Cu(II) complex, the mechanism in Scheme 4.6**B** is essentially the same as that for the hydrolysis of trifluoroacetanilides with good leaving groups (Scheme 4.4**B**; Scheme 4.6C). Between pH 6.8 and 8.5 the Cu-OH is the most effective nucleophile since its nucleophilicity is higher than that of water, and its concentration exceeds that of the hydroxide ion.[56,57] Scheme 4.6**B** shows Lewis acid activation of the carbonyl oxygen followed by intramolecular metal-hydroxide attack to form **T7**. At neutral pH, T7 prefers to revert back to starting material (pKa of the metal-

hydroxide is between 10 and 15 whereas that of N-methyl-*p*-nitroanilide is greater than 27)[59a,b] and the breakdown of **T7** is the rate limiting step. Breakdown of **T7** occurs by rate limiting C-N bond cleavage followed by rapid proton transfer (similar to Scheme 4.4**B**).

Metal complexes are known to increase reaction rates by either trapping intermediates or by stabilizing (or bypassing) the transition states leading to products.[55c,61] One way to increase the rate of amide hydrolysis would be to stabilize the tetrahedral intermediate (**T1**, Scheme 4.4) thereby increasing its steady state concentration. Indeed, due to the formation of **T7** diaqua Cu(II) complexes efficiently catalyze the hydrolysis of **MNTA** (Scheme 4.6**B**).

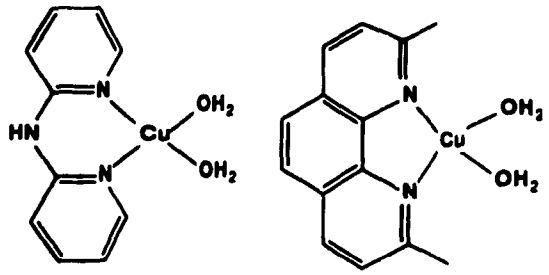

2 **10**

The observed pseudo first order catalyzed rate constant for 5 mM $[(neo)Cu(OH_2)_2]^{+2}$ (**10**) is comparable to that of 1 mM $[(dpa)Cu(OH_2)_2]^{+2}$ (**2**) (Table 3.2 and 3.6). The difference in catalytic efficiency between (**2**) and (**10**) is related to the ease of formation of **T7**. (**2**) can form **T7** more effectively than (**10**) since it has a larger bond angle opposite the four-membered ring. This relationship has been previously observed for Co(III) complexes.[25]

In addition, inhibition by acetate and phosphate buffer, at pH 8.0 and 25°C (Table 3.4), demonstrates (**2**)'s preference for bidentate coordination. The crystal structure for (**2**) bound to acetate in a four-membered ring has been reported.[63]

Mechanistic kinetic studies of diaqua Cu(II) complex catalyzed hydrolysis of **MNTA** favors the bifunctional mechanism displayed in Scheme 4.6**B**. C-N bond cleavage is the rate limiting step in the breakdown path of **T7**.

Cu(II) Complex catalyzed Hydrolysis of NTA

The mechanism for **NTA** hydrolysis is the same as that for **MNTA**. However, **NTA** differs from **MNTA** in that the former has a titratible proton (pKa = 8.2). Scheme

4.7 displays the ionization of the amidic nitrogen. The anionic form of NTA is resistant to hydrolysis.

Scheme 4.7

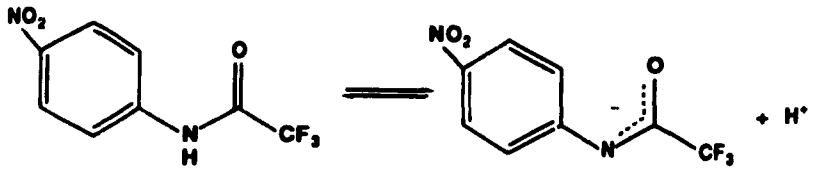

As in MNTA hydrolysis, the water rate predominates between pH 2 and 4 (k_{H2O}=1.2 x 10^{-6} sec^{-1}).[50] Above pH 4, the rate of hydrolysis of NTA increases with an increase in pH but levels off at pH 8.2. The pH dependence of NTA hydrolysis is given by: [50]

$$k_{Corr} = k_{obs}\left\{1 + \frac{Ka}{[H]}\right\} \quad \text{where} \quad k_{obs} = k_1[OH]\left[\frac{k_2 + k_3[OH]}{k_{-1} + k_2 + k_3[OH]}\right]$$

where Ka is the acid dissociation constant for NTA. For k_1, k_{-1}, k_2, and k_3 see equation 10 and Scheme 4.3 in Section 4.2.

$[(dpa)Cu(OH_2)_2]^{+2}$ (2) increases the rate of the hydrolysis of NTA between pH 6.5 and 8.00. (Figure 3.6). Below pH 8 the mechanism for $[(dpa)Cu(OH_2)_2]^{+2}$ (2) catalyzed hydrolysis of NTA and MNTA is the same. However, above pH 8 the copper complex decreases the rate of hydrolysis of NTA. This inhibitory effect is likely due to the coordination of the anionic amide nitrogen to the copper complex. The inactive form of the complex, with NTA, is displayed below. Rate limiting C-N bond cleavage is not facilitated by coordination of the leaving amine to a metal complex since RN-Metal is known to be a worse leaving group than RNH.[56]

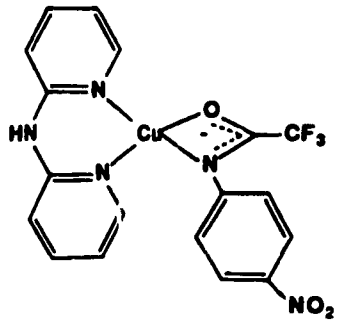

Therefore, an effective amide-cleaving diaqua Cu(II) complex should not bind to the amidic nitrogen of the amide substrate.

4.3 Metal-Buffer Cooperativity

Cu(II) Complex Catalyzed Hydrolysis of an Activated Amide with a Poor Leaving Group (MTA)

It is well known that enzymes facilitate chemical reactions by multifunctional catalysis. The active site of metallopeptidases such as carboxypeptidase, thermolysin, and enkaphalinase contains zinc and, acidic and basic functional groups. The cooperative interactions between the metal and the acidic and basic functional groups is responsible for the enzyme's efficient peptidase activity.

Interesting enzyme models in which the amide bond is hydrolyzed through cooperative interactions between a metal ion and a buffer have been designed and studied. However, in the model systems, the amide is permanently attached to the metal. Some models also include attached acid/base groups which help catalyze the hydrolysis reaction.

Buckingham, Keene, and Sargeson[19] have observed the effects of phosphate buffer in the metal-hydroxide mediated hydrolysis of an amide bond in cis-$[(en)_2Co(OH)(glyglyOC_3H_7)]^+$ (Scheme 4.8). At pH 7.0 and 0.1 M phosphate buffer, a 10^{10} rate enhancement over the uncatalyzed hydrolysis of glycylglycine was observed. Scheme 4.8 displays the possible roles of phosphate buffer.

Scheme 4.8

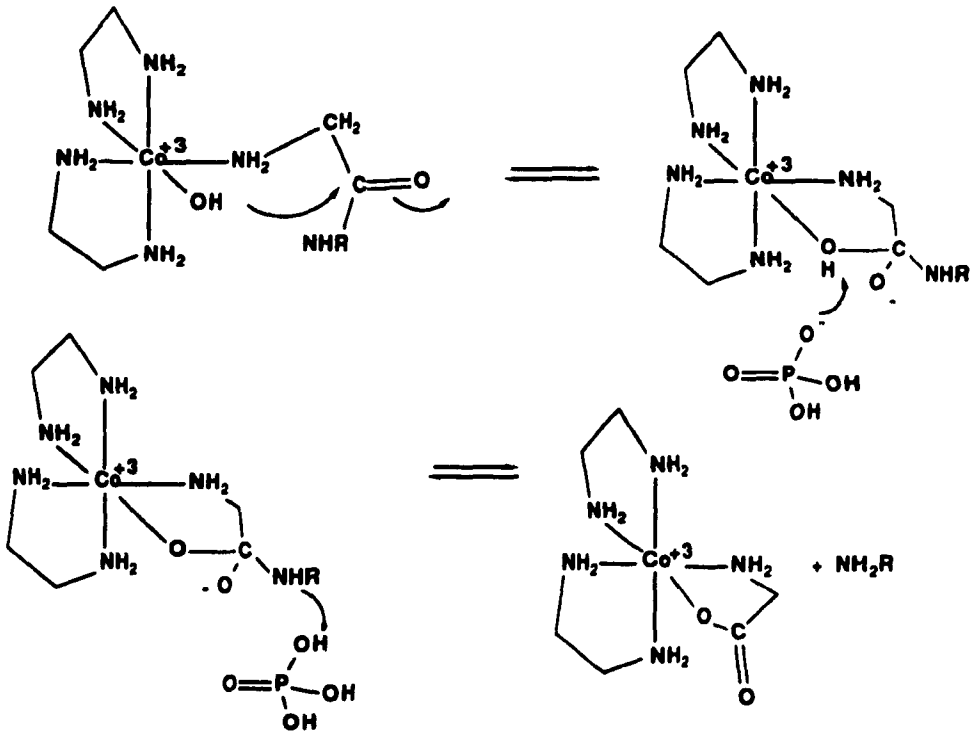

The rate limiting step for the intramolecular reaction in Scheme 4.8 is believed to be deprotonation of the metal-hydroxyl group after its attack onto the carbonyl carbon. Phosphate is believed to facilitate this step. At neutral pH phosphate can act as either a GBC (deprotonating the hydroxyl group) or as a GAC (protonating the leaving amine group, Scheme 4.8).

Intramolecular general acid catalysis by a phenol group and intramolecular catalysis by a carboxyl group was attempted in enzyme models proposed by Breslow[45] (Scheme 4.9**A**) and Groves[44] (Scheme 4.9**B**) respectively. A 50 fold increase in the rate of amide hydrolysis due to the phenol in model **A** was observed whereas a 30 fold increase was observed due to the carboxyl in model **B**.[44,45]

Scheme 4.9

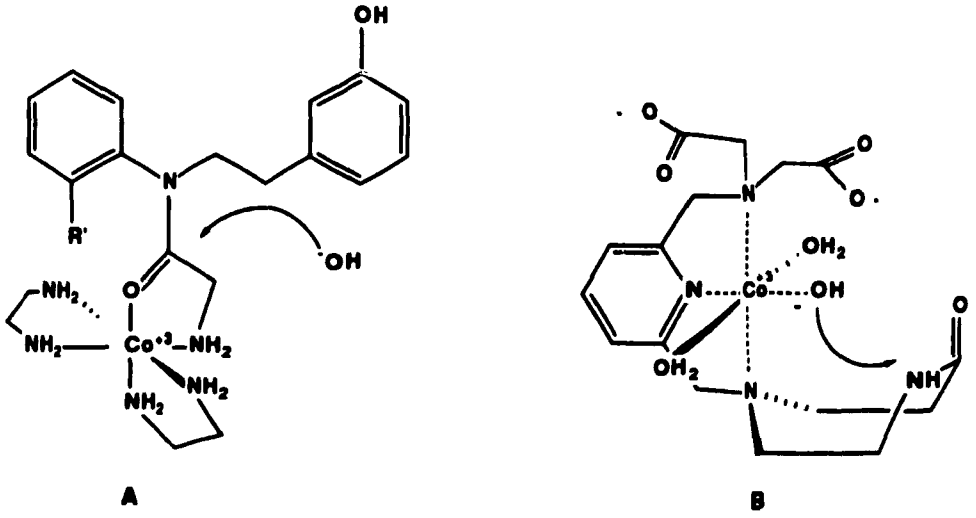

Although valuable lessons can be learned from studies involving intramolecular catalysis, the mechanism for the corresponding intermolecular catalyzed reaction may be different. To investigate metal-buffer cooperativity in a free amide hydrolysis reaction, **MTA** was chosen as the amide substrate. The mechanism for the base hydrolysis of **MTA** differs from that of **MNTA** and **NTA**. Since the pKa of the doubly protonated leaving group of **MTA** is greater than 5, it follows the hydrolysis mechanism displayed in Scheme 4.4**A** where the rate limiting step is proton transfer in **T1**. Rapid C-N bond cleavage follows in **T2** to form products.

The amidic nitrogen in **MTA** has a pKa of 9.65.[30a-d] Unlike **NTA**, the amidic nitrogen does not ionize at neutral pH. At pH 8 and 25°C the hydrolysis of **MTA** is much slower than that of **NTA** and **MNTA**. Since $[(dpa)Cu(OH_2)_2]^{+2}$ (**2**) was found to be the best catalyst for the hydrolysis of **NTA** and **MNTA**, it was chosen for mechanistic studies

of Cu(II) complex catalyzed hydrolysis of **MTA**. The hydrolysis reactions were observed only with (**2**) and $[(dien)Cu(OH_2)]^{+2}$ (**11**) since $[(terp)Cu(OH_2)]^{+2}$ (**3**)'s absorbance, at 270 nm, is too large to monitor a reaction.

Interestingly, both hydroxide and (**2**) catalyzed hydrolysis of **MTA** are buffer catalyzed (Table 3.8). This implies that in both reactions proton transfer is the rate limiting step. (**2**) effectively catalyzes the hydrolysis of **MTA** whereas the monoaqua complex $[(dien)Cu(OH_2)]^{+2}$ gives no observable rate enhancement. In view of our experimental results for (**2**) catalyzed hydrolysis of amides with good leaving groups, we propose a simple mechanism explaining these buffer effects.

Scheme 4.10

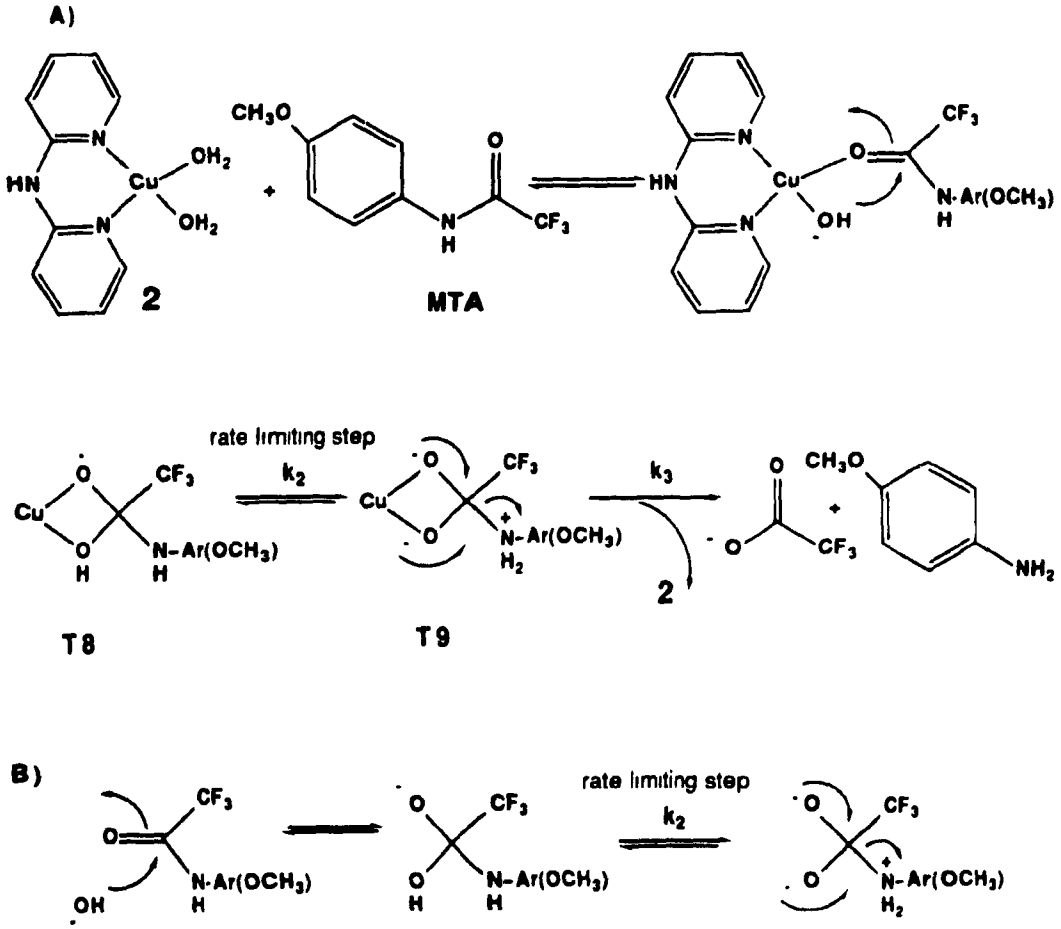

Except for the involvement of the Cu(II) metal the mechanism in Scheme 4.10**A** is identical to that shown in Scheme 4.4**A** and Scheme 4.10**B**. Similar to (**2**) catalyzed

hydrolysis of NTA and MNTA, Lewis acid activation of the carbonyl carbon is followed by metal-hydroxide attack forming the tetrahedral intermediate **T8**. Except for the leaving group **T8** is identical to **T7** in Scheme 4.6**B**. Rate limiting proton transfer occurs to form the zwitterionic intermediate **T9**. Rapid C-N bond cleavage in **T9** leads to products.

When cooperativity occurs between a copper complex and a buffer in an amide hydrolysis reaction, the overall rate constant is given by:

$$k_{obs} = k_{H2O} + k_{Cu}\,[Cu] + k_B\,[B] + k_S\,[B]\,[Cu]$$

or

$$k_{obs} = (k_B + k_S\,[Cu]\,)\,[B] + (k_{H2O} + k_{Cu}\,[Cu]\,)$$

where k_{H2O} is the water mediated hydrolysis rate constant, k_{Cu} is the copper complex catalyzed rate constant, k_B is the buffer catalyzed rate constant, and k_S is the rate constant due to the cooperative effect of the buffer and the catalyst. A plot of k_{obs} vs [B] has a slope equal to $(k_B + k_S\,[Cu]\,)$ and a y intercept equal to $(k_{H2O} + k_{Cu}\,[Cu]\,)$. If a cooperative effect is not present then the slope would be equal to k_B, the rate of the buffer catalyzed reaction.

Figure 3.8 displays the plots of k_{obs} vs [B] for both the buffer catalyzed (slope = 1.2×10^{-3} sec^{-1} M^{-1}) hydrolysis reaction and $[(dpa)Cu(OH_2)_2]^{+2}$ (**2**)-buffer catalyzed (slope = 2.5×10^{-3} sec^{-1} M^{-1}) hydrolysis of **MTA**. The difference in slope between the two plots clearly indicates that NEM and (**2**) cooperate in the catalyzed hydrolysis of **MTA**. $k_B = 1.2 \times 10^{-3}$ sec^{-1} M^{-1}, and $k_S = 4.5$ sec^{-1} M^{-2}.

The addition of equal amounts of (**2**) (0.3 mM) to a 10, 20, 30, 40, and 50 mM NEM solution results in a 1.3, 1.6, 1.5, 1.7 and a 1.9 fold rate increase respectively, over the buffer catalyzed rate (Table 3.8) for the hydrolysis of **MTA** at pH 8 and 50°C. Other than in enzymic systems, such cooperativity between metal and buffer in free amide hydrolysis has not been previously observed.

At pH 8 the non-complexing buffer, NEM (pKa = 7.67), is present in solution in its basic and conjugate acid forms shown below.

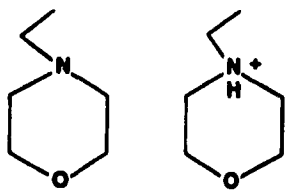

We propose that NEM (**BH,B**) acts as either a GBC or a GAC, or both, facilitating the rate determining proton transfer step in Scheme 4.10. The possible roles of NEM are shown in Scheme 4.11.

Scheme 4.11

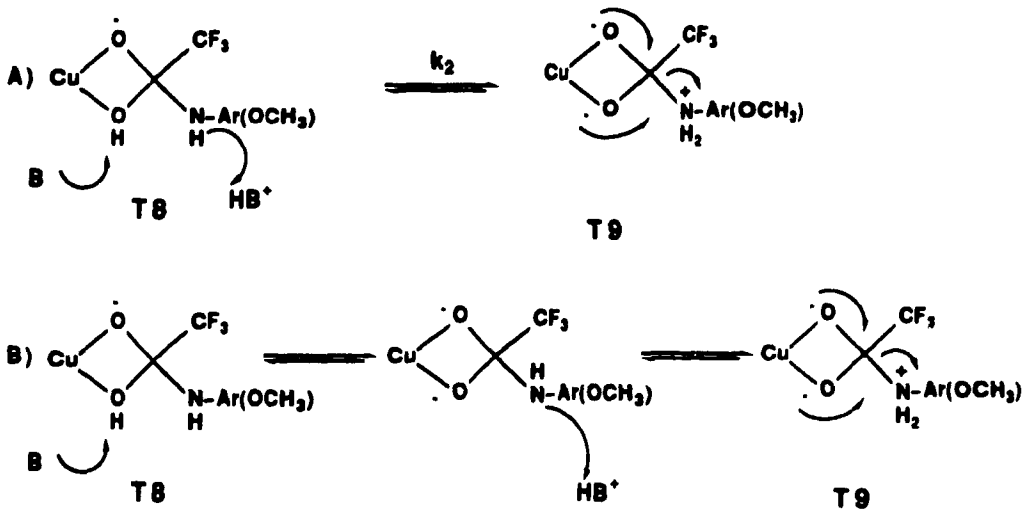

Scheme 4.11A shows concerted GAC/GBC by two NEM species present in solution at pH 8. The anionic tetrahedral intermediate **T8** is converted to the zwitterionic intermediate **T9** in one step. Scheme 4.11**B** shows a stepwise process where NEM first deprotonates **T8** to form an unstable intermediate. NEM then protonates this intermediate to form the most reactive intermediate **T9**. Scheme 4.11**C** displays the possible participations of an external water molecule in a stepwise or concerted reaction. NEM is shown as a GBC/GAC, deprotonating or protonating an external water molecule.

4.4 Hydrolysis of Unactivated Amides

Few true catalysts exist which are efficient at cleaving unactivated amides.[46a] This has been partly due to the stability of the amide bond, and to the lack of a sensitive assay capable of detecting small increases in the rate of amide hydrolysis.[28] Recently, the pseudo first order rate constant for the hydrolysis of a tripeptide, at neutral pH and room temperature, was measured to be 3×10^{-9} sec^{-1}. This corresponds to a half-life of about seven years.[28] Since peptide substrates have a tendency to auto-hydrolyse and cyclize, the Cu(II) complex catalyzed hydrolysis of the simple unactivated amides, formamide (**FA**) and N-methylformamide (**MFA**), were studied. **FA** and **MFA** were chosen because of their lack of reactivity (k_{OH} for **FA** is 3.1×10^{-8} at 100°C, and k_{OH} for **MFA** is 1.5×10^{-9} at 44°C)[53], and for their availability. The study of simple metal complex catalyzed reactions of unactivated amides can give valuable information on the mechanism of action of peptide cleaving proteins, and on the principles of catalysis.

$[(dpa)Cu(OH_2)_2]^{+2}$ (**2**), which was found to be effective in catalyzing the hydrolysis of activated amides, gives large rate enhancements for the hydrolysis of **FA**. The first order rate constants, at 100°C, for (**2**) catalyzed hydrolysis of **FA** and **MFA** are 1.7×10^{-5} sec^{-1} and 7.3×10^{-6} sec^{-1} respectively. This corresponds to a rate enhancement of 170 and 99 respectively over the hydroxide rate at pH 8 and 100°C (Table 3.9).

Similar to the catalyzed hydrolysis of activated amides, the diaqua complex $[(dpa)Cu(OH_2)_2]^{+2}$ (**2**) was found to be more efficient than the monoaqua complex $[(terp)Cu(OH_2)]^{+2}$ (**3**).

For the unactivated amides the simplest mechanism that could account for the difference in reactivity between the two complexes is displayed in Scheme 4.12 below, where R = H, CH_3. The pD rate profiles (Figure 3.11 and 3.12) and the pKa of the complex (7.3 in D_2O) indicate that the reactive form of the catalyst is the aqua-hydroxy species.

Scheme 4.12

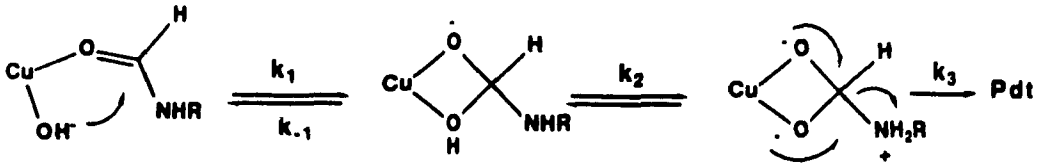

T10 T11

Except for the involvement of the metal the mechanism in Scheme 4.12 is identical to that shown in Scheme 4.4A, for the hydrolysis of acyl-activated amides with poor leaving groups (pKa> 5). The pKa for the leaving groups of **FA** and **MFA** are 9.2 (NH_4^+) and 10.6 ($CH_3NH_3^+$) respectively.[59a,64] One way to accelerate the reaction would be to stabilize **T2** (Scheme 4.4A) thereby increasing its steady state concentration. This is achieved by the formation of **T10.**

For the hydroxide catalyzed hydrolysis of acyl-activated amides with poor leaving groups (pKa > 5) proton-transfer is the rate limiting step.[30a-d,31,32] In Scheme 4.12 **T10** reverts back to starting materials ($k_{-1} > k_2$), therefore breakdown of **T10** to products is the rate determining step (pKa of the attacking metal-hydroxide is between 10 and 15 whereas for ammonia it is about 35).[64] Cu(II) catalyzed hydrolysis of unactivated amides with poor leaving groups has a mechanism similar to that shown in Scheme 4.8A and Scheme 4.8B where proton transfer is the rate limiting step, followed by rapid C-N bond cleavage.

Recently, Guthrie[30e] has proposed similar tetrahedral intermediates for the base catalyzed hydrolysis of the tertiary amide N,N,-dimethyl-*p*-toluamide, at 100°C. A stepwise reaction mechanism is proposed where rate limiting hydroxide attack produces an anionic intermediate **T12.** Oxygen labelling experiments and KIE studies have shown that water mediated proton switch in **T12** gives an anionic zwitterion **T13.** This is followed by C-N bond cleavage.[30e] This is shown in Scheme 4.13 below.

Scheme 4.13

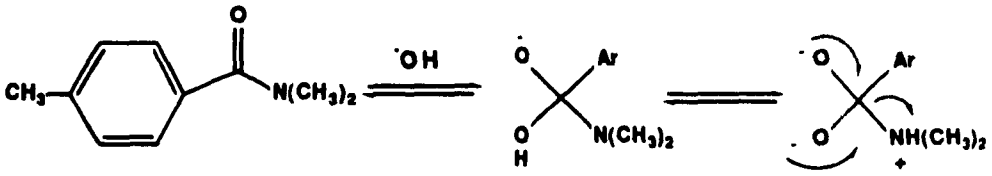

T12 **T13**

T12 and **T13** have short lifetimes since they are interconverted by proton transfers. **T12** is the thermodynamically preferred form of the tetrahedral intermediate. The lifetime of the C-N bond in **T12** has been estimated to be between 2×10^{-9} sec and 2×10^{-8} sec whereas for **T13** the estimated C-N bond's lifetime is 3×10^{-11} sec.[30e]

In theory the metal ion can catalyze the hydrolysis of amides through two kinetically indistinguishable mechanisms. The first is the Lewis acid mechanism involving direct substrate activation (Scheme 4.14A). Following nucleophilic attack, the tetrahedral intermediate formed has a coordinated metal to the alkoxide. This diminishes the basicity of the alkoxide oxygen, without greatly decreasing its nucleophilicity, and this facilitates expulsion of the leaving group.[56] This Lewis acid activation mechanism can therefore

increase the rate of hydrolysis. The second mechanism is the metal-hydroxide mechanism involving water activation (Scheme 4.14**B**). Thirdly, we have proposed a combination of the Lewis acid and the metal-hydroxide mechanisms (Scheme 4.14C). The structural requirements of a catalyst obeying mechanism C have been elucidated by comparing the catalytic efficiencies of $[(dpa)Cu(OH_2)_2]^{+2}$ (**2**) and $[(terp)Cu(OH_2)]^{+2}$ (**3**) in the hydrolysis of activated and unactivated amides.

Scheme 4.14

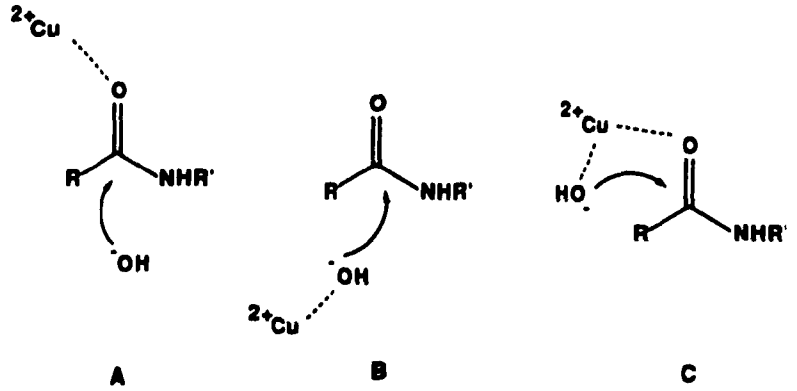

If mechanism **A** or **B** is more efficient than **C** then (**2**) and (**3**) should have comparable reactivities for hydrolyzing amides. However, (**2**) has been shown to be over two orders of magnitude more efficient than (**3**) in the hydrolysis of both activated and unactivated amides (Table 3.1 and 3.11). This difference in reactivity cannot be due to any steric effects for (**3**) since it is slightly more reactive than (**2**) in hydrolyzing *p*-nitrophenylacetate.[23,58] In addition, it is unlikely that an electronic effect is present since the difference in the acidity of the water molecules coordinated to the metal ion, between (**2**) and (**3**), is less than one order of magnitude (pKa values are 7.2 for (**2**) and 8.0 for (**3**)). If we examine the difference in pKa values it is evident that (**2**) is a stronger Lewis acid than (**3**). Using the Brönsted relationship $\log k_{cat} = -\alpha pK_{a_{cat}}$ and $\log k_{cat} = -\beta pK_{a_{cat}}$,[65] if mechanism **A** is correct then (**2**) should be more reactive than (**3**) by $10^{\alpha(pKa2-pKa1)}$. Where β is the Brönsted coefficient and the difference in pKa of (**2**) and (**3**) is 0.8 (8.0-7.2). (**2**) can be no more than $10^{0.8}$ times as reactive as (**3**) since the theoretical maximum of α is 1.0.

Similarly if mechanism **B** is correct, the metal-hydroxide of (**3**) should be more reactive than the metal-hydroxide of (**2**) by $10^{\beta(pKa2-pKa1)}$. Where β is the Brönsted coefficient and the pKa difference is 0.8. (**3**) can be no more than $10^{0.8}$ times as reactive

as (**2**) since the theoretical maximum of β is 1.0. It is therefore unlikely that electronic effects are significant.

In the hydrolysis of activated amides and unactivated amides, the efficiency of the bifunctional catalyst, (**2**), has been related to its unique ability to increase the steady state concentration of the tetrahedral intermediates **T1** and **T2** by forming a stable four membered ring (Scheme 4.6 **T7**; Scheme 4.10 **T8** and **T9**, Scheme 4.12 **T10** and **T11**).

The dpa ligand binds Cu(II) more tightly ($K= 1.15 \times 10^8$ mol^{-1} dm^3) than it binds H^+ ($K= 1.28 \times 10^7$ mol^{-1} dm^3)[66]. This implies that the metal ion does not dissociate from the ligand over a wide pH range (including the pKa range). The ligand allows easy formation of the four membered ring formed during amide hydrolysis. Furthermore, the dpa catalyst does not bind to the amide nitrogen (production of free amine was observed; Figure 3.9) and intramolecular metal-hydroxide attack occurs readily. $[(dpa)Cu(OH_2)_2]^{+2}$ (**2**) is therefore an effective amide-cleaving diaqua complex.

4.5 ^{31}P NMR and Transition State Analogues

The efficient hydrolysis of activated and unactivated amides by diaqua Cu(II) complexes has been shown to be related to the diaqua complex's unique ability to stabilize the reactive tetrahedral intermediate by forming a four-membered ring (Scheme 4.6 **T7**, Scheme 4.10 **T8**, **T9** and Scheme 4.12 **T10**, **T11**). In addition, a structure-reactivity relationship was demonstrated by comparing the catalytic abilities of the diaqua complexes, $[(dpa)Cu(OH_2)_2]^{+2}$ (**2**) and $[(neo)Cu(OH_2)]^{+2}$ (**10**).

We propose that since the disodium salt of phenylphosphonic acid resembles the tetrahedral intermediate formed during Cu(II) complex catalyzed amide hydrolysis studies, it should easily form the four-membered ring intermediate with the diaqua Cu(II) complexes (**T14**).

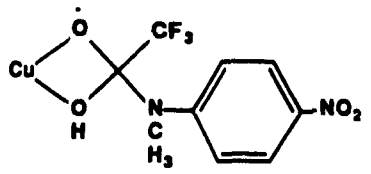

T7

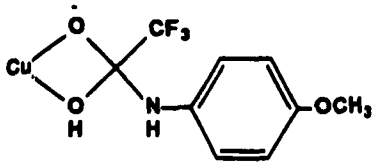

T8

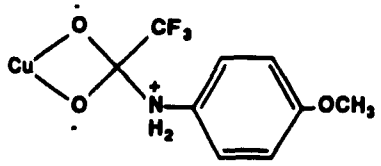

T9

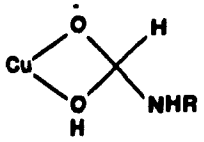

T10

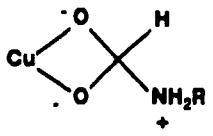

T11

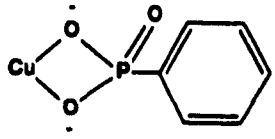

T14

Due to Cu(II)'s paramagnetic nature these observations were investigated through simple NMR binding studies using Co(III) complexes (tren and trpn). The disodium salt of phenylphosphonic acid is a suitable substrate because it mimics the tetrahedral intermediate formed during amide hydrolysis, and its coordination geometry is easily detectable using ^{31}P NMR. ^{31}P NMR signals of phosphates are known to shift progressively downfield with an increase in the number of Co(III) phosphate-oxygen bonds formed.[54]

$[(trpn)Co(OH_2)_2]^{+3}$ was observed to prefer bidentate coordination with the substrate (Figure 3.13(a); 40 ppm; $[(trpn)Co(ArPO_3)]^+$ (**12**)) while $[(tren)Co(OH_2)_2]^{+3}$ preferred monodentate coordination with the substrate ($[(tren)Co(ArPO_3)(OH_2)]^{+2}$ (**13**)).

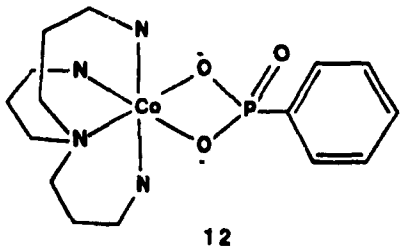

12

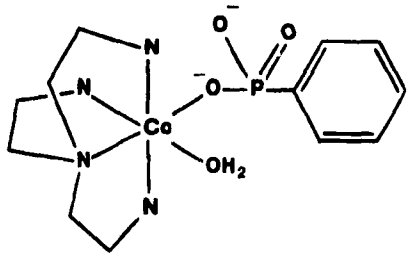

13

^{31}P NMR of one equivalent of the substrate (disodium salt of phenylphosphonic acid) with $[(tren)Co(OH_2)_2]^{+3}$ revealed the presence of free substrate (Figure 3.13(b); 10.4 ppm), structure **13** (Figure 3.13; 23.0 and 24.0 ppm where one isomer has the phosphorus centre opposite the tertiary nitrogen and the other has the phosphorus centre opposite the primary nitrogen), and small amounts of other structures.

It is well known that $[(trpn)Co(OH_2)_2]^{+3}$ forms four membered rings more easily than $[(tren)Co(OH_2)_2]^{+3}$ because of the trpn ligand. Free phenylphosphonate is observed in Figure 3.13(b) whereas none is seen in Figure 3.13(a). This is because bidentate coordination in **12** allows tighter binding of the phosphonate. Similarly, (**2**) may form a more stable four-membered ring complex than (**10**), therefore making (**2**) a more efficient amide-cleaving catalyst.

4.6 Applications to Proteins

Catalytic Antibodies

The binding forces between an enzyme and its complementary substrate are used to deform the substrate into an activated complex for which the enzyme has the greatest binding affinity. Depending on the stability of this interaction the activated complex can revert back to starting material, or it can be broken down to products. Since the enzyme specificity is oriented towards the activated complex, the activation energy for the reaction decreases and a faster reaction proceeds.[67] Because of this, enzyme inhibitors have been designed to mimic the highest energy transition state structure for the reaction catalyzed by the enzyme. Binding studies of transition state analogues, with modified chemical properties, have been used to identify amino acid side chains responsible for catalysis within the enzyme's active site.[68-71] Phosphorus transition state analogues which have successfully inhibited the hydrolysis activity of the peptidase pepsin are shown below.[68] The tetrahedral intermediate center, the carbon ketone hydrate, has been imitated by phosphorus. We propose that since the disodium salt of phenylphosphonic acid resembles the structures depicted below, it is a potential transition state analogue for peptide-cleaving enzymes.

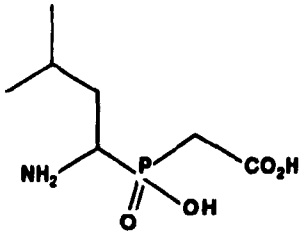

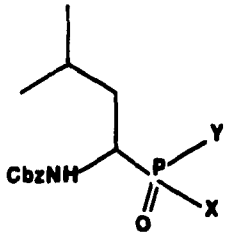

X= Y= OPh
X= Y= OMe
X= OMe, Y= OH
X= OMe, Y= Cl
X= OMe, Y=SPh
X= OMe, Y= CH_2CO_2 - t- Bu

Recently, Schultz, Lerner, and Benkovic have induced the production of cellular monoclonal catalytic antibodies using transition state analogues as haptens.[72] The theory which led to this development was derived from the observation that enzymes selectively bind to the transition state, whereas antibodies selectively bind to the substrate in the ground state.[33,72] Therefore, extending the transition state theory by using various transition state analogues as haptens, antibodies have been generated with catalytic characteristics similar to biological molecules such as restriction enzymes, glycosidases, stereospecific esterases, DNA photolyase, and selective peptidases. These catalytic antibodies are also called abzymes.[72]

Monoclonal antibodies capable of hydrolyzing a *p*-nitroanilide peptide substrate (**14**), with a 250 000 fold rate enhancement over the background rate, were generated using phosphoamidate transition state analogues (**TSA1**, **TSA2**) as haptens. Enzyme-like inhibition of the catalytic antibody was also observed in the presence of excess hapten (*m*- and *p*-nitroanilide).

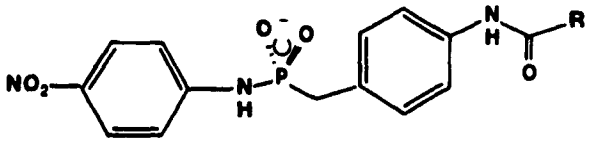

TSA1, TSA2 R= CH_3 , $(CH_2)_3CO_2NC_4O_2$

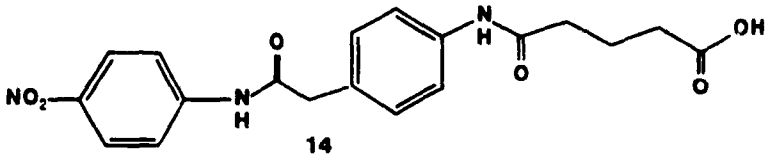

14

The transition state stabilization energy (equivalent to the differential binding energy between **TSA2**, which mimics the zwitterionic tetrahedral intermediate formed during amide hydrolysis, and **14**) could not fully account for the large observed rate enhancements. Additional catalytic functional groups such as acid/base residues and ground state destabilization are believed to be involved. Hapten structures capable of inducing catalytic side chains in an antibody binding site have also been observed.[72]

Sequence specific peptide cleavage catalyzed by an antibody has been induced with the Co(III) triethylenetetramine (trien) peptide hapten (**15**).[72]

15

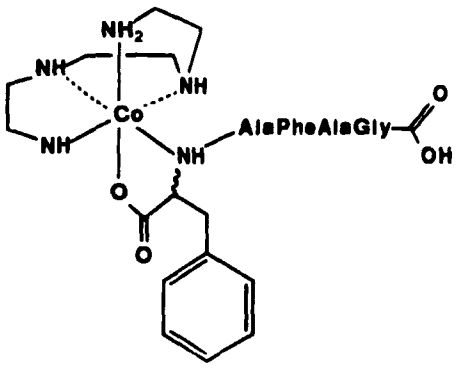

The antibodies produced were observed to bind peptides with the trien complexes of Zn(II), Ga(II), Fe(II), In(III), Cu(II), Ni(II), Lu(III), Mg(II), or Mn(II) as cofactors. Interestingly, binding of either inert or labile metals selectively catalyzed the cleavage of the

Gly-Phe amide bond at pH 6.5. The metal complex is believed to facilitate amide hydrolysis by binding and polarizing the carbonyl group (Lewis acid activation), or by promoting the nucleophilic attack of a metal-hydroxide species, or by a combination of the two. Either pathway would lead to a metal-bound tetrahedral intermediate prior to product formation.[72]

Although **15** induces the antibody to have a binding pocket complementary to a metal-complex cofactor which binds a peptide in a stereospecific manner, it does not imitate the metal-tetrahedral intermediate, and therefore is not a true transition state analogue. A potential hapten which may generate catalytic antibodies with a binding site complementary to the transition state of a metal-catalyzed amide hydrolysis reaction is compound **12**.

We propose that since **12** closely resembles the tetrahedral intermediates formed during Cu(II) complex catalyzed amide hydrolysis (**T7**, **T8**, **T9**, **T10**, **T11**), it should be considered a potential hapten for the production of catalytic metalloantibodies with peptidase activity.

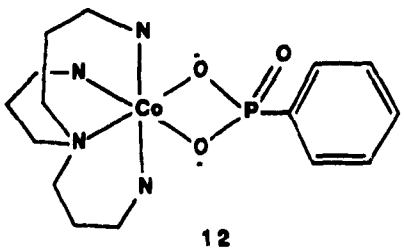

12

An Enzyme Model: Carboxypeptidase A

Detailed mechanistic studies of metal-complex systems have enlightened the chemist's understanding of the mode of action of metalloenzymes.

Bovine carboxypeptidase A[73] is a Zn containing exopeptidase of molecular weight 34 472 daltons. Its optimum activity occurs around neutral pH. The residues responsible for binding and catalysis are Glu-270, Arg-71, Arg-127, Asn-144, Arg-145, Tyr-248, Zn bound to a single polypeptide chain, and a Zn-OH_2 molecule Binding studies have indicated that Tyr-248 endures a large conformational change when the substrate binds to the active site. Several model studies have emerged to determine the catalytic mechanism of this enzyme which efficiently cleaves peptides ($k_{cat} = 10^2$ sec^{-1}) and esters ($k_{cat} = 10^3$ sec^{-1}).[73]

A Lewis acid mechanism for the Zn metal was proposed through the study of a Co(III) model with a coordinated glycine amide fixed in place (Scheme 4.15).[45] To determine the roles of Tyr-248 and Glu-270, the catalytic effects of a phenol (Scheme 4.15; **16-18**) and a carboxylate (**19-21**) functional group were examined.

Scheme 4.15

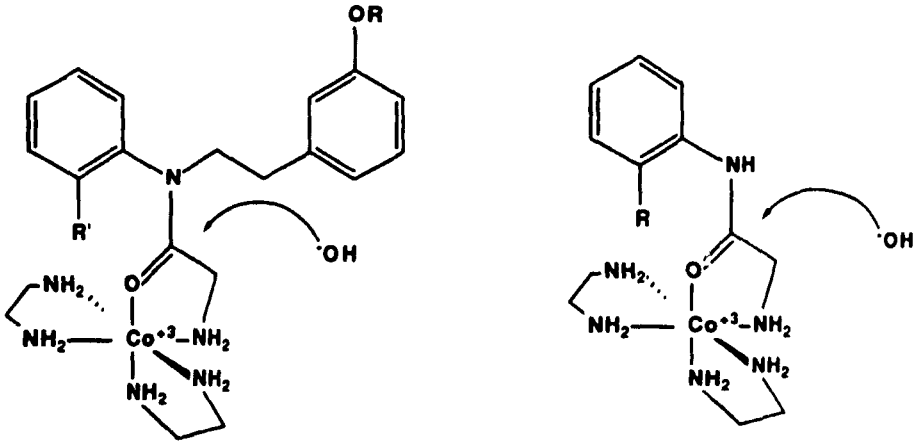

16. R = H, R' = CO_2 H

17. R = R' = H

18. R = CH_3 , R' = H

19. R = CO_2H

20. R = CO_2CH_3

21. P = H

The carboxylate gave no additional rate enhancement however, when a protonated phenol was present, between pH 7.5 and 9, a 100 fold increase in the hydrolysis rate was observed (Scheme 4.15, **17**). The phenol is believed to function as a GAC protonating the nitrogen in the rate limiting breakdown of the tetrahedral intermediate.

At neutral pH, the bifunctional buffer phosphate ($H_2PO_4^-/HPO_4^{-2}$) catalyzed the hydrolysis of **16**, **17** and **18**, while at 50°C, acetate buffer catalyzed the hydrolysis of **17** and **18**. The buffers are believed to act in a bifunctional manner catalyzing the breakdown of the tetrahedral intermediate. Scheme 4.16 displays the phosphate and acetate buffers acting as a GAC/GBC in the breakdown of the tetrahedral intermediate.

Scheme 4.16

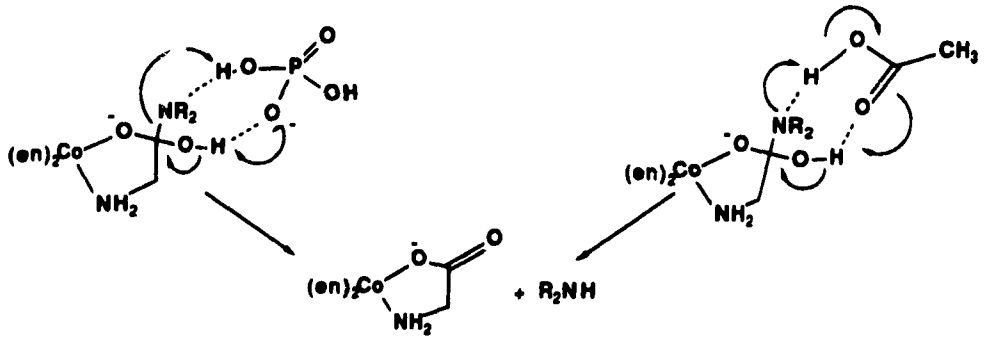

When site-directed mutagenesis revealed the non-catalytic role of Tyr-248, efforts diverged towards determining the catalytic role of Glu-270.[45] Glu-270 can function as a nucleophile or a general base (Scheme 4.17 **A** and **B** respectively).

Scheme 4.17

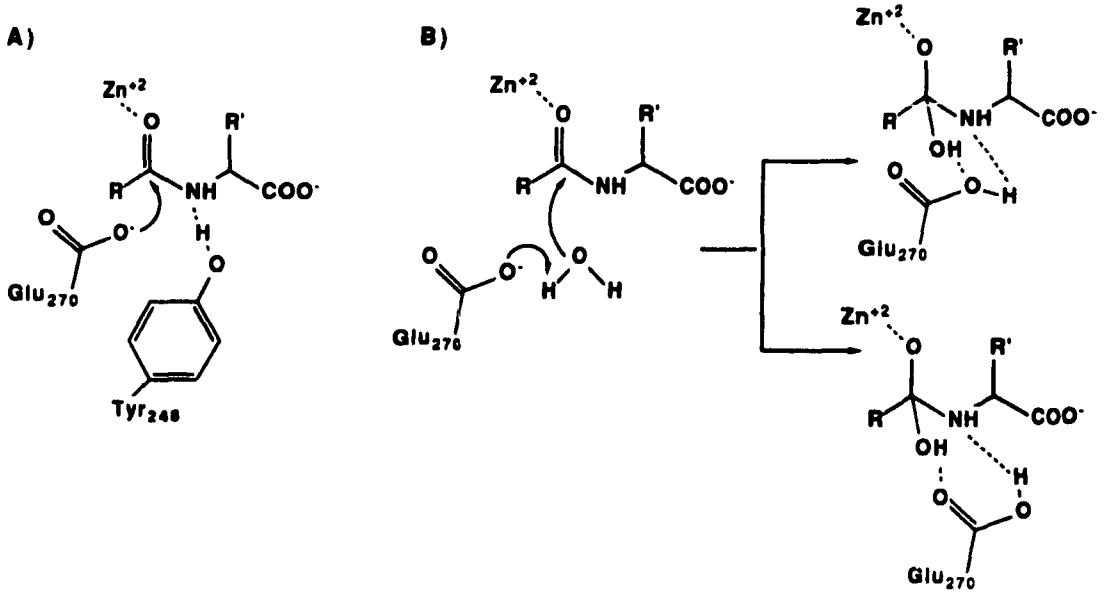

The mechanism in Scheme 4.17**A** is unlikely since Tyr-248 is not involved in catalysis. The preferred mechanism for Carboxypeptidase A, Scheme 4.17**B**, shows

Lewis acid activation of the carbonyl with Glu-270 acting as a GBC promoting the attack of an external water molecule. The protonated Glu-270 then acts as a bifunctional catalyst. The breakdown of the tetrahedral intermediate is facilitated as Glu-270 protonates the leaving amine group (GAC) and stabilizes the hydroxide group.

A Zn-OH mechanism for Carboxypeptidase A was proposed with a coordinated lactam Co(III) complex (Scheme 4.18; **22** and **23**).[44] The boat configuration of the azalactam properly positions the attacking metal-hydroxide (L-Co-OH) and metal-water species (L-Co-OH_2). First order kinetic results, and a hydrolysis rate faster than the rate of ligand exchange, proved that the hydrolysis reaction was intramolecular.

Scheme 4.18

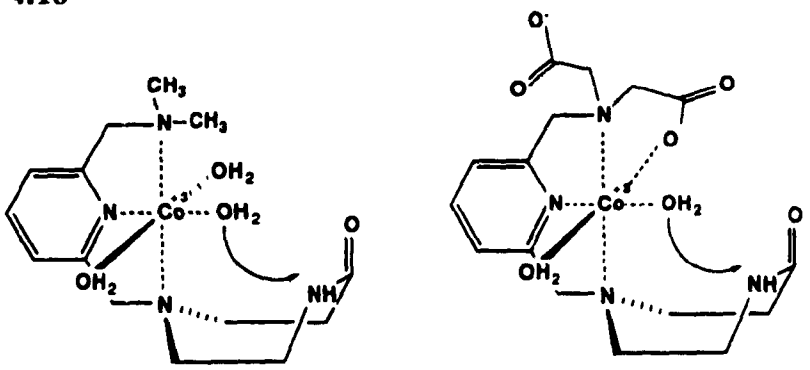

22 **23**

The mechanism for the hydrolysis reaction catalyzed by the L-Co-OH_2 species, at acidic and neutral pH, is displayed in Scheme 4.19. The rate limiting step is believed to be the formation of the tetrahedral intermediate, followed by rapid proton transfer and C-N bond cleavage (in a step-wise or concerted fashion).[44]

Scheme 4.19

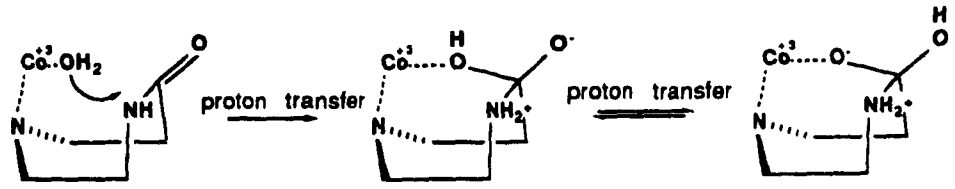

For the L-Co-OH catalyzed hydrolysis reaction the mechanism is displayed in Scheme 4.20 below. Intramolecular Co-OH attack forms **TA**. In path **A**, proton transfer in **TA** forms **TB**. This is followed by GAC and GBC to form **TD** and **TE** respectively. In path **B**, GBC in **TA** forms **TC**. GAC follows to form **TE**. **TE** is converted to products by rapid C-N bond cleavage.

Buffer catalysis was observed around neutrality where the breakdown of the tetrahedral intermediate is rate limiting. The reaction rate was observed to increase with the addition of phosphate buffer. For example, at pH 6.78 the reaction is 20 fold faster in the presence of phosphate (0.2 M). This was interpreted as a buffer assisted breakdown of the tetrahedral intermediate **TA** in a concerted process.

The rate enhancements for the Co(III) promoted hydrolysis of **22** and **23** at pH 7, and 25°C, are 1.7 X 10^7 and 5.3 x 10^8 respectively. The carboxylate in **23** is responsible for a 30 fold rate increase in the rate constant of the Co-OH promoted amide hydrolysis reaction. A correctly positioned pendant carboxylate is believed to facilitate the rate limiting breakdown of the tetrahedral intermediate by proton transfer in **TA**, thus forming **TE**. Glu-270 in Carboxypeptidase A is proposed to behave as a GBC/GAC, similar to this carboxylate (**23**).

Scheme 4.20

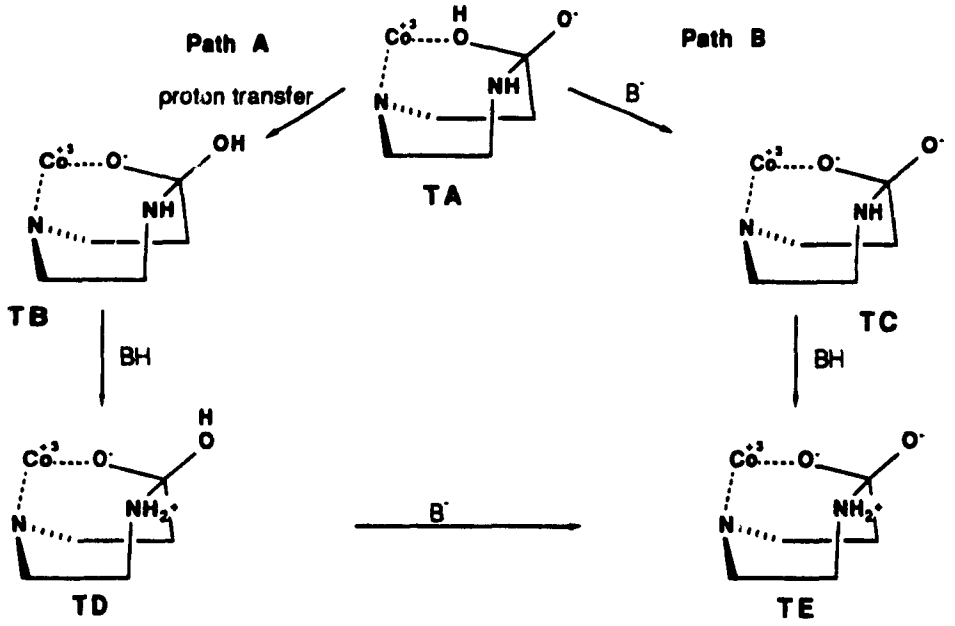

The production of free amine revealed that during the hydrolysis reaction the amidic nitrogen is never coordinated to the metal. Furthermore, stereoelectronic arguments, stating that the cleavage of a carbon-oxygen or a carbon-nitrogen bond is

facilitated only when the two heteroatoms of the tetrahedral intermediate each have a lone pair of electrons (or exchangeable protons) oriented antiperiplanar to the departing O-alkyl or N-alkyl group, were used to explain these results. These factors have proven to be important in the understanding of metal-catalyzed amide hydrolysis reactions.

Christianson and Lipscomb have reported an X-ray structure of an inhibitor bound substrate to carboxypeptidase A (**CPA**).[73] Scheme 4.21 displays the hydrated ketone coordinated in a bidentate fashion to the active site zinc of **CPA**, where one of the gem-diol oxygens is hydrogen bonded to Glu-270 and the other is hydrogen bonded to Arg-127. In light of our experimental results for Cu(II) complex catalyzed hydrolysis of amides, the bifunctional mechanism we propose can also be used to explain the catalytic activity of **CPA**. Indeed, Lewis acid activation of the carbonyl carbon, followed by intramolecular Zn-OH attack forms the tetrahedral intermediate (analogous to the hydrated ketone enzyme inhibitor in Scheme 4.21 below). Since in Cu(II) catalyzed hydrolysis of **MTA** (Section 4.3) the rate limiting proton transfer step was found to be facilitated by buffer catalysis (cooperative effect) we propose that in **CPA** Glu-270 acts as a GBC/GAC removing the proton from the metal-hydroxide and protonating the amine leaving group in the anionic tetrahedral intermediate. This may occur in a concerted or stepwise fashion (Scheme 4.21).

Scheme 4.21

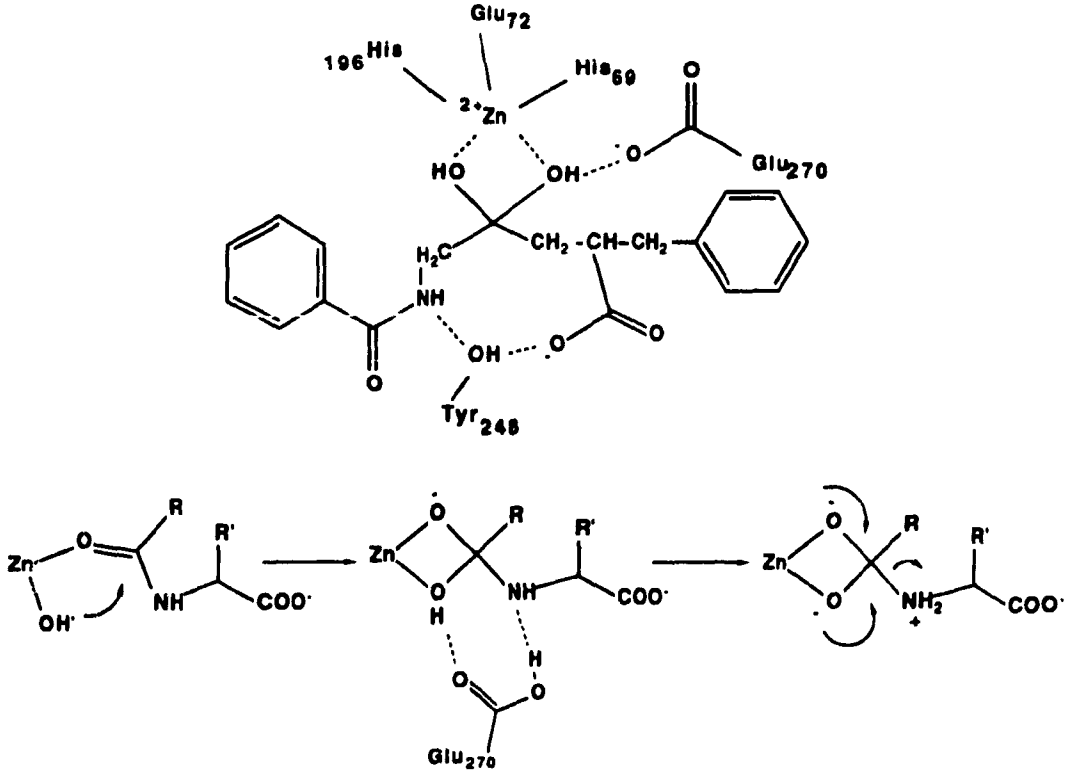

4.7 Future Plans

For the first time a metal-buffer cooperative effect is observed in free amide hydrolysis. The complex $[(dpa)Cu(OH_2)_2]^{+2}$ is an effective amide-cleaving catalyst which cooperates with NEM buffer in the hydrolysis of an acyl-activated amide with a poor leaving group (i.e. **MTA**).

Since greater rates of intramolecular reactions compared to the corresponding intermolecular reactions have been observed[33,40], an interesting future plan is to study the effects of attaching non-complexing acid/base functional groups, such as NEM, either to the amide substrate to be cleaved by a cis-diaqua metal complex (i.e. $[(dpa)Cu(OH_2)_2]^{+2}$), or, to the cis-diaqua metal complex catalyzing the hydrolysis of the amide substrate. The intramolecular metal-buffer cooperativity effect can increase the catalyzed hydrolysis reaction rates of a free amide with a poor leaving group (i.e. **MTA**). Ultimately, through the study of these simple metallocomplexes, cleavage of peptides and proteins may be achieved.

Contributions to Knowledge

The study of simple transition metal-complex systems contributes to the understanding of the mechanisms of hydrolysis reactions, the principles of catalysis, and to the role of the metal ion in the active site of metalloproteins.

1. The structural requirements of a Cu(II) catalyst capable of catalyzing the hydrolysis of activated amides with catalytic turnover has been elucidated through detailed mechanistic studies. The diaqua Cu(II) complex $[(dpa)Cu(OH_2)_2]^{+2}$, was observed to be a more efficient catalyst than the monoaqua Cu(II) complexes $[(terp)Cu(OH_2)]^{+2}$ and $[(dien)Cu(OH_2)]^{+2}$, in the hydrolysis of activated and unactivated amides.

2. A cooperative effect has been observed between $[(dpa)Cu(OH_2)_2]^{+2}$ and NEM buffer in the catalyzed hydrolysis of an activated amide with a poor leaving group. Other than in enzymic systems, such a metal-buffer cooperativity in free amide hydrolysis has not been previously detected.

3. A bifunctional mechanism for the $[(dpa)Cu(OH_2)_2]^{+2}$ catalyzed hydrolysis of both activated and unactivated amides has been proposed. A Lewis acid activation of the carbonyl carbon, followed by metal-hydroxide intramolecular attack forms the tetrahedral intermediate. The relative rate enhancement has been related to the complex's ability to stabilize the tetrahedral intermediate through the formation of a key four-membered ring. For the hydrolysis of amides with good leaving groups C-N bond cleavage is the rate limiting step, whereas for amides with poor leaving groups proton transfer is the rate limiting step.

4. These Cu(II) complex catalyzed amide hydrolysis studies have been related to simple metalloprotein systems. Firstly, a potential hapten capable of generating catalytic metalloanitbodies with peptidase activity has been proposed with the help of ^{31}P NMR binding studies of a transition state analogue. Secondly, the metal ion in the peptidase, CPA, was assigned a role similar to that of the Cu(II) metal ion in $[(dpa)Cu(OH_2)_2]^{+2}$.

As a result of my Masters study I have contributed to the following papers:

1. Jik Chin, Vrej Jubian, and Karen Mrejen.
"Catalytic Hydrolysis of Amides at Neutral pH."
Journal of the Chemical Society: Chemical Communications, 1990, 1326-1328.

2. Jik Chin, Mariusz Banaszczyk, Vrej Jubian, Jung-Hee Kim, and Karen Mrejen.
Bioorganic Chemistry Frontiers (ed), Artificial Hydrolytic Metalloenzymes.
Springer-Verlag: New York, 1990.

3. Jik Chin and Karen Mrejen.
"Metal-Buffer Cooperativity in Free Amide Hydrolysis"
To be submitted for publication.

References

1. a) Richards, F.M.; *Scientific American* **1991**, 54.

2. a) Zubay, G.; *Biochemistry;* Addison-Wesley Publishing Company: Don Mills, **1983**. b) Bruice, T.C.; Benkovic, S.; *Bioorganic Mechanisms*, Vol I, W.A. Benjamin inc.: New York, **1966**.

3. Creighton, T.E.; *Proteins; Structures and Molecular Properties;* W.H. Freeman and Co.: New York, **1984**.

4. Roques, B. P.; *La Science* **1989**, 140, 40.

5. Matthews, B.W.; *Acc. Chem. Res.* **1988**, 21, 333.

6. Stein, R.L.; Izquierdo, M.C.; *J. Am. Chem. Soc.* **1990**, 112, 6062.

7. a) Blow, D.M.; *Acc. Chem. Res.* **1976**, 9, 145. b) Tollato, U.; Anoardi, L.; *J. Chem. Soc., Chem. Comm.* **1977**, 401.

8. Fruton, J.S.; *Acc. Chem. Res.* **1974**, 8, 241.

9. a) Fife, T.H.; Przystas, J.T.; *J. Am. Chem. Soc. Perkin Trans 2* **1990**, 393. b) Fife, T.H.; Przystas, J.T.; *J. Am. Chem. Soc.* **1986**, 108, 4631.

10. a) Page, M.I.; Proctor, P.; Gensmantel, N.P.; *J Am. Chem. Soc Perkin Trans 2* **1980**, 1725. b) Page, M.I.; Webster P.S.; Ghosez, L.; *J Am. Chem. Soc., Perkin Trans 2* **1990**, 805. c) Page M.I.; *Acc. Chem. Res.* **1984**, 17,144.

11. a) Cram, D.J.; Lam, P.Y.; Ho, S.P.; *J. Am. Chem. Soc.* **1986**, 108,839. b) Lehn, J.M.; Sirlin, C.; *J. Chem. Soc., Chem. Commun.* **1987**,949. c) D'Souza, V.T.; Bender, M.L.; *Acc. Chem. Res.* **1987**, 20, 146. d) Breslow, R.; *Pure Appl. Chem.* **1990**, Vol. 62, 10, 1859.

12. Carey, F.A.; Sundberg, R.J.; *Advanced Organic Chemistry, Part A. Structure and Mechanisms*, 3rd Ed.; Plenum Press: New York, **1984**.

13. Lowry,T.; Richardson, K.S.; *Mechanism and Theory in Organic Chemistry*, 3rd Ed.; Harper & Row: New York, **1987**.

14. Jencks, W.P.; Kirsch, J.F.; *J. Am. Chem. Soc.* **1964**, 86, 837.

15. Ritchie, C.D.; *J. Am. Chem. Soc.* **1975**, 97, 1170.

16. Menger, F.M.; Ladika, M.; *J. Am. Chem. Soc.* **1987**, 109, 3145.

17. a) Breslow, R.; Trainor, G.; Veno, A.; *J. Am. Chem. Soc.* **1983**, 105, 2739. b) Breslow, R.; Czarniecki, M.F.; Emert, J.; Hamaguchi, H.; *J. Am. Chem. Soc.* **1980**, 102, 762.

18. Kroll, H.; *J. Am. Chem. Soc.* **1952**, 74, 2036.

19. Buckingham, D.A.; Sutton, P.A.; *Acc. Chem. Res.* **1987**, 87, 357. (and references therein)

20. Chin, J.; Zou, X.; *J. Am. Chem. Soc.* **1984**, 106, 3687.

21. Moore, J.W.; Pearson, R.G.; *Kinetics and Mechanism*; John Wiley & Sons: New York, **1981**, 363.

22. Cotton, F.A.; Wilkinson, G.; *Adv. Inorg. Chem.* John Wiley & Sons: New York, **1972**, 503.

23. Chin, J.; Jubian, V.; *J. Chem. Soc., Chem. Commun.* **1989**, 13, 840.

24. Chin, J.; Banaszczyk, M.; *J. Am. Chem. Soc.* **1989**, 111, 2724.

25. a) Banaszczyk, M.; *Ph.D. Thesis* McGill University, Montreal: **1989**. b) Moore, A.; *Ph.D. Thesis*, McGill University, Montreal: **1990.**

26. Chin,J.; Banaszczyk, M.; Jubian, V.; Kim, J.H.; Mrejen, K.; *Bioorganic Chemistry Frontiers (ed), Artificial Hydrolytic Metalloenzymes: A Unified Approach;* Springer-Verlag, New York, **1990**.

27. a) Schepartz, A.; Cuenoud, B.; *J. Am. Chem. Soc.* **1990**, 112, 3247. b) Meares, F.; Rana, M.T.; *J. Am. Chem. Soc.* **1990**, 112, 2457.

28. Still, W.C.; Kahne, D.; *J. Am. Chem. Soc.* **1988**, 110, 7529.

29. Dugas, H.; *Bioorganic Chemistry; A Chemical Approach to Enzyme Action,* 2nd Ed.; Springer-Verlag: New York, **1989**.

30. a) Schowen, R.L.; Zuorick, G.W.; *J. Am. Chem. Soc.* **1966**, 88, 1223. b) Schowen, R.L.; Kershner, L.; Jayaraman, H.; *J. Am. Chem. Soc.* **1966**, 88, 3373 c) Schowen, R.L.; Kershner, L.D.; *J. Am. Chem. Soc.* **1971**, 93, 2014. d) Schowen, R.L.; Drake, D.; Jayaraman, H.; *J. Am. Chem. Soc.* **1973**, 95, 454. e) Guthrie, J.P.; Brown, R.S.; Jodhan, A.; Keillor, JW.; Bennet, A.J.; Slebocka-Tilk, H.; *J. Am. Chem. Soc.* **1990**, 112, 8507.

31. Pollack, R.M.; Dumasha, T.C.; *J. Am. Chem. Soc.* **1973**, 95, 4463.

32. Schowen L.R.; Gandour R.D.; *Transition States of Biochemical Processes,* Plenum Press: New York, **1978**, 529.

33. Jencks, W.P.; *Catalysis in Chemistry and Enzymology;* Dover Ed; John Wiley & Sons: New York, **1975**, 7-41.

34. Kirby, A.J.; Fersht, A.R.; *Prog. Bioorg. Chem.* **1971**, 1,

35. Menger, F.M.; *Acc. Chem. Res.* **1985**, 18, 128.

36. Knowles, J.R.; *Science* **1987**, 236, 1252.

37. a) Bender, M.L.; Bergeron, R.J.; Kamiyama, M.; *The Bioorganic Chemistry of Enzyme Catalysis,* John Wiley & Sons: New York, **1984**. b) Rebek, J. Jr.;

Acc. Chem. Res. **1984**, 17, 258.

38. Bruice, T.C.; Marquardt, F.H.; *J. Am. Chem. Soc.* **1962**, 66, 365.

39. a) Gandour, D.R.; *Bioorg. Chem.* **1981**, 10, 169. b) Kirby, A.J.; Lancaster P.W.; *J. Am. Chem. Soc. Perkin Trans.* **1972**, 1206. c) Klugar, R.; Chin, J.; *J. Am. Chem. Soc.* **1982**, 104, 4154. d) Breslow, R.; Chin, J.; *Tetrahedron Lett.* **1982**, 23, 4221.

40. Koshland, D.E.; Daffom, G.A.; *Bioorg. Chem.* **1971**, 1, 129.

41. Sigel, S.; *Metal Ions in Biological Systems, Volume 2; Metal-Ligand complex,* Marcel Dekker, Inc.: New York, **1973**, 207.

42. Meriwether, L.; Westheimer, F.H.; *J. Am. Chem. Soc.* **1956**, 78, 5119.

43. Chin, J.; Jubian, V.; Mrejen, K.; *J. Chem. Soc., Chem. Commun.* 1990, 19, 1326.

44. a) Groves, J.T.; Baron, L.A.; *J. Am. Chem. Soc.* **1989**, 111, 5442.
b) Groves, J.T.; Chambers, R.R. Jr.; *J. Am. Chem. Soc.* **1984**, 106, 630.

45. a) Breslow, R.; Schepartz, A.; *J. Am. Chem. Soc.* **1987**, 109, 1814.
b) Breslow, R.; Schepartz, A.; *Chem. Lett.* **1987**, 1.

46. a) Czarnik, A.W.; Duerr, B.F.; *J. Chem. Soc., Chem. Commun.* **1990**, 1707. b) Czarnik, A.W.; Nanjappan, P; *J. Am. Chem. Soc.* **1987**, 87, 1826.

47. Tatlow, J.C.; Tatlow, C.E.M.; Henry, S.H.; Bourne, E.J.; *J. Am. Chem. Soc.* **1952**, 74, 1695.

48. Reference 33, 565.

49. Trogler W.C.; Morrow, J.R.; *Inorg. Chem.* **1988**, 27, 3387.

50. Segretain, A.M.; Beugelmans-Verrier, M.; Laloi-Diard, M.; *Bull. Soc. Chim. Fran.* **1972**, 9, 3375.

51. Bell, R.P.; *The Proton in Chemistry*, Methuen & Co.: London, **1959**, 183.

52. Bruice, T.C.; Fife, T.H.; *J. Am. Chem. Soc.* **1961**, 65, 1079

53. a) Khan, A.A.; Ahmad, R.; Khan, M.N.; *Ind. J. Chem* **1976**, 14A, 12, 96.
b) Reference 2b, p. 91.

54. a) Haight, G.P. Jr;. *Coord. Chem. Rev.* **1987**, 79, 293-319.
b) Sargeson, A.M.; Lindoy, L.F.; Jones, D R.; *J. Am. Chem. Soc.* **1984**, 106, 7807-7819. c) Milburn, R.M.; Anderson, B.; Harrowfield, J.M.; Robertson, G.B.; Sargeson, A.M. et al.; J. *Am Chem Soc.* **1977**, 99, 2652. d) J. Chin; Banaszczyk, M.; *J. Am. Chem Soc.* **1989**, 111, 4103.

55. a) Orgel, L.E.; *An Introduction to Transition-Metal Chemistry: Ligand-Field Theory;* John Wiley & Sons: New York, **1965**, 59. b) Guenther, B.W.;

Chemical Equilibrium; A Practical Introduction for the Physical and Life Sciences, Plenum Press: New York, **1975**. c) Kurz, J.K.; *J Am. Chem. Soc.* **1963**, 85, 987. d) Basolo, F.; Pearson, R.G.; *Mechanisms of Inorganic Reactions. A Study of Metal Complexes in Solutions*; John Wiley & Sons: New York, **1968**, 421.

56. Sayre, L.M.; *J. Am. Chem. Soc.* **1986**, 108, 1632; and references therein.

57. Martell, A.E.; Gustafson, R.L.; *J. Am. Chem. Soc.* **1959**, 81, 525.

58. Jubian, V.; *Ph.D. Thesis*, McGill University, Montreal: **1991**.

59. Guthrie, J.P.; *J. Am. Chem. Soc.* **1974**, 96, 3608. Dolman, D.; Stewart, R.; *Can. J. Chem.* **1967**, 45, 911.

60. Dolman, D.; Stewart, R.; *Can. J. Chem.* **1967**, 45, 911.

61. Jencks, W.P.; *Acc. Chem. Res.* **1976**, 9, 425.

62. Jencks, W.P.; *Chem. Rev.* **1972**, 72(6), 705.

63. Ray, N.; Tyagi, S.; Hathaway, B.; *Acta Crystallogr., Sect. B* **1982**, 38, 1574.

64. Reference 51, 65

65. Caldin, E.; Gold, V.; *Proton-transfer Reactions*, John Wiley & Sons: New York, **1975**, 166.

66. Anderegg, G.; *Helv. Chim. Acta* **1971**, 54, 509.

67. Pauling, L.; *Am. Scien.* **1948**, 36, 51

68. Bartlett, P.A.; *J. Am. Chem. Soc.* **1984**, 106, 4282.

69. Carter, P.; Wells, J.A.; *Nature* **1988**, 332 (7), 564

70. Leinhard, G.E.; *Science* **1973**, 180, 149.

71. Wolfenden, R.; *Acc. Chem. Res.* **1972**, 5,10.

72. Schultz, P.G.; Lerner, R.A.; Benkovic, S.J.; *Chem. Eng. News, Special Report* **1990**, 26; and references therein.

73. Lipscomb, W.N.; Christianson, D.W.; *Acc. Chem. Res.* **1989**, 22, 62.